



The
University
Of
Sheffield.

Immobilised Transition Metal
Photosensitisers: Robust, Sustainable,
Solar-Driven Systems for Water
Purification

Dylan Pritchard

*A thesis submitted in partial fulfilment of the requirements for the
degree of Doctor of Philosophy*

The University of Sheffield
Faculty of Science
Department of Chemistry

August 2020

Abstract

The aim of this work is to produce a point-of-use water disinfecting technology that harnesses the power of sunlight to disinfect water through generation of singlet oxygen by metal complex photosensitisers attached to solid supports. To that end a number of Ru(II) and Cu(I) complex photosensitisers based on bipyridyl-type ligands have been synthesised and immobilised onto various supports. The compounds were tested with regards to their singlet oxygen generating abilities and bactericidal efficiencies against *Staphylococcus aureus* and *Escherichia coli*.

Chapter 1 contains an introduction to the topic of singlet oxygen photosensitisation, photodynamic inactivation of bacteria, and a literature survey of the field of solar purification of water using supported singlet oxygen photosensitisers.

Chapter 2 discusses the main synthetic work: synthesis of a wide range of Ru(II) and Cu(I) complexes with polypyridyl ligands, followed by spectroscopic characterisation using UV-Vis, steady-state and time-resolved fluorescence spectroscopy. The complexes' immobilisation onto solid supports is described and the resulting immobilised compounds were also characterised using UV-Vis, Infrared and fluorescence spectroscopy. The ruthenium complex [Ru(bpy)₂(bpy-silatrane)]Cl₂ (RuBS) was synthesised and covalently grafted onto chromatography silica (40-60 mesh), SBA-15 and MCM-41 with surface coverages of 38, 50 and >80 μmol g⁻¹ respectively. A number of other Ru(II) polypyridyl complexes were synthesised with the aim of improving singlet oxygen quantum yield. Tetrasodium Ruthenium tris(bathophenanthroline disulfonate) (RuBPS) was ionically bound onto the surface of Amberlite® IRA900 with a surface loading of 1.20 μmol g⁻¹. To PDMS were covalently grafted two Ru(II) polypyridyl complexes. This was performed by two methods: amination with 3-

amino(propyl triethoxysilane) (APTES) and 3-mercapto(propyl trimethoxysilane) (MPTS). A number of Cu(I) diamine diphosphine complexes ($\{\text{Cu}(\text{NN})(\text{PP})\}^+$) were also synthesised with optimisation of singlet oxygen quantum yield and absorption in the visible spectrum being evaluated. Of all of the synthesised complexes the known compound $[\text{Cu}(2,9\text{-dimethyl-1,10-phenanthroline})(\text{xantphos})]\text{tfpb}$ was dry-loaded onto chromatography grade silica to produce the compound CuXD-CS, with surface loading of $11 \mu\text{mol g}^{-1}$ of the active complex.

Chapter 3 describes the quantification of singlet oxygen production by the synthesised compound, both in solution and when grafted onto solid supports. The singlet oxygen quantum yields of the following Ru(II) complexes was measured: RuBS ($\Phi_{\Delta} = 0.55 \pm 0.03$), RuBMS ($\Phi_{\Delta} = 0.60 \pm 0.04$) and RuPS ($\Phi_{\Delta} = 0.88 \pm 0.03$); along with the Cu(I) complexes $\{\text{Cu}(\text{dmp})(\text{xant})\}^+$ ($\Phi_{\Delta} = 0.30 \pm 0.04$), $\{\text{Cu}(\text{BC})(\text{xant})\}^+$ ($\Phi_{\Delta} = 0.41 \pm 0.03$), $\{\text{Cu}(\text{BCS})(\text{xant})\}^+$ ($\Phi_{\Delta} = 0.42 \pm 0.08$), $\{\text{Cu}(\text{dmp})(\text{DPEPhos})\}^+$ ($\Phi_{\Delta} = 0.40 \pm 0.09$).

In Chapter 4 the singlet-oxygen based bactericidal activity of two of the solid support-immobilised complexes was tested on *S. aureus* and *E. coli* with varying degrees of success following an introduction into the cell wall structure of Gram-positive and Gram-negative bacteria. RuBS covalently grafted onto chromatography silica (RuBS-CS) was unable to reduce colonies of *S. aureus* and *E. coli* after 2 hours of illumination by 455 nm light (2.5 mWcm^{-2}). The complex $[\text{Cu}(2,9\text{-dimethyl-1,10-phenanthroline})(\text{xantphos})]\text{tfpb}$ also showed no photodynamic bactericidal activity on its own. However, the same Cu(I) complex dry-loaded onto chromatography silica, CuXD-CS, reduced colonies of *S. aureus* and *E. coli* by 99.9999% (6-log_{10}) after 2 and 3 hours of illumination by 405 nm light (14.3 mW cm^{-2}) respectively.

Chapter 5 includes all synthesis and characterisation data of the complexes presented in this work.

Acknowledgements

An enormous thank you to my two PhD project supervisors: Mike Ward and Julia Weinstein for all the support, encouragement and helpful criticism that led to the completion of this degree. I couldn't have asked for a more welcoming and reassuring pair of supervisors.

A big thanks to my collaborators and all those who aided with my research, including but not limited to: Martin Appleby, Professor Dave Kelly, Pete G. Walker, Jamie Wright, Luke Mckenzie for all the help with experiments. It was a joy to work alongside you all.

I would like to express my very great appreciation to Denise and Louise Richards, the university Financial Administrators, for guiding me through the administrative nightmare that is a PhD project, like they have for so many others.

A special thanks to all my fellow lab mates for showing me the ropes, being generally fun to work around and being incredibly patient with me: Jenny Train, Andy Sadler, Beth Crowston, Tom Roseveare, James Shipp, Simon Parker, Tao Cheng, Samantha Peralta, Marta Martinez Alonso to name a few.

To the countless technical staff, the backbone of the chemistry department that have aided me and every other researcher in the department I know.

Big thanks the occupants of D85 who made working in an office bearable.

Thank you to the British Council, The University of Cairo and the University of Warwick for funding my research project.

Table of contents

Abstract.....	i
Acknowledgements.....	iv
Table of Contents.....	v
Glossary.....	vi
1 Introduction	1
2 Synthesis and characterisation.....	35
3 Singlet Oxygen Generation.....	73
4 Bactericidal Experiments.....	98
5 Experimental.....	117
6 Conclusions and Future Work.....	140
Appendix.....	150

List of Abbreviations

A	Acceptor	DMF	Dimethylformamide
APTES	(3-Aminopropyl)triethoxysilane	DMSO	Dimethylsulfoxide
ATR	Attenuated total reflectance	EI	Electron ionisation
BODIPY	Distyryl boron dipyrromethane	EDC	1-Ethyl-3-(3-dimethylaminopropyl)carbodiimide
bpy	2,2'-bipyridyl	ESI MS	Electrospray Ionization Mass Spectrometry
bpy-sil	2,2'-bipyridyl-4,4'-dicarboxylic acid bis-[(3-triethoxysilylpropyl)amide]	$f_{1O_2}^T$	fraction of the molecular oxygen that quenches the excited state that produces singlet oxygen
bu	butyl	FTIR	Fourier transform infrared
cm	centimetre	g	gram
CDCl ₃	Deuterated chloroform	HOMO	Highest occupied molecular orbital
conc.	concentrated	Hz	Hertz
CS	Chromatography grad silica (40-60 mesh)	IR	Infrared
CuXD	[Cu(xantphos)(2,9-dimethyl-1,10-phenanthroline)]tfpb	IRA900	Amberlite IRA-900 macroporous anion exchange polymer
CuXD-CS	Cu(xantphos)(2,9-dimethyl-1,10-phenanthroline dry loaded onto chromatography silica (40-60 mesh)	J	Coupling constant
d	Doublet	$k_{TQ}^{O_2}$	sum of rates of quenching of the triplet state
dcbpy	2,2'-Bipyridine-4,4'-dicarboxylic acid	LED	Light Emitting Diode
DCM	Dichloromethane	LUMO	Lowest unoccupied molecular orbital
dd	Doublet of doublets	LLCT	Ligand-to-ligand charge transfer
dm	decimetre	LUMO	Lowest unoccupied molecular orbital
DCM	dichloromethane	m	multiplet

DMA	9,10-Dimethylanthracene	M	molar
MCM-41	Mobil Composition of Matter No. 41, Mesoporous Silica	PN	perinaphthenone
MeOH	Methanol	PS	Photosensitiser
MeCN	Acetonitrile	ROS	Reactive oxygen species
mg	milligram	RuBS	Ru(bpy) ₂ (bpy-silatrane)Cl ₂
mins	minutes	RuBS-CS	Ru(bpy) ₂ (bpy-silatrane)Cl ₂ covalently immobilised onto chromatography silica (40-60 mesh)
ml	millilitre	RuBPS	tetrasodium Ruthenium tris(bathophenanthroline disulfonate)
MNP	Magnetic nanoparticle	RuPS	[Ru(phen) ₂ (phen-silatrane)]Cl ₂
		rt	room temperature
mmol	millimole	s	Seconds
MLCT	Metal-to-ligand charge transfer	SBA-15	Santa Barbara Amorphous-15, Mesoporous silica
MLCT/LLCT	Mixed metal-ligand-to-ligand charge transfer	SiO ₂	Silica
MS	Mass spectrometry	SODIS	Method of water disinfection
nm/ns	nanometers/nanoseconds	SOSG	Singlet oxygen sensor green
NMR	Nuclear magnetic resonance	t	triplet
¹ O ₂	Singlet oxygen	tBu	tertiary butyl
OD	Optical density	tfpb	tetrakis[3,5-bis(trifluoromethyl)phenyl]borate
$P_T^{O_2}$	proportion of excited triplet state quenched by molecular oxygen	THF	Tetrahydrofuran
PDMS	Polydimethylsiloxane	TiO ₂	Titanium dioxide
phen	1,10-phenanthroline	TLC	Thin layer chromatography
PoU	Point-of-Use	UV-vis	Ultraviolet-visible

XPS	X-ray Photoelectron Spectroscopy
δ	Chemical shift
ϵ	Extinction coefficient
$\lambda/\lambda_{\text{abs}}/\lambda_{\text{em}}$	Wavelength(absorption/emission)
$\mu\text{m}/\mu\text{s}$	micrometer/microsecond
ν	Frequency
τ/τ_{em}	lifetime/emission lifetime
χ	Pauling's electronegativity
Φ_{em}	Emission quantum yield
Φ_{Δ}	Singlet oxygen quantum yield
$\tilde{\nu}$	Wavenumber
\AA	Angstrom, $10\text{E}-10\text{ m}$

1 Introduction

Contents

1	Introduction	1
1.1	Current Non-photosensitiser Water Disinfection Technologies.....	3
1.2	Photosensitisers.....	7
1.2.1	Photophysics of photosensitiser compounds and excitation of molecular oxygen	7
1.2.2	$^1\text{O}_2$ Generation kinetics and measuring $^1\text{O}_2$ production	10
1.2.3	Existing non-metal immobilised photodynamic antimicrobial compounds	12
1.2.4	Ruthenium Compounds	22
1.2.5	Copper Complexes	25
1.3	Conclusions	27
1.4	References	27

1.1 Current Non-photosensitiser Water Disinfection Technologies

Access to drinking water free from microbiological and chemical contaminants continues to prove itself an international issue to be overcome. Globally, roughly 2.4 million deaths annually are caused by lack of adequate sanitation methods and potable water.¹ A study from 2015 by the World Health Organisation found that 663 million people did not have access to clean drinking water and over 80% of these people live in rural areas.² Thorough sewage waste systems and water treatment are the most effective ways of reducing risk of drinking contaminated water and spreading disease. However, in rural areas these facilities are either sparse or non-existent, meaning more local, point-of-use (POU) methods are necessary for providing safe drinking water to households.

A solution utilising chemistry and materials sciences to create a piece of batch technology should be possible. It would ideally: be cheap, effectively removing all microbes and pollutants; be easy to use; have a simple and green method of preparation; be easy to transport; and would not require any form of costly infrastructure. As water cleaning requires a large amount of energy and many rural areas with little access to drinking water have an abundance of unharnessed solar energy, it follows that a water purification method utilising energy from sunlight could be used.

Various methods and technologies already employ the harvesting of energy from sunlight to produce clean drinking water. Some have been tested more thoroughly than others and many have not seen testing on-site. However, it is likely that in the following decade these technologies will see the light of day. The following examples are provided as a background for a study on photosensitisers. For a more in depth comparison of these methods see the review by Loeb *et al.*³

Solar Disinfection (SODIS) is a commonly used POU method of water disinfection recommended by the WHO. The method consists of exposing water sealed in glass or polyethylene terephthalate (PET) bottles to sunlight over an extended period of time ranging between 5-48 hrs.⁴ This method has seen some success in various developing countries, and countries in a state of emergency.⁴⁻⁷ When the temperature exceeds the pasteurization point (>70 °C) and is maintained for over 4 hours, the water can be considered safe to drink. UV-A also has germicidal effects in water as it is absorbed by dissolved organic matter to produce reactive oxygen species (ROS),⁸ including singlet oxygen, the hydroxyl radical, peroxides and superoxides, which are biocidal. While displaying bactericidal inactivation of up to 99.99%, it is generally unsuccessful at eliminating viruses from drinking water, achieving around 80% reductions.⁹



Figure 1 Picture of SODIS in use in Indonesia.

SODIS has a few clear advantages that lie in its simplicity: it is very easy to understand and use and it is cheap and sustainable – due to it only requiring sealable plastic bottles that can be reused. However, its simplicity is also the source of its disadvantages. As the water needs to be stored in bottles the disinfection can only occur on very small scales, a very large

sealable container would be required otherwise. It requires the untreated water to be relatively clear, with the presence of turbidity greatly increasing the necessary exposure time. As SODIS relies partly on the germicidal effects of UV-A in water this method only harvests a small proportion of sunlight with germicidal wavelengths constituting a small band in the region of 320-400 nm. Furthermore, SODIS requires a large amount of inactive PET and glass bottles as well as a large area exposed to the sun to leave them in.

Light emitting diode (LED) lamps used with Photovoltaic Solar cells can be used to produce Ultraviolet (UV) light in the UV-C region (100 – 280 nm). This represents a promising investment for POU water disinfection in rural areas. These hybrid systems depend on the germicidal nature of light in the UV-C region and are powered by current generated by photovoltaic cells, so can be used in remote areas far from conventional power sources. UV-C lamps would offer a robust and stable method of eliminating a broad range of microorganisms without the use of chemical consumables. Ibrahim *et al.* theorised that UV-C LEDs would be commercially viable within the next 10 years.¹⁰ Although LED's reach shorter wavelengths and higher efficiencies year-by-year, they are still far from reaching the full UV-C spectrum.¹¹ UV-C lamps are also marred by low quantum efficiency, high operating voltage and high production cost as well as UV-C posing an eye and skin hazard.¹²

Photocatalysts such as titanium dioxide (TiO₂) have been studied extensively as potential photodynamic antimicrobial compounds, and have been used in a variety of environmental applications.¹³⁻¹⁸ TiO₂ can convert UV light energy into a redox potential on its surface, by promoting electrons from the insulating to the conducting bands, and thereby acting as a semiconductor. Semiconductors with valence bandgaps in the UV to visible range can absorb photons with an energy greater than or equal to that bandgap to create a charge separated conduction band electron (e⁻) and a valence band hole (h⁺) across the bandgap, and

these generate bacteriocidal 'reactive oxygen species' (ROS). Valence band holes, which are 1-electron oxidising agents, can then react with water to produce the hydroxyl radical ($\bullet\text{OH}$); and the excited e^- (a 1-electron reducing agent) with oxygen in water to produce the superoxide anion (O_2^-). The hydroxyl radical is highly reactive and is thus germicidal.¹⁹ In addition the superoxide anion quickly reacts to form hydrogen peroxide (H_2O_2) a long-lived compound and known disinfectant. TiO_2 was also capable of reducing colonies of oocyst *C. parvum* 99% (\log_{10}).²⁰ Oocysts are another type of parasitic microbe present in dirty drinking water that can lead to disease, and while larger than bacteria and viruses (so they can thus be filtered out of solution), they are harder to kill through exposure to ROS. A recent study by Teng et al.²¹ showed promising results utilizing carbon nitride nanosheets as a photocatalyst for water disinfection: these displayed complete inactivation of bacterial cultures after 30 minutes of irradiation with white light. This photocatalyst was found to produce the superoxide radical in larger quantities than other forms of ROS. The superoxide reacts quickly with water to form hydrogen peroxide, which is far longer lived than other ROS.

Photocatalysts provide a promising method for water disinfection, however, they are marred by inefficiencies. For one, only the small proportion of the sun's light which is UV light (<380 nm) is generally harvested. However, research is being conducted to broaden titania's absorption spectrum into the visible region.²² Another drawback is that the hydroxyl radical is heavily quenched by natural organic matter in the water.¹³

Upconversion phosphors have been of particular interest due to their ability to convert lower energy photons into higher energy photons. They achieve this by sequential absorption of two photons by a single activator ion or two neighboring ions each absorb a photon and one then transfers its energy to the other.²³ These compounds take the form of crystalline powders or ceramics doped with lanthanide ions that are insoluble in water,

allowing a filterable and reusable product for treatment of water. In the case of water disinfection, upconverters capable of absorbing light in the visible region and emitting in the UV-C region have been developed.²³ These compounds, however, are still in very preliminary stages of development and only one has been tested on microorganisms. It currently suffers from very poor quantum efficiency.²⁴

1.2 Photosensitisers

Photosensitisers (PS) produce highly reactive singlet oxygen ($^1\text{O}_2$) by absorption of light and interacting with ground state oxygen ($^3\text{O}_2$). They are extremely desirable due to their high quantum yields (QY) and the strong biocidal action of singlet oxygen. A high quantum yield means that PS can very efficiently harvest incident solar energy and thus require the smallest energy input at POU. PSs are often employed for photodynamic therapy (PDT) to kill cancer cells in chemotherapy. However, they tend to be more complex and costly for this application as the drugs need to be suitable for use *in vivo* they have to operate within strict transparency windows and toxicity levels.²⁵ There are, however, numerous examples of far simpler and cheaper PS more suited for use in environmental applications.²⁶

1.2.1 Photophysics of photosensitiser compounds and excitation of molecular oxygen

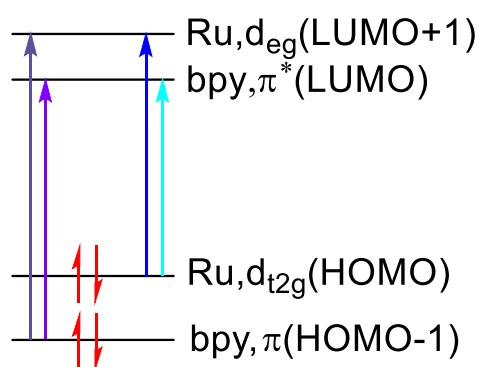


Figure 2 Frontier orbital diagram showing the various possible electronic transitions: **MLCT**, **d-d**, **$\pi-\pi^*$** , **LMCT**.

Transition metal-diimine complexes have rich excited state chemistry with numerous applications. No transition metal complex is more studied perhaps than ruthenium (II)

tris(bipyridine). In this complex the Ru^{2+} metal ion center is coordinated to three 2,2'-bipyridine ligands to form an (approximately) octahedral dicationic complex (more accurately a complex with D_3 symmetry) with d^6 electron configuration. A strong crystal field gives a low spin formation of full t_{2g} orbitals, which form the highest occupied molecular orbitals (HOMO). The large crystal field splitting also yields the empty ligand p -antibonding (π^*) orbitals as the lowest unoccupied molecular orbital (LUMO). Thus, the lowest energy excitation that can occur to the complex in the ground state is from the metal t_{2g} orbital into the ligand π^* orbital (Figure 2). This is a metal-to-ligand charge transfer (MLCT). The next in energy is from the metal center t_{2g} to e_g , called a $d-d$ transition or metal-centered (MC) transition. This is followed by the intraligand transition $\pi-\pi^*$ and then ligand-to-metal transfer (LMCT).

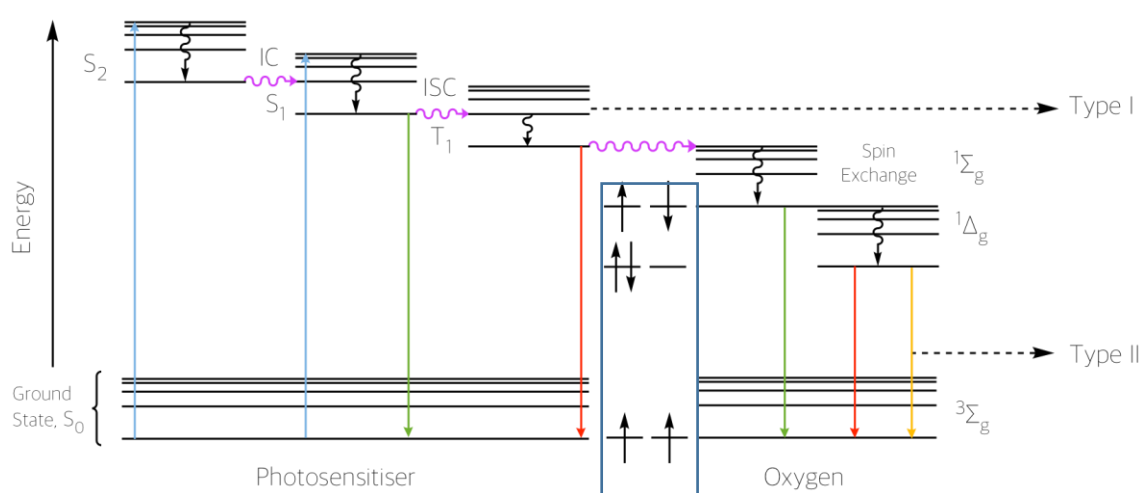


Figure 3: Jablonski diagram displaying the different modes of excitation and relaxation of a photosensitiser. Blue box contains molecular orbital diagram showing oxygen pi electrons.

The photophysics involved in production of singlet oxygen are displayed using a Jablonski diagram in Figure 3. Photosensitisers work by first absorbing the energy of a photon, thereby promoting it to an energetically excited singlet state (S_2 or S_1). If the molecule is in a higher excited state (S_2) it can then undergo vibrational relaxation, followed by an internal conversion to reach the lowest excited state S_1 . The molecule can return to its ground state by fluorescence, vibrational relaxation (green arrows) or undergo intersystem crossing (ISC),

effectively reversing the spin of the electron, bringing the complex to a triplet state (T_1). In metal coordination complexes this is the $^3\text{MLCT}$ state. In this triplet state the excited electron is no longer spin-paired with the electron as in the ground state, but is spin-opposed, meaning that the relaxation is spin-spin forbidden. This gives the triplet excited state a longer lifetime and accounts for the long-lasting glow in phosphorescence (red arrow). This PS can produce reactive oxygen species through two photoprocesses (Type I and Type II). The Type I pathway involves the PS triplet state undergoing electron-transfer interactions with substrates creating cytotoxic radical species.²⁷

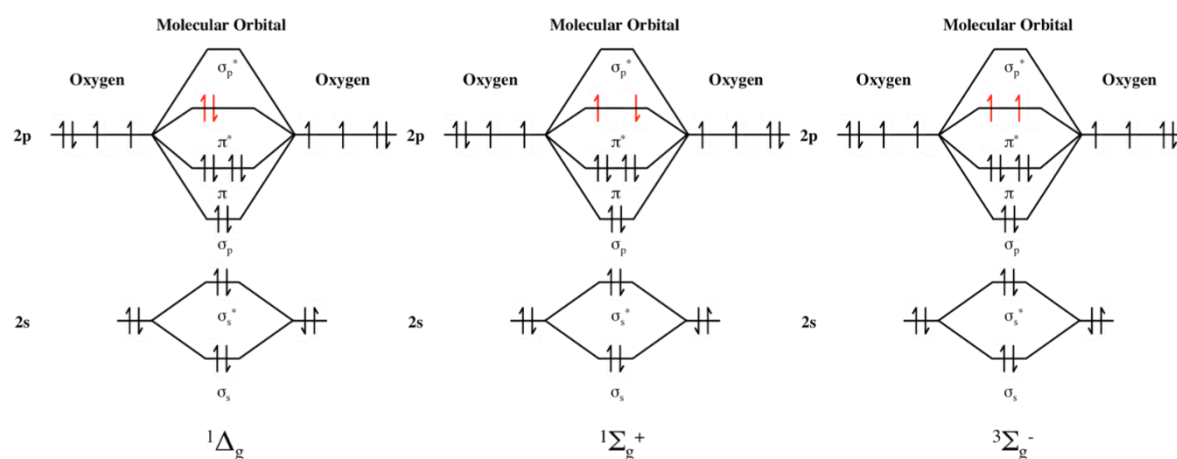


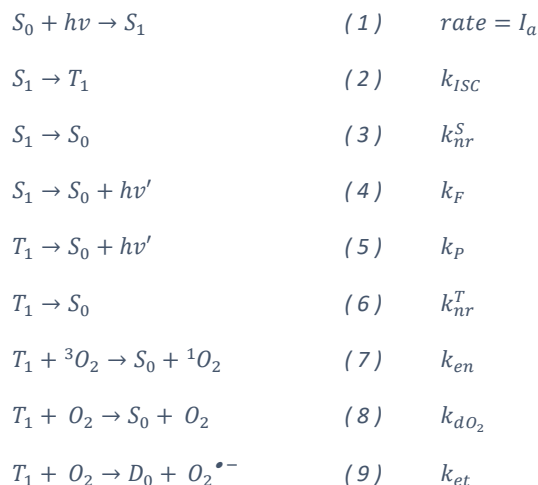
Figure 4 Molecular orbital diagrams showing the electronic structure of the different excited states of molecular oxygen.

In the Type II pathway, the PS has a direct energy-transfer interaction with molecular oxygen, which has a triplet ground state. The $^3\text{O}_2$ quenches the excited state PS and is itself excited to a singlet state, $^1\Sigma_g$ (Figure 4), which can then reach oxygen's lowest excited state ($^1\Delta_g$) through isoenergetic processes. In this diamagnetic state, interactions with many organic molecules (also in the singlet state) are allowed in terms of spin restriction, making it a potent oxidiser and electrophile. This low-energy excited state, generally termed 'singlet oxygen', is highly reactive and is capable of oxidising many biological molecules, leading to cytotoxicity.^{28,29}

1.2.2 $^1\text{O}_2$ Generation kinetics and measuring $^1\text{O}_2$ production

To quantify the amount of singlet oxygen produced by a photosensitising species the quantum yield of singlet oxygen production (Φ_{Δ}) can be used. There are a few ways in which this can be measured, for example: using a pulsed laser to measure singlet oxygen phosphorescence at 1270 nm; measuring thermal lensing in solution; and time dependent quencher disappearance.³⁰

Type I reactions which generate the O_2 excited state results in either abstraction of a hydrogen atom or electron transfer, yielding radicals or radical ions, competing with the quantum yield of singlet oxygen phosphorescence. Type II reactions leads to the production of singlet oxygen by energy transfer from the PS triplet state. To understand the quantum yield of a photosensitiser we must therefore consider the rates of some of the photoprocesses at play:



In these equations S_0 , S_1 and T_1 represent the photosensitiser in its ground state, first excited singlet state and first triplet excited state respectively. Equation 1 represents the absorption of a photon by the ground state PS and internal conversion/vibrational relaxation from higher lying ground states; its rate constant can be derived from the absorbance of the PS at a given wavelength. k_{ISC} is the rate of intersystem crossing from S_1

to T_1 (Equation 2). Deactivation of the excited states by molecular oxygen (k_{dO_2}) and electron transfer interactions (k_{et}) compete with energy transfer (k_{et}).

$$k_{TD} = k_{nr}^T + k_P \quad (10)$$

$$k_{TQ}^{O_2} = k_{en} + k_{dO_2} + k_{et} \quad (11)$$

The sum of the rates of quenching of T_1 by oxygen can be expressed as $k_{TQ}^{O_2}$ (Equation 11). And the sum of the rates of radiative and non-radiative emissions leading to the deactivation of T_1 can be expressed as k_{TD} (Equation 10). From these rates we can find the proportion of T_1 quenched by oxygen, $P_T^{O_2}$ (Equation 12) and the fraction of T_1 quenched by oxygen to give singlet oxygen, $f_{^1O_2}^T$ (Equation 13).

$$P_T^{O_2} = \frac{k_{TQ}^{O_2}[O_2]}{k_{TD} + k_{TQ}^{O_2}[O_2]} \quad (12)$$

$$f_{^1O_2}^T = \frac{k_{en}}{k_{TQ}^{O_2}} \quad (13)$$

The quantum yield of singlet oxygen produced can therefore be written as the sum of the contributions from the two excited states. (NB: Only a small amount of singlet oxygen will be produced by interactions with S_1 as the quantum yield for triplet-state formation in transition metal complexes is usually near unity. For simplicity's sake, its calculation is not included in the calculations. However, its contribution will be noted as $\Phi_\Delta(S)$ (Equation 14).

$$\Phi_\Delta = \Phi_\Delta(S) + \Phi_\Delta(T) \quad (14)$$

$$\Phi_\Delta(T) = \Phi_T^{O_2} \phi_{en} = \Phi_T^{O_2} P_T^{O_2} f_{^1O_2}^T \quad (15)$$

Or, it can be written in terms of rate constants and oxygen concentration:

$$\Phi_\Delta(T) = \Phi_T^{O_2} \frac{k_{en}[O_2]}{k_{TD} + k_{TQ}^{O_2}[O_2]} \quad (16)$$

Where $\Phi_T^{O_2}$ is the quantum yield of triplet formation. The population of this excited state has two contributors: intersystem crossing and the quenching of S_1 by oxygen to give T_1 .

1.2.3 Existing non-metal immobilised photodynamic antimicrobial compounds

Numerous 1O_2 PS compounds, dyes with extended triplet-state lifetimes, have been developed and investigated for their photodynamic inactivation of bacteria: Rose Bengal, phenathiazinium compounds (such as methylene blue), anthraquinones, metal-organic frameworks (MOFs), porphyrins, phthalocyanins, ruthenium polypyridyl complexes and BODIPYs.³¹⁻³⁵

When producing a new 1O_2 photosensitising material there are numerous considerations: Economic viability of active compound and support; photo/chemical stability of the compound as well as mechanical durability (little to no leaching of active material from the support for example); strong absorption in the visible in order to effectively utilize sunlight; good triplet quantum yield, rate of ISC and singlet oxygen quantum yield; and a low rate constant of singlet oxygen quenching.

In solution PSs are often very effective, by virtue of being able to be absorbed by bacteria and thus aggregate on the inside, drawing itself nearer to vital parts of the cell. However, they do not need to be free in solution to function as effective antimicrobials, as singlet oxygen can be effective acting from outside of the cell as well.^{36,37} In addition, due to their frequently high production costs, recovery of the PSs is highly desirable. Thus, a large proportion of research in the area is coupled with effective immobilisation of photosensitisers. Immobilisation does have its setbacks: the quantum yield for 1O_2 generation of immobilised photosensitisers is generally smaller than for the free species, likely due to limitations by the diffusion of oxygen to the surface of the material.³⁸ However the

advantages of immobilization onto support media are clear; recovery and reuse of the species but also easy separation from medium being cleaned, which is vital in water purification.

Bacteria can be divided into two categories: Gram positive (+) and Gram negative (-). The distinction between these two types is that Gram(+) bacteria lack the additional outer plasma membrane that Gram(-) bacteria have, making them less resistant to antibiotics. Both Gram(+) and Gram(-) bacteria are generally deactivated by exposure to singlet oxygen. However, Gram(+) bacteria seem to be more susceptible to photosensitisers due to their cell wall lacking the outer plasma membrane (this is expanded in Chapter 4). The additional thick, negatively charged outer membrane on Gram(-) bacteria attracts cationic species. It is therefore beneficial for the photosensitising compound to have a net positive charge as it will allow the photosensitiser to aggregate at the bacterium or *vice versa*.

Rose Bengal

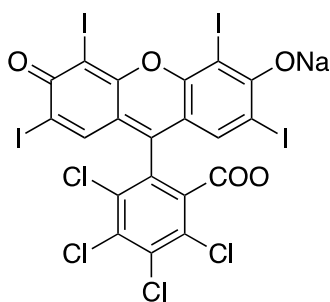


Figure 5 Rose Bengal

Rose Bengal (Fig. 5) is a well-known dye and effective photosensitiser due to a strong absorption band in the visible region (550 nm – 700 nm), a high quantum yield for $^1\text{O}_2$ generation ($\Phi_{\Delta} = 0.76$),²⁸ and a very high antimicrobial activity against Gram(+) bacteria in solution.^{32,39} The compound also has antimicrobial properties not related to its photosensitising abilities. It has been incorporated into polymeric chitosan and cellulose acetate,^{40–44} and has been immobilised on various synthetic polymers.^{45–47} A study by

Nakonechny et al. even saw Rose Bengal, supported on silicon, successfully reducing colonies of *S. aureus* under irradiation with radio waves.⁴⁸

Rose Bengal has been immobilised onto silica nanoparticles by Zhang *et al.* with surprising results: although the immobilised photosensitiser has a lower quantum yield for singlet oxygen generation than when free in solution, its antibacterial activity increases, deactivating more bacteria by two orders of magnitude.⁴⁶ This is likely due to the increased surface area making access to molecular oxygen by the PS easier, increasing cell damage. Rose Bengal has an extensive literature of antibacterial activity in solution and on supported media. While Rose Bengal has many excellent properties, it is held back by its lastingness, in that it undergoes photobleaching by reacting with the singlet oxygen such that it is permanently unable to fluoresce or produce singlet oxygen.

Phenothiazinium compounds

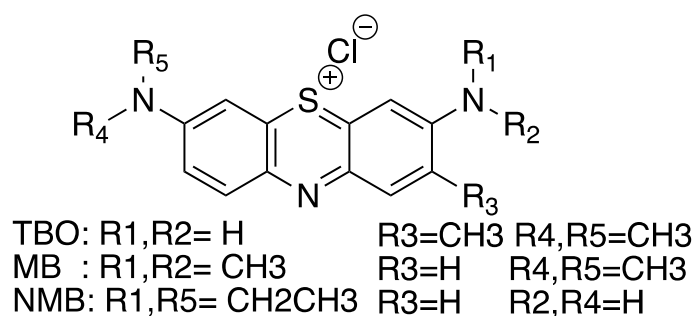


Figure 6: Phenothiazinium compounds

Methylene Blue (MB), New Methylene Blue (NMB) and Toluidine Blue O (TBO) (Fig. 6) are amongst the cationic aromatic photosensitisers that together constitute the phenothiazinium compounds. Due to their overall positive charge, they are effective antibiotics against both Gram(+) and (-) bacteria,^{34,49,50} and have been found to be effective against a number of antibiotic-resistant strains of bacteria in solution.^{34,51} Phenothiazinium

compounds have strong absorbance in 550 nm – 700 nm and a reasonable quantum yield ($\Phi_{\Delta} = 0.52$).²⁸ Phenothiazinium compounds have been incorporated in polymers such as silicone, polyurethane, polyethylene and cellulose acetate mainly for use in antimicrobial surfaces and materials in hospitals.⁵²⁻⁵⁷

The dyes have been encapsulated into medical grade polymers along with nanogold through a “swell-encapsulate-shrink” method. These polymers showed strong antimicrobial activity when exposed to white light for 24 hrs and for 1-10 minutes when exposed to a low-power 660 nm laser.^{52,58,59}

A cheap and easy method of immobilising dyes on a polyethylene film by spreading a mixture of Rose Bengal, MB, TBO and poly(vinylidene fluoride) nanobeads onto its surface using a heat press (95 °C, 1 hr) was developed by Cahan et al. This material showed bacterial inactivation of Gram(+) and (-) strains. However, Gram(+) bacteria were far more sensitive to this method of inactivation.⁶⁰

Piccirillo *et al.* reported covalently bonding TBO to the surface of an activated silicone polymer. This material had very strong bactericidal properties, rendering 99.999% of *E. coli* and *S. epidermis* inviable after only 4 minutes exposure from a low-power laser. This is despite the fact that very low levels of dye were actually bound to the silicone and is likely due to the PS being bound in the best possible position (at the surface) to be as close as possible to the bacteria.⁵⁶ TBO immobilised on silica nanoparticles exhibited antimicrobial activity towards *S. epidermis* and *E. coli*. Using a low-power laser at 630 nm the bacteria populations showed a 99% reduction after only 2 (*S. epidermis*) and 3 (*E. coli*) minutes of irradiation.⁶¹

Porphyrins

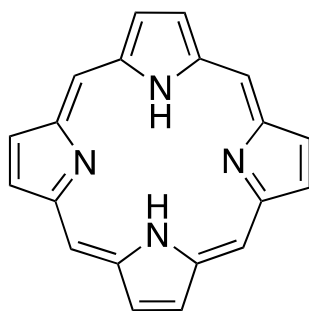


Figure 7: Porphyrin general structure

Porphyrin compounds (Fig. 7) have very high quantum yields for singlet oxygen production in specific solvents (Φ_{Δ} up to 0.95); however due to their relatively narrow absorption bands they do not exploit the full solar emission spectrum.⁶² Porphyrins are present in natural systems, indicating that they do not have cytotoxicity in the absence of light. This makes them ideal candidates for *in vivo* and environmental applications. The ability to coordinate metal ions to porphyrins in the centre of the ring allows further additions of ligands for fine-tuning or for immobilisation onto support media. Free porphyrins tend to have better QYs for singlet oxygen generation than do phthalocyanins and porphycenes, as they do not dimerise in solution which leads to self-quenching of the triplet state.⁶²

Porphyrins have been successfully incorporated into a wide variety of natural polymers including chitosan⁶³, cellulose⁶⁴ and dextran⁶⁵. These make environmentally friendly materials with great potential in household, medical and industrial applications. There have been multiple reports of creating effective antimicrobial agents through the binding of porphyrins to cotton (cellulose), which constitutes a promising support through sheer availability and sustainability.⁶⁴ Nanocrystalline cellulose (NCC) also offers many benefits as a support, including a large surface area; high mechanical strength; availability and biodegradability. Porphyrin PSs bound to NCC have been successfully used to effectively reduce bacterial growth in many strains of Gram(+) and (-) bacteria.^{66,67}

Synthetic polymer conjugates also provide an eco-friendly and efficient way of immobilisation of substrates on solid supports. A considerable amount of research has been done on incorporating porphyrins into polymers, some resulting in cheap and robust materials which are easily recovered. Giulio Jori *et al.* reported the synthesis of a poly-*S*-lysine conjugate that eliminated numerous strains of antibiotic-resistant Gram(+) and (-) bacteria. The added conjugation from the polymer also significantly improved the activity of the PSs.⁶⁸

A bridged polysilsesquioxane doped with 5-(4-carboxyphenyl)-10,15,20-tris(4-methylphenyl)porphyrin was synthesized to make a mechanically stable film that was moldable. Under exposure to light the material exhibited good antifungal effects on *C. Albicans*.⁶⁹

Porphyrin-conjugated carbon nanotubes (NT-P) have been successfully synthesized to yield a chemically and mechanically stable material capable of killing *S. aureus* in water, which also shows antimicrobial action as a flexible macroscopic film. As a powder in water it is easily separated and reusable (it was still found to be effective after the 5th use), making it economically and environmentally friendly option for water purification.⁷⁰⁻⁷²

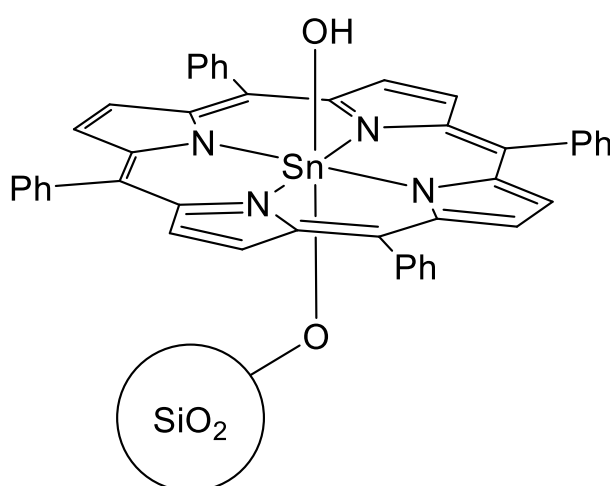


Figure 8: $[Sn(TPP)(OH)]-O-(SiO_2)$ axially coordinated to silica (TPP = tetraphenylporphyrin)

Coordination to the porphyrin through the axial coordination site holds promising possibilities through ease of binding to silica. Silica nanoparticles present a cheap and practical support medium. Porphyrins supported on silica have shown low levels of photobleaching and high activity against Gram(+) and (-) bacteria.⁷³ This conjugate was also easily filtered from its aqueous suspension and showed high reusability. Tin- and antimony- based, silica-bound metalloporphyrins have both been successfully produced. This tin metalloporphyrin (Fig. 6) was found to effectively produce singlet oxygen, however its photobactericidal activity has not been investigated.^{74,75} The antimony analogue has been found to effectively inactivate *E. coli* and *Legionella pneumophila*.^{76,77}

Silica coated magnetic nanoparticles for the attachment of porphyrins have gained a lot of interest because of their easy separation and purification from suspension utilizing a magnetic field.⁷⁸ This clever modification could find significant use in water disinfection. Recent research has produced a photostable product with high bacterial inactivation which retains its bactericidal activity after 6 uses.⁷⁸

Porphyrin-based conjugated microporous polymers (CMPs) are novel, non-toxic materials with good photosensitizing ability and high stability. They consist of a 3-dimensional framework of covalently bonded conjugate networks that allow fine tuning of porphyrin unit positions. Their good photo- and chemical stability, with a high singlet oxygen production quantum yield and reusable nature, makes them promising candidates for use in antimicrobial surfaces and water disinfection agents. More research needs to be done with respect to their antimicrobial strength.⁷⁹

Metalloporphyrins can also be incorporated into metal-organic frameworks (MOFs). MOFs are microporous (pore sizes <2 nm) which would allow fast diffusion of water through them. This would mean very high surface area and large number of active sites for singlet

oxygen production. Zhang *et al.* studied the photosensitizing ability of a zirconium-metalloporphyrin MOF and found it to be a possible photosensitiser with low water solubility and cheap starting materials, making it of interest in the disinfection of drinking and waste water.⁸⁰

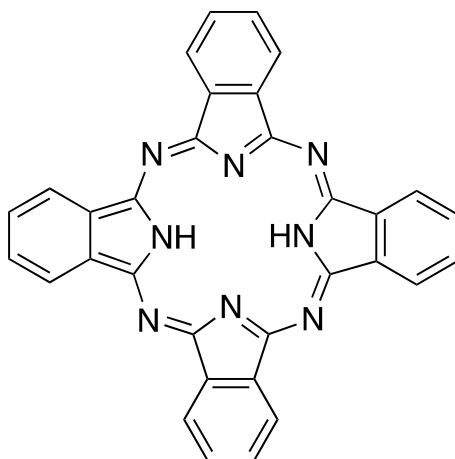


Figure 9 Phthalocyanin general structure

Phthalocyanins (Fig. 9) are macrocyclic molecules similar to porphyrins in structure and conjugation. Like porphyrins, they are amenable to immobilisation on surfaces, and good quantum yields are observed on-support.⁸¹ Phthalocyanins have found success in being spun into polystyrene polymer nanofibers to produce recyclable photo- and chemically stable materials.⁸¹⁻⁸³

Other Photosensitisers

In the past few years fullerenes have come under the spotlight as potentially potent PSs. Their strong absorption in the UV and throughout the visible regions, along with excellent singlet oxygen photogeneration and low water solubility, make them very promising heterogeneous antimicrobial materials.⁸⁴⁻⁸⁶

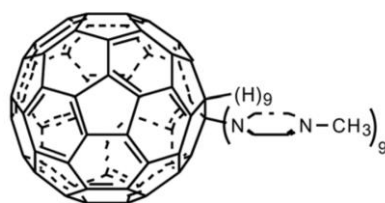


Figure 10: 1-(4-Methyl)-piperazinyll fullerene (MPF) used by Manjon *et al.* reproduced from from ref. [81] with permission from the Royal Society of Chemistry

Manjon *et al.* tested the photodynamic disinfecting ability of a silica-supported $[C_{60}]$ – fullerene (Fig. 10) in water against a similarly-supported Ru(II) polypyridyl complex. Although the fullerene saw excellent loading rate and singlet oxygen lifetime, it showed surprisingly poor bacterial deactivation. Due to the hydrophobic nature of 1-(4-Methyl)-piperazinyll fullerene (MPF), a limited amount of the PS can be loaded onto the anionic porous silica, failing to neutralise a negative net surface charge.⁸⁷

Another recent study by the Moor group focused on the immobilisation of C_{60} -fullerene onto silica particles through covalent attachment (Fig. 11). A simple synthetic method produced a material with good inactivation of bacteriophage MS2 which did not suffer from significant leaching or photobleaching. Although this is a promising result, further research has to be carried out on its bacterial deactivation properties.⁸⁸

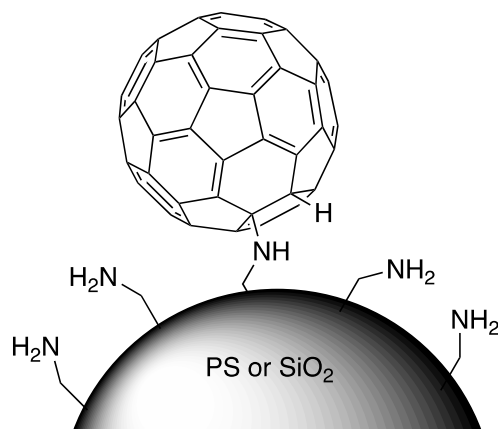


Figure 11: C_{60} -fullerene covalently bound to silica or porous silica

Porphyrin-fullerene C₆₀ dyads provide a unique approach to photosensitiser immobilisation. The dyad contains three carbazoyl groups covalently attached to tetrapyrrolic macrocycle porphyrins (Fig. 12). The porphyrin units act as a light-harvesting array, with the carbazoyl groups acting as antennae, transmitting energy to the fullerene units. This interesting method of coupling increases the lifetime of the charge separated state, giving a higher yield of singlet oxygen.^{89–91}

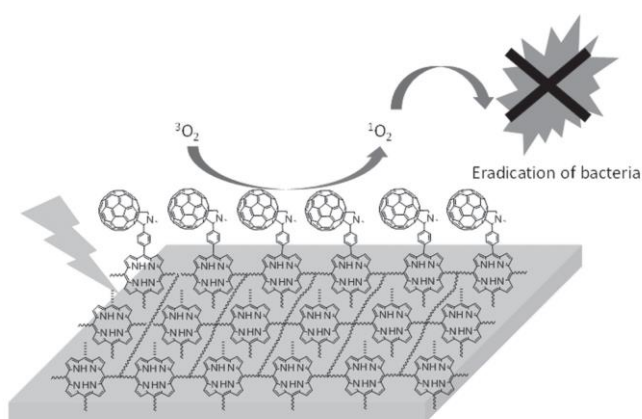


Figure 12: Porphyrin-fullerene thin film developed by Duratini et al. reproduced from ref [88]

This biofilm effectively eliminated 99.99% of *S. aureus* after 30 minutes and *E. coli* after an hour in cell suspensions. This material shows overall promise with good absorbance across the solar spectrum, excellent bactericidal activity and sees little effect from scavenging natural organic materials in water. The cost of the materials makes this currently unviable however, and more tests have to be done on the films' performance with wastewaters.

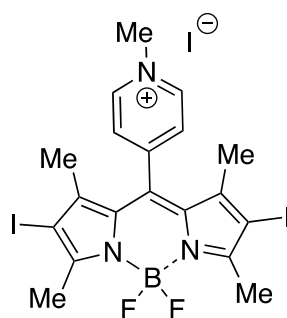


Figure 13: DIMPy-BODIPY photosensitiser

Distyryl boron dipyrromethane (BODIPY) compounds are strongly luminescing dyes, widely used for bio-imaging. They have more recently been found to be effective photosensitisers and have been tested as PDT drugs.⁹² A cationic BODIPY free in solution (Fig. 13) has been shown to cause 6-log deactivation (99.9999% reduction) of *S. xylosus* and *E. coli* after just 5 minutes of illumination under green light.⁹³ Another study by the Ghiladi group showed that the same compound was extremely effective in killing bacteria, viruses and fungi in solution even at low concentrations utilising light in the visible range (400-700 nm).⁹⁴

BODIPY dyes do tend to aggregate in solution giving lower efficiencies.⁹² This problem could be solved by immobilisation on solid supports. Recent research by the Parkin group has produced a novel PDMS material with two BODIPY complexes covalently bound to the surface.⁹⁵ The materials were produced for use on medical surfaces and a bromo-analogue BODIPY on the surface of PDMS saw a 99.9% reduction of bacteria after 5 hrs under hospital light. The method for attachment by Brook et al. allows for monolayer coverage of PDMS by the PS, meaning less of the costly materials are wasted.⁹⁶

1.2.4 Ruthenium Compounds

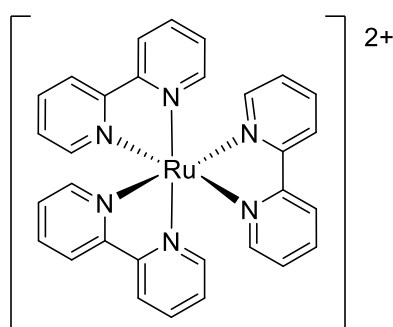


Figure 14: Ruthenium tris-bipyridyl ion.

Ruthenium polypyridyl complexes provide a great foundation for versatile photosensitisers in antimicrobial applications. Ligands can be easily added to the ruthenium ion to tune its properties whilst being strong enough to retain shape and form stable, robust

compounds which are less likely to photodegrade compared to organic dyes.⁹⁷ The ability to select the coordinating ligand also opens an opportunity to immobilise the photosensitiser on a wide variety of supports.

Excitation of Ru(II) polypyridyl complexes in the 180 – 500 nm region followed by fast intersystem crossing from the initially-generated ¹MLCT state leads to the formation of the metal-to-ligand charge transfer triplet excited state (³MLCT). Fast ISC means quantum yields for triplet production are of near unity in ruthenium(II) complexes and long ³MLCT lifetime gives excellent quantum yields of oxygen production (See figure 3 where S₀ is the ground state Ru, S₁ is ¹MLCT state and T₁ is the ³MLCT excited state.).^{98,99}

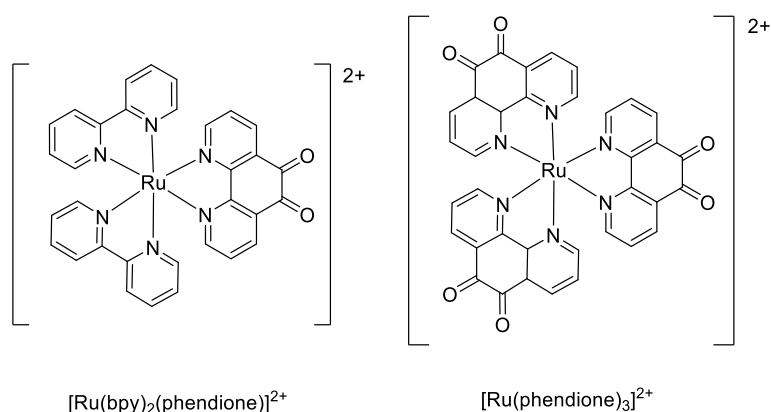


Figure 15 Bactericidal photosensitisers utilized by Prakash *et al.* ref [100].

Prakash *et al.* tested the bactericidal activity of the two complexes $[\text{Ru}(\text{bpy})_2(\text{phendione})](\text{PF}_6)_2 \cdot 2\text{H}_2\text{O}$ and $[\text{Ru}(\text{phendione})_3]\text{Cl}_2 \cdot 2\text{H}_2\text{O}$ (Fig. 15). They were found to effectively deactivate *B. subtilis*, *S. aureus*, *E. coli*, *P. aeruginosa* (in order of sensitivity). These compounds were then successfully adsorbed onto activated carbon as a means of removal from solution. This seems a promising method of disinfecting water followed by removal of PS. However, the compounds could not be desorbed from the carbon, and the effectiveness of the carbon with the PS adsorbed was not tested, meaning the PS material may be effectively lost.¹⁰⁰

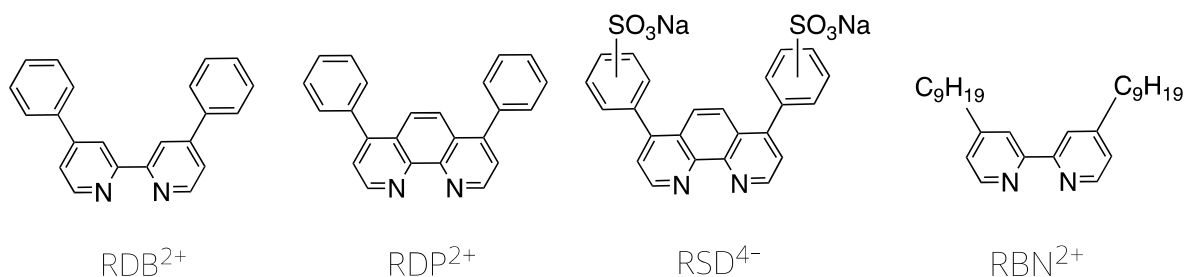


Figure 16: Ligands (L) used by Orellana et al. to make [RuL₃] complexes as silica-immobilised ruthenium photosensitisers. The labels refer to the [RuL₃] complex where the ligand shown is L.

Orellana *et al.* successfully immobilised two Ru(II) polypyridyl PSs (RSP²⁺ and RSD⁴⁻) in hydrophilic cationic polymers or on hydrophobic porous silicone. Silicone rubber has high oxygen permeability, high photogenerated singlet oxygen lifetime,¹⁰¹ is optically translucent, mechanically- and photo-stable, chemically inert and commercially available. As such, it looks to be an excellent prospect for the immobilisation of PSs. RDP²⁺ showed no leaching from its support and good singlet oxygen production. RSD⁴⁻ immobilised in hydrophilic cationic polymers showed poor singlet oxygen production and high PS leaching, likely due to singlet oxygen interaction with hydroxyl groups in the polymer.^{57,102,103}

RDP²⁺ and RDB²⁺ ruthenium compounds were loaded onto porous silicone and tested for waterborne *E. faecalis* inactivation using a solar simulator and a compound parabolic collector (CPC) solar photo reactor. It was found that bacterial inactivation was 4 times as efficient when using reloaded material compared to the original. This is likely due to the aggregation of silicone supported PS at the surface of the polymer.⁵⁷ The CPC reactor has an effective disinfection time (giving less than 10% of viable *E. faecalis* and *E. coli*) of 5 h, which is an improvement over SODIS, which requires over twice the solar dose for similar operating times.^{5,103} Overall this shows great promise as a method for production of potable water in rural areas. However, there are a few issues associated with the reactor. Photobleaching is always an issue – as with any PS – as it reduces the efficiency and durability of the system.

Although attaching the PS to a support can help, it is not a definitive solution to the problem. In the CPC system there is an operational time of roughly 6 months before RDP²⁺/pSiI needs to be reloaded into the system. Although the reloading cost has an estimated price of \$20 USD, the cumulative price for many reactors may be high. In addition to this the CPC array consists of numerous large mirrors, this would require setting up by a technician and might involve high maintenance costs.

1.2.5 Copper Complexes

In an effort to phase out expensive, less abundant transition-metal photosensitisers and catalysts, Copper (I) complexes have drawn considerable attention in recent years.^{104–106} Copper is a group 11 transition metal with three common oxidation states: 0, +1 and +2. Cu(0) is $d^{10}4s^1$, Cu(I) is d^{10} and Cu(II) is d^9 . Cu(II) complexes prefer a square planar or square pyramidal geometry. Cu(I) complexes on the other hand prefer tetrahedral complex geometry and upon MLCT excitation the metal centre in these complexes is formally oxidised to Cu(II), resulting in a transient change in geometry in the excited state which may lead to irreversible photo-decomposition, often generating Cu(II) products. By choosing the correct ligands these Cu(I) complexes can be rendered highly stable; for example use of sterically hindering diimine ligands, with bulky substituents at the positions adjacent to the coordinating N atoms, can form a complex that does not undergo oxidative decomposition following excitation but relaxes back to the Cu(I) ground state (Fig. 17).¹⁰⁷ These ligands successfully limit oxidative decomposition. However, the flattening distortion of the complex is a severe enough distortion to kill the MLCT excited state or can cause the complex undergo exciplex formation.¹⁰⁸ By preventing the flattening process the MLCT excited state lifetime is extended, enhancing its luminescent properties but also increasing its oxygen encounter probability which increases singlet oxygen generation.

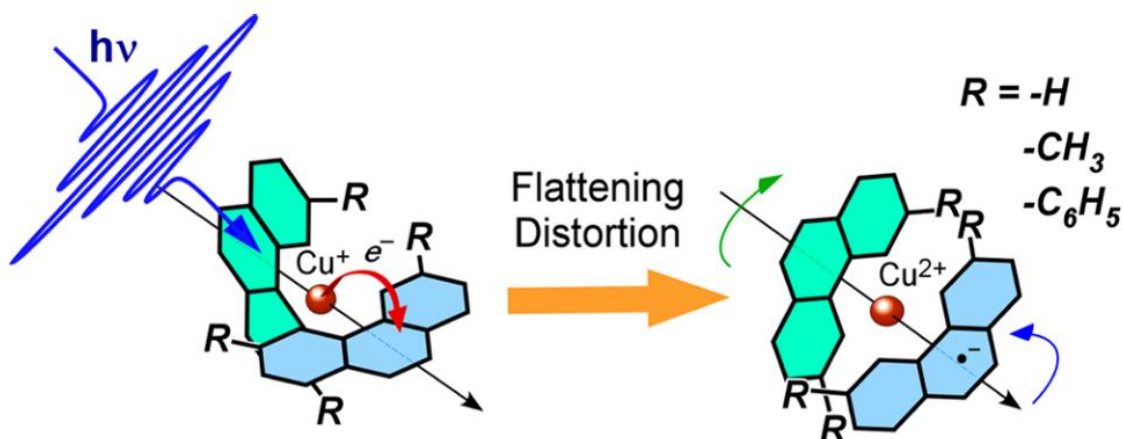


Figure 17 Photoexcitation and subsequent structural distortion of Cu(I) bis-diimine complexes. From reference [95].

Ligands with even greater steric bulk can therefore further stabilise the $^3\text{MLCT}$ state of Cu(I) complexes. Notably, Cu(I) diphenylphosphino-diimine heteroleptic complexes (Fig. 18) with long-lived ($>1 \mu\text{s}$ under nitrogen) $^3\text{MLCT}$ excited states have been reported.^{105,109} Smith et al. found that oxygen could quench the $^3\text{MLCT}$ excited state of solid-state $[\text{Cu}(\text{xantphos})(\text{dmp})]\text{tfpb}$ (from $38.5 \mu\text{s}$ under nitrogen to $5 \mu\text{s}$ in air);¹¹⁰ however the singlet oxygen producing abilities of this complex were not explored.

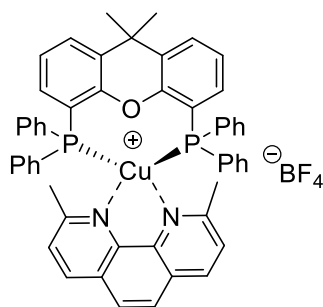


Figure 18 $\text{Cu}(\text{xantphos})(\text{dmp})$ complex by Smith et al.

The main disadvantage of current $\text{Cu}(\text{PP})(\text{NN})^+$ complexes is their poor absorbance in the visible spectrum, with $^3\text{MLCT}$ absorptions normally lying in the 380-400 nm range. Red-shifting the $^3\text{MLCT}$ absorption band further into the visible region has thus become a key area of research in order to allow these photocatalysts to harvest sunlight.¹⁰⁵

1.3 Conclusions

Throughout this work, we will examine the singlet-oxygen generating and antimicrobial photoactivity of numerous synthesised Ruthenium polypyridyl and Cu(PP)(NN)⁺ complexes, along with photophysical characterisation of the complexes by absorption spectroscopy, time-resolved and steady-state fluorescence measurements, in order to produce a cheap and efficient photodynamic antimicrobial material. Numerous Cu(I) complexes have also been synthesised in an attempt to produce a complex with broad absorption in the visible light region.

1.4 References

1. Prüss-Üstün, A., Bos, R., Gore, F. & Bartram, J. Safer water, better health. *World Heal. Organ.* 53 (2008). doi:ISBN 9789241596435
2. WHO/UNICEF. 2015 Update and MDG Assessment. *World Heal. Organ.* 90 (2015). doi:10.1007/s13398-014-0173-7.2
3. Loeb, S., Hofmann, R. & Kim, J. H. Beyond the Pipeline: Assessing the Efficiency Limits of Advanced Technologies for Solar Water Disinfection. *Environmental Science and Technology Letters* **3**, 73–80 (2016).
4. Oates, P. M., Shanahan, P. & Polz, M. F. Solar disinfection (SODIS): Simulation of solar radiation for global assessment and application for point-of-use water treatment in Haiti. *Water Res.* **37**, 47–54 (2003).
5. McGuigan, K. G. *et al.* Solar water disinfection (SODIS): A review from bench-top to roof-top. *J. Hazard. Mater.* **235–236**, 29–46 (2012).
6. Hunter, P. R. Household water treatment in developing countries: Comparing different intervention types using meta-regression. *Environ. Sci. Technol.* **43**, 8991–8997 (2009).
7. Du Preez, M., McGuigan, K. G. & Conroy, R. M. Solar disinfection of drinking water in the prevention of dysentery in South African children aged under 5 years: The role of participant motivation. *Environ. Sci. Technol.* **44**, 8744–8749 (2010).
8. Meierhofer, R. & Wegelin, M. *Solar Water Disinfection: A Guide for Applications of SODIS. SANDEC (Water & Sanitation in Developing Countries) at EAWAG (Swiss Federal Institute for Environmental Science and Technology)* (2002).
9. Polo, D., García-Fernández, I., Fernández-Ibáñez, P. & Romalde, J. L. Solar water disinfection (SODIS): Impact on hepatitis A virus and on a human norovirus surrogate under natural solar

- conditions. *Int. Microbiol.* **18**, 41–49 (2015).
10. Ibrahim, M. a S., MacAdam, J., Autin, O. & Jefferson, B. Evaluating the impact of LED bulb development on the economic viability of ultraviolet technology for disinfection. *Environ. Technol.* **35**, 400–6 (2014).
 11. Lui, G. Y. *et al.* Photovoltaic powered ultraviolet and visible light-emitting diodes for sustainable point-of-use disinfection of drinking waters. *Sci. Total Environ.* **493**, 185–196 (2014).
 12. Lui, G. Y., Roser, D., Corkish, R., Ashbolt, N. J. & Stuetz, R. Point-of-use water disinfection using ultraviolet and visible light-emitting diodes. *Sci. Total Environ.* **553**, 626–635 (2016).
 13. Murray, C., Goslan, E. & Parsons, S. TiO₂/UV: Single stage drinking water treatment for NOM removal? *J. Environ. Eng. Sci.* **6**, 311–317 (2007).
 14. Gelover, S., Gómez, L. A., Reyes, K. & Teresa Leal, M. A practical demonstration of water disinfection using TiO₂ films and sunlight. *Water Res.* **40**, 3274–3280 (2006).
 15. Salthammer, T. & Fuhrmann, F. Photocatalytic surface reactions on indoor wall paint. *Environ. Sci. Technol.* **41**, 6573–6578 (2007).
 16. Youssef, Z. *et al.* Titania and silica nanoparticles coupled to Chlorin e6 for anti-cancer photodynamic therapy. *Photodiagnosis Photodyn. Ther.* **22**, 115–126 (2018).
 17. Rokicka-Konieczna, P., Wanag, A., Sienkiewicz, A., Kusiak-Nejman, E. & Morawski, A. W. Antibacterial effect of TiO₂ nanoparticles modified with APTES. *Catal. Commun.* **134**, 0–3 (2020).
 18. Vatansever, F. *et al.* Antimicrobial strategies centered around reactive oxygen species - bactericidal antibiotics, photodynamic therapy, and beyond. *FEMS Microbiol. Rev.* **37**, 955–989 (2013).
 19. Cho, M., Chung, H., Choi, W. & Yoon, J. Linear correlation between inactivation of E. coli and OH radical concentration in TiO₂ photocatalytic disinfection. *Water Res.* **38**, 1069–1077 (2004).
 20. Ryu, H., Gerrity, D., Crittenden, J. C. & Abbaszadegan, M. Photocatalytic inactivation of *Cryptosporidium parvum* with TiO₂ and low-pressure ultraviolet irradiation. *Water Res.* **42**, 1523–1530 (2008).
 21. Teng, Z. *et al.* Edge-Functionalized g-C₃N₄ Nanosheets as a Highly Efficient Metal-free Photocatalyst for Safe Drinking Water. *Chem* **5**, 664–680 (2019).
 22. Etacheri, V., Di Valentin, C., Schneider, J., Bahnemann, D. & Pillai, S. C. Visible-light activation of TiO₂ photocatalysts: Advances in theory and experiments. *J. Photochem. Photobiol. C Photochem. Rev.* **25**, 1–29 (2015).
 23. Cates, S. L., Cates, E. L., Cho, M. & Kim, J. H. Synthesis and characterization of visible-to-UVC upconversion antimicrobial ceramics. *Environ. Sci. Technol.* **48**, 2290–2297 (2014).
 24. Cates, E. L. & Kim, J. H. Bench-scale evaluation of water disinfection by visible-to-UVC upconversion under high-intensity irradiation. *J. Photochem. Photobiol. B Biol.* **153**, 405–411 (2015).
 25. Huang, Z. A review of progress in clinical photodynamic therapy. *Technol. Cancer Res. Treat.* **4**, 283–93 (2005).

26. Spagnul, C., Turner, L. C. & Boyle, R. W. Immobilized photosensitizers for antimicrobial applications. *J. Photochem. Photobiol. B Biol.* **150**, 11–30 (2015).
27. Athar, M., Mukhtar, H. & Bickers, D. R. Differential role of reactive oxygen intermediates in photofrin-I- and photofrin-II-mediated photoenhancement of lipid peroxidation in epidermal microsomal membranes. *The Journal of investigative dermatology* **90**, 652–657 (1988).
28. Redmond, R. W. & Gamlin, J. N. A compilation of singlet oxygen yields from biologically relevant molecules. *Photochem. Photobiol.* **70**, 391–475 (1999).
29. Redmond, R. W. & Kochevar, I. E. Spatially Resolved Cellular Responses to Singlet Oxygen. *Photochem. Photobiol.* **82**, 1178–1186 (2006).
30. Wilkinson, F., Helman, W. P. & Ross, A. B. Rate Constants for the Decay and Reactions of the Lowest Electronically Excited Singlet State of Molecular Oxygen in Solution . An Expanded and Revised Compilation . 1–17 (1993).
31. Wainwright, M. Non-porphyrin photosensitizers in biomedicine. *Chemical Society Reviews* **25**, 351 (1996).
32. Jemli, M., Alouini, Z., Sabbahi, S. & Gueddari, M. Destruction of fecal bacteria in wastewater by three photosensitizers. *J. Environ. Monit.* **4**, 511–516 (2002).
33. Aydın Tekdaş, D. *et al.* Antimicrobial activity of a quaternized BODIPY against Staphylococcus strains. *Org. Biomol. Chem.* **14**, 2665–2670 (2016).
34. Wainwright, M., Phoenix, D. A., Marland, J., Wareing, D. R. A. & Bolton, F. J. A study of photobactericidal activity in the phenothiazinium series. *FEMS Immunol. Med. Microbiol.* **19**, 75–80 (1997).
35. I. Ramos, A., M. Braga, T. & S. Braga, S. Ru(II)-Based Antimicrobials: Looking Beyond Organic Drugs. *Mini-Reviews Med. Chem.* **12**, 227–235 (2012).
36. Dahl, T. A., Midden, W. R. & Hartman, P. E. Comparison of killing of gram-negative and gram-positive bacteria by pure singlet oxygen. *J. Bacteriol.* **171**, 2188–2194 (1989).
37. Dahl, T. A., RobertMiddenand, W. & Hartman, P. E. Pure Singlet Oxygen Cytotoxicity for Bacteria. *Photochem. Photobiol.* **46**, 345–352 (1987).
38. Schaap, A. P., Thayer, A. L., Blossey, E. C. & Neckers, D. C. Polymer-Based Sensitizers for Photooxidations. *J. Am. Chem. Soc.* **97**, 3741–3745 (1975).
39. Dahl, T. A., Midden, W. R. & Neckers, D. C. Comparison of Photodynamic Action By Rose Bengal in Gram Positive and Gram Negative Bacteria. *Photochem. Photobiol.* **48**, 607–612 (1988).
40. Shrestha, A., Hamblin, M. R. & Kishen, A. Characterization of a conjugate between rose bengal and chitosan for targeted antibiofilm and tissue stabilization effects as a potential treatment of infected dentin. *Antimicrob. Agents Chemother.* **56**, 4876–4884 (2012).
41. Shrestha, A., Hamblin, M. R. & Kishen, A. Photoactivated rose bengal functionalized chitosan nanoparticles produce antibacterial/biofilm activity and stabilize dentin-collagen. *Nanomedicine Nanotechnology, Biol. Med.* **10**, 491–501 (2014).
42. Moczek, Ł. & Nowakowska, M. Novel water-soluble photosensitizers from chitosan. *Biomacromolecules* **8**, 433–438 (2007).
43. Decraene, V., Pratten, J. & Wilson, M. Cellulose acetate containing toluidine blue and rose

- bengal is an effective antimicrobial coating when exposed to white light. *Appl. Environ. Microbiol.* **72**, 4436–4439 (2006).
44. Decraene, V., Pratten, J. & Wilson, M. Novel light-activated antimicrobial coatings are effective against surface-deposited *Staphylococcus aureus*. *Curr. Microbiol.* **57**, 269–273 (2008).
 45. Pessoni, L., Lacombe, S., Billon, L., Brown, R. & Save, M. Photoactive, porous honeycomb films prepared from rose bengal-grafted polystyrene. *Langmuir* **29**, 10264–10271 (2013).
 46. Guo, Y., Rogelj, S. & Zhang, P. Rose Bengal-decorated silica nanoparticles as photosensitizers for inactivation of gram-positive bacteria. *Nanotechnology* **21**, 065102 (2010).
 47. Ferreira, A. M. *et al.* Surface modification of poly(dimethylsiloxane) by two-step plasma treatment for further grafting with chitosan-Rose Bengal photosensitizer. *Surf. Coatings Technol.* **223**, 92–97 (2013).
 48. Nakonechny, F. *et al.* Dark antibacterial activity of rose Bengal. *Int. J. Mol. Sci.* **20**, (2019).
 49. Tardivo, J. P. *et al.* Methylene blue in photodynamic therapy: From basic mechanisms to clinical applications. *Photodiagnosis and Photodynamic Therapy* **2**, 175–191 (2005).
 50. Wainwright, M. The development of phenothiazinium photosensitisers. *Photodiagnosis and Photodynamic Therapy* **2**, 263–272 (2005).
 51. Kömerik, N. *et al.* In vivo killing of *Porphyromonas gingivalis* by toluidine blue-mediated photosensitization in an animal model. *Antimicrob. Agents Chemother.* **47**, 932–940 (2003).
 52. Naik, A. J. T., Ismail, S., Kay, C., Wilson, M. & Parkin, I. P. Antimicrobial activity of polyurethane embedded with methylene blue, toluidene blue and gold nanoparticles against *Staphylococcus aureus*; Illuminated with white light. *Mater. Chem. Phys.* **129**, 446–450 (2011).
 53. Wilson, M. Light - Activated Antimicrobial Coating for the Continuous Disinfection of Surfaces. *Cambridge Univ. Press behalf Soc. Healthc. Epidemiol. Am. Concise Commun. Theor.* **24**, 782–784 (2003).
 54. Perni, S. *et al.* Antibacterial Activity of Light-Activated Silicone Containing Methylene Blue and Gold Nanoparticles of Different Sizes. *J. Clust. Sci.* **21**, 427–438 (2010).
 55. Perni, S., Prokopovich, P., Parkin, I. P., Wilson, M. & Pratten, J. Prevention of biofilm accumulation on a light-activated antimicrobial catheter material. *J. Mater. Chem.* **20**, 8668 (2010).
 56. Piccirillo, C. *et al.* Antimicrobial activity of methylene blue and toluidine blue O covalently bound to a modified silicone polymer surface. *J. Mater. Chem.* **19**, 6167 (2009).
 57. Manjón, F., Santana-Magaña, M., García-Fresnadillo, D. & Orellana, G. Singlet oxygen sensitizing materials based on porous silicone: photochemical characterization, effect of dye reloading and application to water disinfection with solar reactors. *Photochem. Photobiol. Sci.* **9**, 838–45 (2010).
 58. Perni, S. *et al.* Toluidine blue-containing polymers exhibit potent bactericidal activity when irradiated with red laser light. *J. Mater. Chem.* **19**, 2715 (2009).
 59. Ismail, S., Perni, S., Pratten, J., Parkin, I. & Wilson, M. Efficacy of a Novel Light-Activated Antimicrobial Coating for Disinfecting Hospital Surfaces. *Infect Control Hosp Epidemiol* **32**, 1130–1132 (2011).

60. Cahan, R., Schwartz, R., Langzam, Y. & Nitzan, Y. Light-activated antibacterial surfaces comprise photosensitizers. *Photochem. Photobiol.* **87**, 1379–1386 (2011).
61. Perni, S., Drexler, S., Ruppel, S. & Prokopovich, P. Lethal photosensitisation of bacteria using silica-TBO nanoconjugates. *Colloids Surfaces A Physicochem. Eng. Asp.* **510**, 293–299 (2016).
62. Wöhrle, D., Hirth, A., Bogdahn-Rai, T., Schnurpfeil, G. & Shopova, M. Photodynamic therapy of cancer: Second and third generations of photosensitizers. *Russ. Chem. Bull.* **47**, 807–816 (1998).
63. Bonnett, R., Krysteva, M. A., Lalov, I. G. & Artarsky, S. V. Water disinfection using photosensitizers immobilized on chitosan. *Water Res.* **40**, 1269–1275 (2006).
64. Ringot, C. *et al.* Triazinyl porphyrin-based photoactive cotton fabrics: Preparation, characterization, and antibacterial activity. *Biomacromolecules* **12**, 1716–1723 (2011).
65. Lucas, R. *et al.* Synthesis and cellular uptake of superparamagnetic dextran-nanoparticles with porphyrinic motifs grafted by esterification. *E-Polymers* 1–8 (2007).
66. Carpenter, B. L., Feese, E., Sadeghifar, H., Argyropoulos, D. S. & Ghiladi, R. A. Porphyrin-cellulose nanocrystals: A photobactericidal material that exhibits broad spectrum antimicrobial activity. *Photochem. Photobiol.* **88**, 527–536 (2012).
67. Properties, A., Carolina, N. & States, U. Photobactericidal Porphyrin-Cellulose Nanocrystals: Synthesis, Characterization, and Antimicrobial Properties. 3528–3539 (2011).
68. Tomé, J. P. C. *et al.* Synthesis and antibacterial activity of new poly-S-lysine-porphyrin conjugates. *J. Med. Chem.* **47**, 6649–6652 (2004).
69. Alvarez, M. G., Gómez, M. L., Mora, S. J., Milanesio, M. E. & Durantini, E. N. Photodynamic inactivation of *Candida albicans* using bridged polysilsesquioxane films doped with porphyrin. *Bioorganic Med. Chem.* **20**, 4032–4039 (2012).
70. Li, Q. *et al.* Antimicrobial nanomaterials for water disinfection and microbial control: Potential applications and implications. *Water Res.* **42**, 4591–4602 (2008).
71. Banerjee, I., Douaisi, M. P., Mondal, D. & Kane, R. S. +++ Light-activated nanotube–porphyrin conjugates as effective antiviral agents. *Nanotechnology* **23**, 105101 (2012).
72. Banerjee, I., Mondal, D., Martin, J. & Kane, R. S. Photoactivated Antimicrobial Activity of Carbon Nanotube–Porphyrin Conjugates. *Langmuir* **26**, 17369–17374 (2010).
73. Magaraggia, M., Jori, G., Soncin, M., Schofield, C. L. & Russell, D. a. Porphyrin-silica microparticle conjugates as an efficient tool for the photosensitised disinfection of water contaminated by bacterial pathogens. *Photochem. Photobiol. Sci.* **12**, 2170–6 (2013).
74. Kim, H. *et al.* Selective oxidative degradation of organic pollutants by singlet oxygen-mediated photosensitization: Tin porphyrin versus C60 aminofullerene systems. *Environ. Sci. Technol.* (2012). doi:10.1021/es301775k
75. Kim, W., Park, J., Jo, H. J., Kim, H. J. & Choi, W. Visible light photocatalysts based on homogeneous and heterogenized tin porphyrins. *J. Phys. Chem. C* **112**, 491–499 (2008).
76. Yokoi, H. *et al.* Bactericidal effect of a silica gel-supported porphyrinatoantimony (V) complex under visible light irradiation. *J. Microbiol.* 559–563 (2003).
77. FUEDA, Y. *et al.* Visible-Light Bactericidal Effect of Silica Gel-supported Porphyrinatoantimony(V) Catalyst on *Legionella* Species Occurring in the Living

- Environmental Fields. *Biocontrol Sci.* **10**, 55–60 (2005).
78. Alves, E. *et al.* A new insight on nanomagnet-porphyrin hybrids for photodynamic inactivation of microorganisms. *Dye. Pigment.* **110**, 80–88 (2014).
 79. Hynek, J., Rathouský, J., Demel, J. & Lang, K. Design of porphyrin-based conjugated microporous polymers with enhanced singlet oxygen productivity. *RSC Adv.* **6**, 44279–44287 (2016).
 80. Zhang, G.-Y. *et al.* Zirconium–metalloporphyrin frameworks as a three-in-one platform possessing oxygen nanocage, electron media, and bonding site for electrochemiluminescence protein kinase activity assay. *Nanoscale* **8**, 11649–11657 (2016).
 81. Masilela, N. *et al.* Photodynamic inactivation of *Staphylococcus aureus* using low symmetrically substituted phthalocyanines supported on a polystyrene polymer fiber. *Dye. Pigment.* **96**, 500–508 (2013).
 82. Mosinger, J. *et al.* Photofunctional polyurethane nanofabrics doped by zinc tetraphenylporphyrin and zinc phthalocyanine photosensitizers. *J. Fluoresc.* **19**, 705–713 (2009).
 83. Masilela, N. & Nyokong, T. The synthesis and photophysical properties of novel cationic tetra pyridiloxo substituted aluminium, silicon and titanium phthalocyanines in water. *J. Lumin.* **130**, 1787–1793 (2010).
 84. Hou, W.-C. & Jafvert, C. T. Photochemistry of aqueous C₆₀ clusters: Evidence of ¹O₂ formation and its role in mediating C₆₀ phototransformation. *Environ. Sci. Technol.* **43**, 5257–5262 (2009).
 85. Moor, K. J., Snow, S. D. & Kim, J.-H. Differential Photoactivity of Aqueous [C₆₀] and [C₇₀] Fullerene Aggregates. *Environ. Sci. Technol.* **49**, 5990–5998 (2015).
 86. Milanesio, M. E., Spesia, M. B., Cormick, M. P. & Durantini, E. N. Mechanistic studies on the photodynamic effect induced by a dicationic fullerene C₆₀ derivative on *Escherichia coli* and *Candida albicans* cells. *Photodiagnosis Photodyn. Ther.* **10**, 320–327 (2013).
 87. Manjón, F., Santana-Magaña, M., García-Fresnadillo, D. & Orellana, G. Are silicone-supported [C₆₀]-fullerenes an alternative to Ru(II) polypyridyls for photodynamic solar water disinfection? *Photochem. Photobiol. Sci.* **13**, 397–406 (2014).
 88. Moor, K. J. & Kim, J. Simple Synthetic Method Toward Solid Supported C₆₀ Visible Light-Activated Photocatalysts. *Environ. Sci. Technol.* **48**, 2785–2791 (2014).
 89. Ballatore, M. B. *et al.* Photodynamic Inactivation of Bacteria Using Novel Electrogenerated Porphyrin-Fullerene C₆₀ Polymeric Films. *Environ. Sci. Technol.* **49**, (2015).
 90. Ballatore, M. B., Spesia, M. B., Milanesio, M. E. & Durantini, E. N. Synthesis, spectroscopic properties and photodynamic activity of porphyrin-fullerene C₆₀ dyads with application in the photodynamic inactivation of *Staphylococcus aureus*. *Eur. J. Med. Chem.* **83**, 685–694 (2014).
 91. Jiang, L., Gan, C. R. R., Gao, J. & Loh, X. J. A Perspective on the Trends and Challenges Facing Porphyrin-Based Anti-Microbial Materials. *Small* 3609–3644 (2016). doi:10.1002/smll.201600327
 92. Kamkaew, A. *et al.* BODIPY dyes in photodynamic therapy. *Chem. Soc. Rev.* **42**, 77–88 (2013).
 93. Caruso, E., Banfi, S., Barbieri, P., Leva, B. & Orlandi, V. T. Synthesis and antibacterial activity of

- novel cationic BODIPY photosensitizers. *J. Photochem. Photobiol. B Biol.* **114**, 44–51 (2012).
94. Carpenter, B. L. *et al.* Antiviral, antifungal and antibacterial activities of a BODIPY-based photosensitizer. *Molecules* **20**, 10604–10621 (2015).
 95. Peveler, W. J. *et al.* Covalently Attached Antimicrobial Surfaces Using BODIPY: Improving Efficiency and Effectiveness. *ACS Appl. Mater. Interfaces* **10**, 98–104 (2018).
 96. Zhang, J., Chen, Y. & Brook, M. A. Facile functionalization of PDMS elastomer surfaces using thiol-ene click chemistry. *Langmuir* **29**, 12432–12442 (2013).
 97. Cooper, A. T. & Goswami, D. Y. Evaluation of Methylene Blue and Rose Bengal for Dye Sensitized Solar Water Treatment. *J. Sol. Energy Eng.* **124**, 305 (2002).
 98. Liu, Y. *et al.* Ru(II) complexes of new tridentate ligands: Unexpected high yield of sensitized TiO_2 . *Inorg. Chem.* **48**, 375–385 (2009).
 99. Garcia-Fresnadillo, D., Georgiadou, Y., Orellana, G., Braun, A. M. & Oliveros, E. Singlet-Oxygen production by Ruthenium(II) Complexes Containing Polyazaheterocyclic Ligands in Methanol and Water. *Helv. Chim. Acta* **79**, 1222–1238 (1996).
 100. Parakh, P., Gokulakrishnan, S. & Prakash, H. Visible light water disinfection using [Ru(bpy)₂(phenadione)](PF₆)₂·2H₂O and [Ru(phenadione)₃](ClO₄)₂·2H₂O complexes and their effective adsorption onto activated carbon. *Sep. Purif. Technol.* **109**, 9–17 (2013).
 101. Jimenez-Hernandez, M. E., Manjon, F., Garcia-Fresnadillo, D. & Orellana, G. Solar water disinfection by singlet oxygen photogenerated with polymer-supported Ru(II) sensitizers. *Sol. Energy* **80**, 1382–1387 (2006).
 102. Villén, L., Manjón, F., García-Fresnadillo, D. & Orellana, G. Solar water disinfection by photocatalytic singlet oxygen production in heterogeneous medium. *Appl. Catal. B Environ.* **69**, 1–9 (2006).
 103. Manjón, F., Villén, L., García-fresnadillo, D. & Orellana, G. On the Factors Influencing the Performance of Solar Reactors for Water Disinfection with Photosensitized Singlet Oxygen. *Environ. Sci. Technol.* **42**, 301–307 (2008).
 104. Keller, S. Heteroleptic light-emitting copper(I) complexes with possible applications in light-emitting electrochemical cells. (2017). doi:10.5451/unibas-006772759
 105. Takeda, H., Monma, Y., Sugiyama, H., Uekusa, H. & Ishitani, O. Development of visible-light driven Cu(I) complex photosensitizers for photocatalytic CO₂ reduction. *Front. Chem.* **7**, 1–12 (2019).
 106. Leoni, E. *et al.* Heteroleptic Copper(I) Complexes Prepared from Phenanthroline and Bis-Phosphine Ligands: Rationalization of the Photophysical and Electrochemical Properties. *Inorg. Chem.* **57**, 15537–15549 (2018).
 107. Iwamura, M., Takeuchi, S. & Tahara, T. Ultrafast Excited-State Dynamics of Copper(I) Complexes. *Acc. Chem. Res.* **48**, 782–791 (2015).
 108. McMillin, D. R., Kirchoff, J. R. & Goodwin, K. V. Exciplex quenching of photo-excited copper complexes. *Coord. Chem. Rev.* **64**, 83–92 (1985).
 109. Cuttell, D. G., Kuang, S. M., Fanwick, P. E., McMillin, D. R. & Walton, R. A. Simple Cu(I) complexes with unprecedented excited-state lifetimes. *J. Am. Chem. Soc.* **124**, 6–7 (2002).
 110. Smith, C. S., Branham, C. W., Marquardt, B. J. & Mann, K. R. Oxygen gas sensing by

luminescence quenching in crystals of Cu(xantphos)(phen)⁺ complexes. *J. Am. Chem. Soc.* **132**, 14079–14085 (2010).

2 Synthesis and characterisation of Complexes

Contents

2	Synthesis and characterisation of Complexes	35
2.1	Ruthenium Complexes	37
2.1.1	[Ru(bpy) ₂ (bpy-Silatrane)]Cl ₂ (RuBS)	37
2.1.2	[Ru(bpy) ₂ (bpy-Me-Silatrane)]Cl ₂ (RuBMS)	42
2.1.3	[Ru(phen) ₂ (phen-silatrane)]Cl ₂ , RuPS	45
2.2	Ruthenium Materials.....	47
2.2.1	Silica-bound Ru-BS	47
2.2.2	PDMS-ruthenium materials	53
2.2.3	Tetrasodium tris(bathophenanthroline disulfonate)ruthenium(II) (Ru-BPS) Supported on Amberlite IRA-900.	57
2.3	Copper Complexes	61
2.3.1	Synthesis	63
2.3.2	UV-visible and Luminescence spectra and Excited State Lifetime.	64
2.4	Copper complexes adsorbed onto solid supports	67
2.4.1	Silica-bound Cu(xant)(dmp).tfpb (CuXD-CS)	67
2.5	Conclusions.....	69
2.6	References.....	71

2.1 Ruthenium Complexes

2.1.1 $[\text{Ru}(\text{bpy})_2(\text{bpy-Silatrane})]\text{Cl}_2$ (RuBS)

2.1.1.1 Synthesis

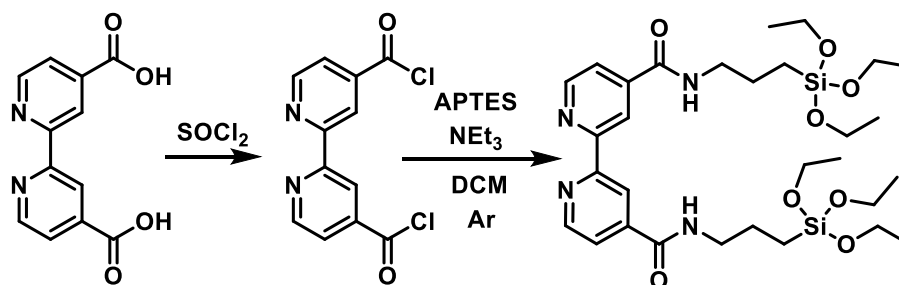


Figure 1 Synthesis of *bpy-sil*

For the purpose of converting solar energy into bactericidal killing power, it was decided that ruthenium polypyridyl complexes would be an effective choice. These compounds are known to produce sizable amounts of singlet oxygen by reaction of their $^3\text{MLCT}$ excited state with ground-state $^3\text{O}_2$. Thus, a reusable photo-activated antibacterial material could be made through attachment of such a complex to a solid support *via* a stable linker.

A ligand was chosen that would effectively and easily coordinate to Ru(II), confer the appropriate photophysical properties on the complex, and also effectively chemisorb onto a surface. Initially, silica was chosen as the substrate due to its availability and stability. A linker based on APTES was used to provide the Ru(II) complexes with the ability to covalently attach to silica (or, indeed, any other supports with OH groups pendant from the surface). The ligand *bpy-sil* (Fig. 1) was successfully synthesised based on a modified method from previous literature.¹ The NMR and MS data are consistent with literature values.² However, when coordinated to a $\{\text{Ru}(\text{bpy})_2\}^{2+}$ fragment the resulting complex $[\text{Ru}(\text{bpy})_2(\text{bpy-sil})]^{2+}$ is not stable, frequently polymerising after purification. This was likely due to the reactive nature of the

triethoxy-silane groups.

The ligand was modified to protect the trialkoxysilane units until they were required for chemisorption onto silica. This was done by reaction of APTES with triethanolamine (TEA) to produce APSilatrane (Fig. 2).



Figure 2 APSilatrane synthesis

This modification not only made a product that was more stable but is also a solid at room temperature and is easily purified via washing with hexane. Bpy-Silatrane was then synthesised using the same method as above and successfully coordinated to $\text{Ru}(\text{bpy})_2\text{Cl}_2$ to form the complex $[\text{Ru}(\text{bpy})_2(\text{bpy-silatrane})]\text{Cl}_2$, abbreviated as RuBS (Fig. 3A). The ^1H NMR spectrum shows 11 signals with 4 visibly overlapping signals in the aromatic region (Fig. 3B). This accounts for 16 hydrogen environments. Although the complex does have 17 hydrogen environments the amide singlet is not visible. This is likely due to proton exchange with the solvent (MeOD). Compared to the ^1H NMR of the bpy-sil complex, the silatrane moieties replace those of the ethoxysilane tail. The quartet of intensity 12H and a triplet of intensity 18H, which came from the ethyl hydrogens on the siloxane tails, were replaced in Ru-BS by two signals of equal intensity, coming from the silatrane hydrogens.

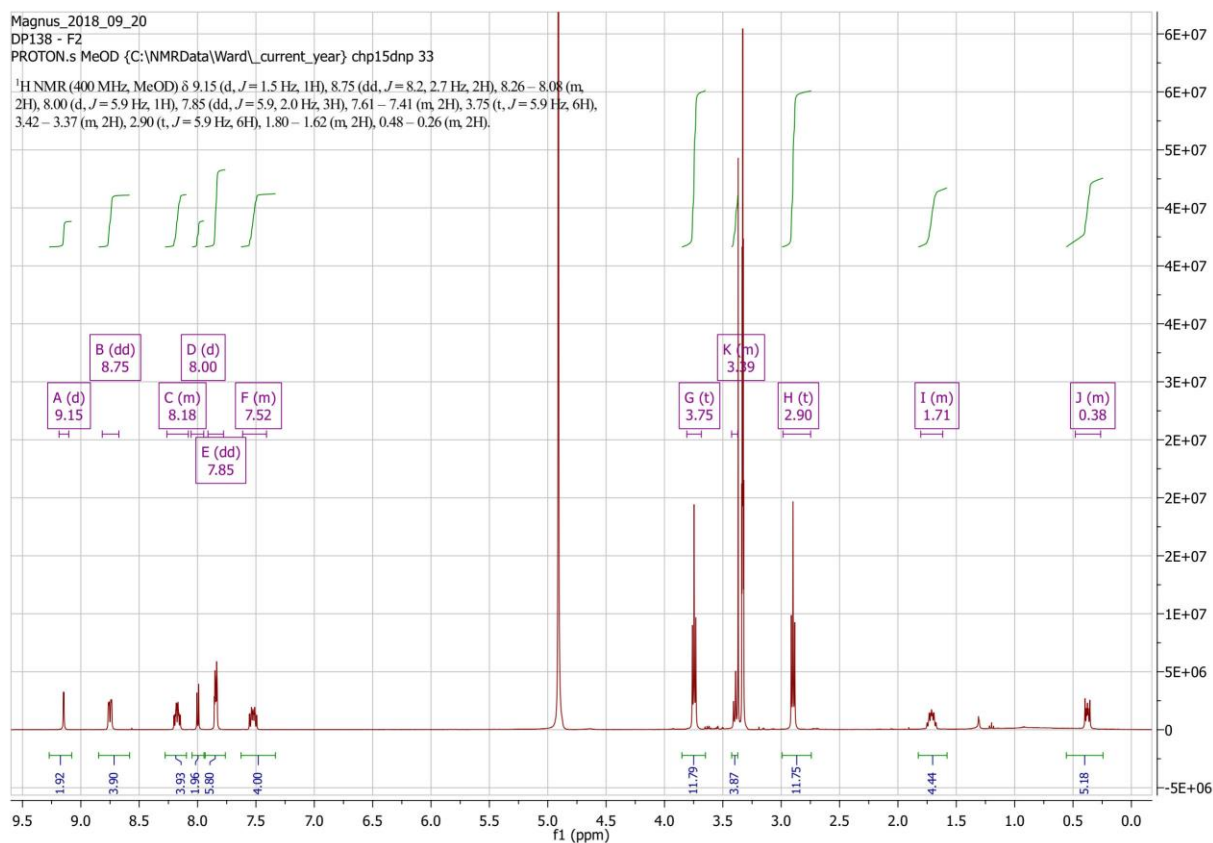
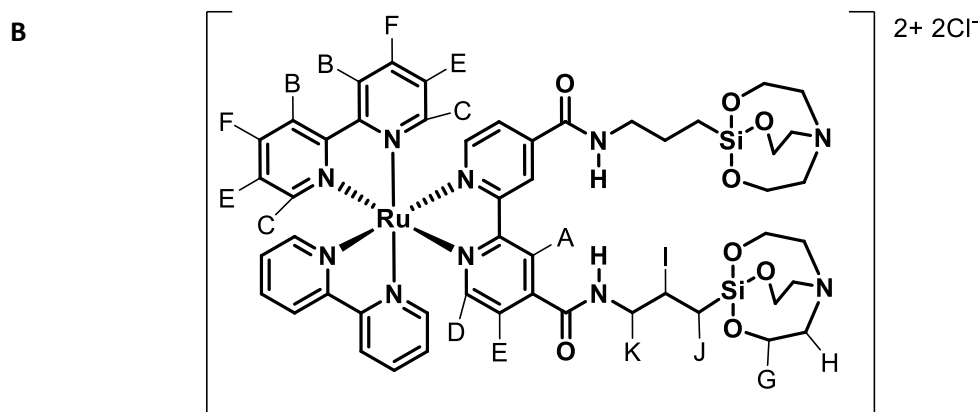
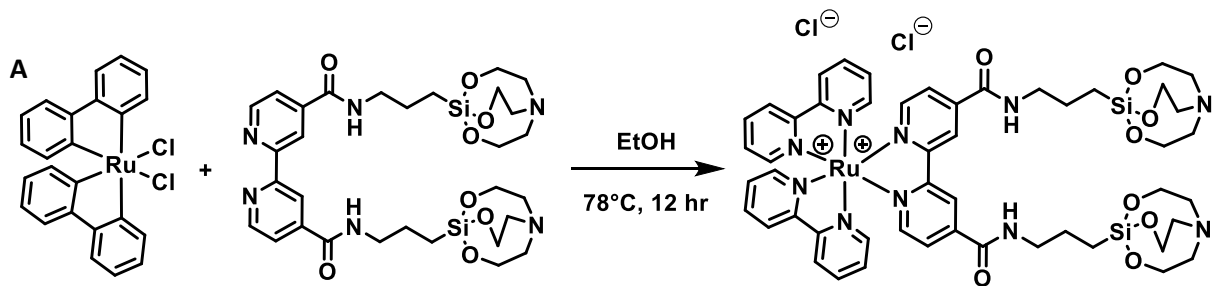


Figure 3 A: Synthesis of $[Ru(bpy)_2(bpy-Silatrane)]Cl_2$ (RuBS) B: Structure of RuBS with labelled protons and 1H NMR spectrum in MeOD. Labels on peaks in spectrum correspond to those labelled on the structure.

2.1.1.2 Characterisation

2.1.1.2.1 UV-Vis spectroscopy

The UV-Vis absorption spectrum (Fig. 4) of RuBS was measured in MeCN. The characteristic $^1\text{MLCT}$ absorption peak is clearly visible at 460 nm (table 1), this is the lowest energy transition. The higher energy $\pi^*\leftarrow\pi$ is visible at 287 nm and is far more intense. By comparison to the $^1\text{MLCT}$ band of $[\text{Ru}(\text{bpy})_3]^{2+}$ it is red-shifted by around 10 nm.³ This is due to the two amide moieties on the linker ligand, which withdraw electron density from the ligand, lowering the energy of the LUMO and thus decreasing the energy gap for the $^1\text{MLCT}$ transition.

Wavelength (nm)	ϵ ($\text{M}^{-1} \text{cm}^{-1}$)	Transition
287	67,000	$\pi^*\leftarrow\pi$
460	16,000	MLCT

Table 1 UV-vis spectroscopy absorption values for Ru-BS in acetonitrile.

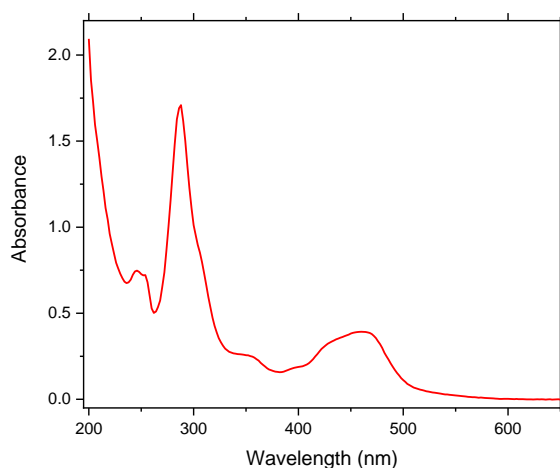


Figure 4 UV-vis spectrum of RuBS in MeCN

2.1.1.2.2 Luminescence properties

Emission studies show a clear emission maximum around 650 nm in the luminescence spectrum, associated with decay of the characteristic $^3\text{MLCT}$ state, and a maximum in the excitation maximum at 460 nm (Fig. 5). This large Stokes shift is expected for Ru(II) polypyridyl

complexes as the absorption is to the singlet excited state, whereas the emission is from the lower-energy triplet state following intersystem crossing. This triplet emission is lower in energy compared to that of $[\text{Ru}(\text{bpy})_3]\text{Cl}_2$ (620 nm), which is again consistent with the electron-withdrawing effect of the amide substituents.

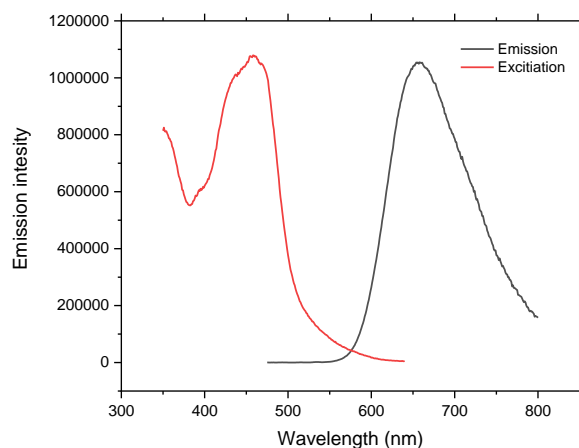


Figure 5 Excitation spectrum (red) and Emission spectrum (black) of RuBS in MeCN

The lifetime of this luminescence in air-equilibrated acetonitrile at 298 K is 353 ns, relatively long compared to $[\text{Ru}(\text{bpy})_3]^{2+}$, which has an excited-state lifetime of 160 ns under the same conditions. The lifetime after the solution had been degassed with argon for 30 minutes was 1167 ns (Fig. 6), 3.3 times lifetime in the air-equilibrated solvent. This indicates that a large component of the emissive excited state is being quenched by molecular oxygen in its triplet ground state ($^3\Sigma_g^-$).

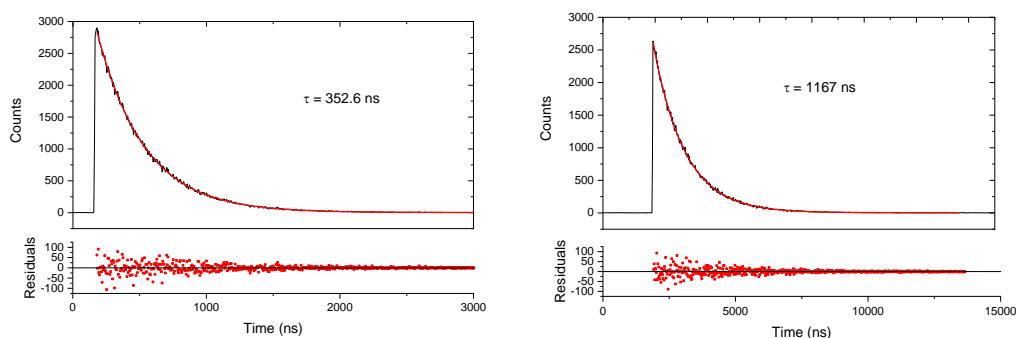


Figure 6 Emission lifetime at 460 nm RuBS in (left) air-equilibrated, and (right) MeCN degassed by bubbling Ar through it for 30 minutes.

2.1.2 [Ru(bpy)₂(bpy-Me-Silatrane)]Cl₂ (RuBMS)

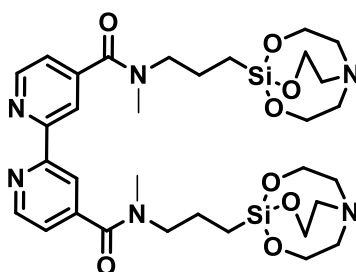


Figure 7 Structure of RuBMS

2.1.2.1 Synthesis

This complex was made in order to test the importance of the amide NH group in singlet oxygen quenching. The amide NH was changed to an N-Me group in the hope that this might improve the efficiency of singlet oxygen generation. RuBMS (Fig. 7) was successfully synthesised in good yields, utilising the same synthesis as for RuBS, however *N*-methylaminotrimethoxysilane was used in the ligand preparation instead of APTES. Similarly, the silanes were protected by capping with triethanolamine. Coordination to the {Ru(bpy)₂}²⁺ unit was carried out in good yield (78%) and the resulting complex RuBMST was purified on Sephadex LH20 in MeOH. Successful synthesis was confirmed by NMR spectroscopy, and ES⁺ MS, and elemental analysis.

2.1.2.2 Characterisation

2.1.2.2.1 UV-Vis spectroscopy

The absorption spectrum of RuBMS varied slightly from that of RuBS (Fig. 8). While the π - π^* absorption band is at the same wavelength in the UV region, it has a higher extinction coefficient than for RuBS, and the $^1\text{MLCT}$ absorption is blue-shifted by 5 nm (table 2).

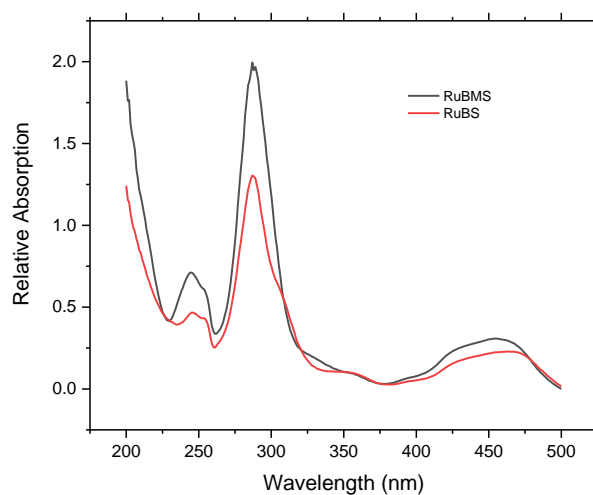


Figure 8 Absorption spectra of RuBS (red) and RuBMS (black) in MeCN

Wavelength (nm)	ϵ ($\text{M}^{-1} \text{cm}^{-1}$)	Transition
287	91,000	$\pi^* \leftarrow \pi$
460	17,500	MLCT

Table 2 UV-visible spectroscopy absorption values for RuBMS in acetonitrile.

2.1.2.2.2 Luminescence spectra

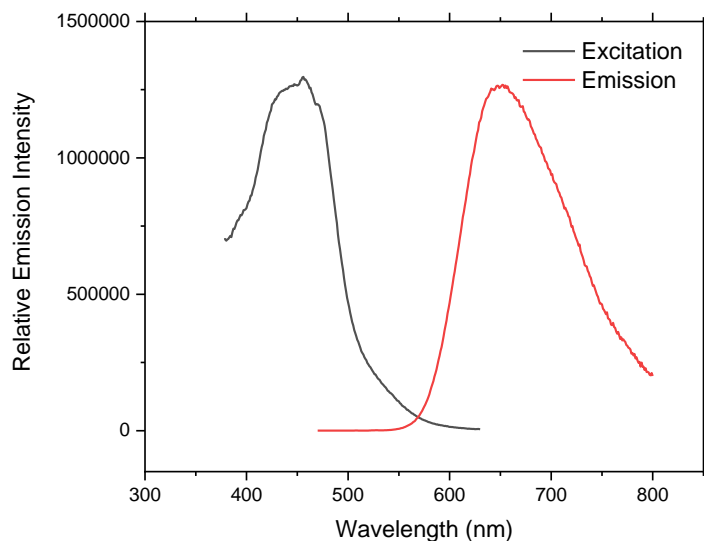


Figure 9 Excitation and emission spectra of RuBMS in MeCN

RuBMS has a similar emission spectrum (Fig. 9) to that of RuBS, with the emission maximum at 650 nm and a maximum in the excitation spectrum that matches the UV/Vis absorption maximum. Lifetimes are similar to those for RuBS, with a 3-fold increase in lifetime under degassed conditions compared to air-equilibrated conditions (Fig. 10). This again indicates that the excited state is being quenched by oxygen.

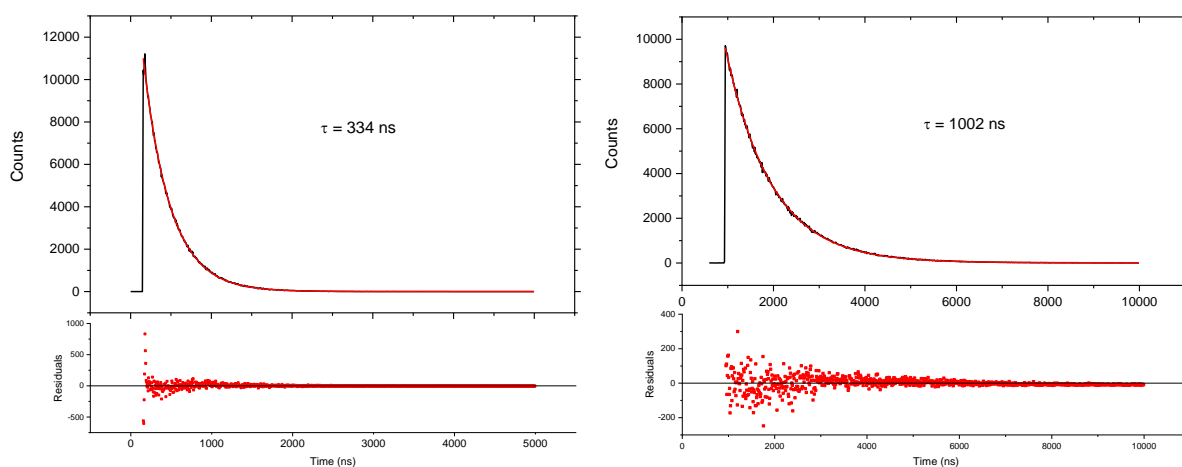


Figure 10 Emission lifetime at 460 nm for RuBMS in (left) air-equilibrated, and (right) degassed MeCN.

2.1.3 [Ru(phen)₂(phen-silatrane)]Cl₂, RuPS

2.1.3.1 Synthesis

The synthetic method for the phen-silatrane ligand (Fig. 12) was similar to that used for bpy-silatrane, the difference being the initial oxidation step to produce the phen-dialdehyde. Whereas 2,2'-dimethyl-4,4'-bipyridine can be oxidised directly to the di-carboxylic acid using potassium dichromate / conc. sulfuric acid, 4,7-dimethyl-1,10-phenanthroline must first be oxidised to the aldehyde through a Riley oxidation, followed by a separate oxidation step with concentrated nitric acid to yield the di-acid (Fig. 11).

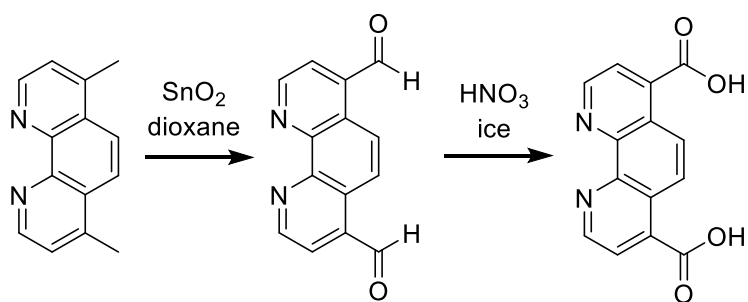


Figure 11 Synthesis of phenanthroline-4,7-dicarboxylic acid.

Beyond this point the synthesis follows the same route as for the bpy-based ligand: formation of the acyl chloride then reaction with APSilatrane. However this reaction mixture is refluxed overnight rather than just stirred at room temperature.

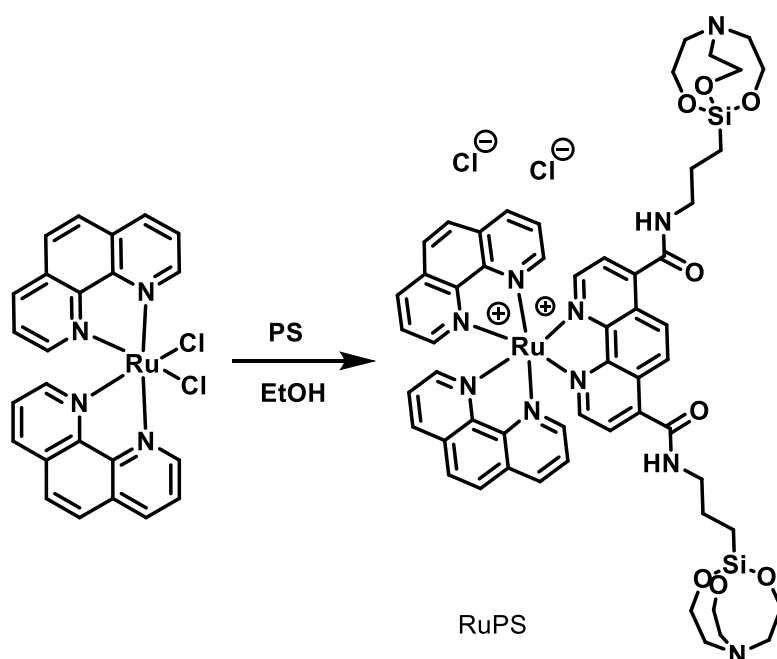
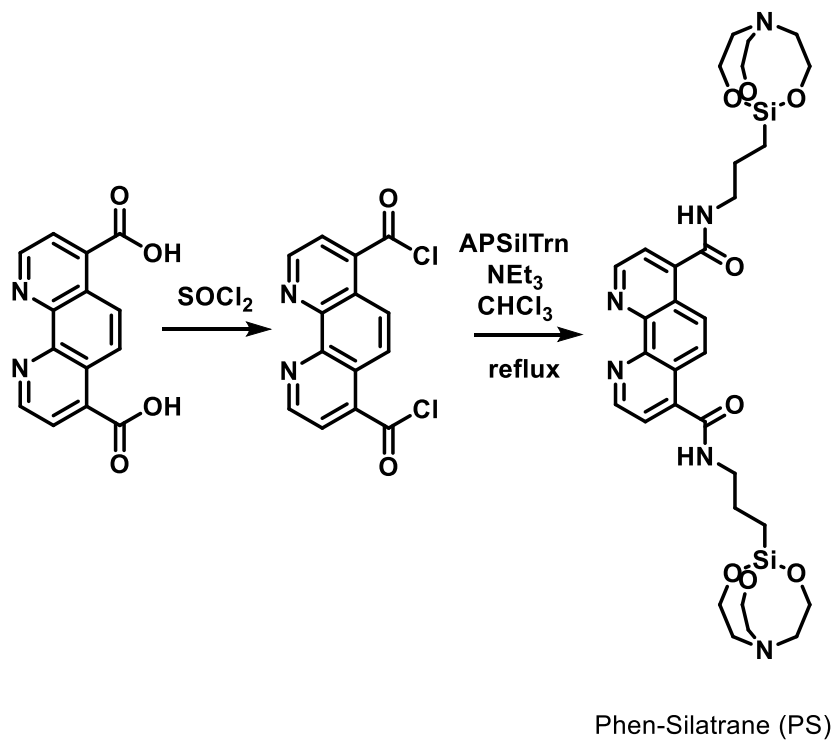


Figure 12 Synthesis of $[Ru(phen)_2(phen-silatrane)]Cl_2$ (RuPS).

RuPS was synthesised in a similar manner to RuBS: the ligand Phen-Silatrane (Fig. 12) and $Ru(phen)_2Cl_2$ were boiled in ethanol for 8 hours, before filtration and then removal of solvent under reduced pressure. The complex was purified on Sephadex LH20 in MeOH. RuPS

was characterised by ES⁺ MS and ¹H NMR spectroscopy, both of which were consistent with the target structure.

2.1.3.2 Characterisation

2.1.3.2.1 UV-Vis and Luminescence properties

Complex	Absorbance		Emission		Lifetime		
	λ_{\max} /nm	ϵ / M ⁻¹ cm ⁻¹	λ_{\max} /nm	Φ_P	τ_{O_2} / μ s	τ^a / μ s	P _{O₂}
{Ru(bpy) ₃ } ²⁺	450	14600	625	0.062	0.16	0.87	0.82
RuBS	455	16000	650	0.14	0.35	1.17	0.70
RuBMS	460	17500	650	0.15	0.334	1	0.67
RuPS	440	14200	650	0.27	0.307	3.18	0.90

Table 3 Values for Spectroscopic data of Ruthenium Complexes in MeCN. a) degassed lifetimes performed in acetonitrile bubbled through with argon for 30 minutes.

As expected, the lifetime of the phenanthroline-based ruthenium complex RuPS in the absence of oxygen is longer than the analogous bipyridine complex RuBS. This is due to the greater rigidity of the phen-based ligands meaning the excited state is less likely to follow non-radiative decay pathways. However their lifetimes in the presence of oxygen are similar. This indicates that a larger proportion of the excited state is being quenched by molecular oxygen (P_{O₂}, discussed in Chapters 1 and 3) for RuPS compared to RuBS.

2.2 Ruthenium Materials

2.2.1 Silica-bound Ru-BS

2.2.1.1 General Immobilisation Method

The complex Ru-BS was successfully bound to silica by dissolving it in a minimum amount of MeCN, then adding it to a stirred suspension of the silica in MeCN (1 g: 10 mL). This mixture was then heated to 50 °C for 4 hours. This can be completed in sealed sample vials in a sand bath: flasks and condensers are unnecessary. Any physisorbed complex still on the silica was removed by sonication in a large amount of MeOH for 30 minutes. The resulting

orange powder was then dried in a vacuum oven at 70 °C overnight. This process permits a facile attachment of the silane-functionalised complex to any silica surface.

2.2.1.2 *Chromatography grade silica gel*

Chromatography-grade silica gel was initially chosen as a support for its thermal and chemical stability, high surface area and relatively low price. The silica used was technical grade, pore size 60 Å, 230-400 mesh particle size, 40-63 µm particle size with a surface area of 500 m² g⁻¹.

2.2.1.2.1 *Surface coverage*

The surface coverage of the complex on silica was measured by addition of varying amounts of a stock solution of the complex to samples of Silica gel. The initial concentration of the solution was then compared to the concentration of the solution after reacting with silica, which was determined by measuring the absorbance at 460 nm. It was found that the number of moles of Ru(II) complex that bound to the silica surface plateaued at around 38 µmol g⁻¹ (Fig. 13). Given the surface area of chromatography silica is 500 cm² g⁻¹, this equates to a surface coverage of around 76 nmol cm⁻².

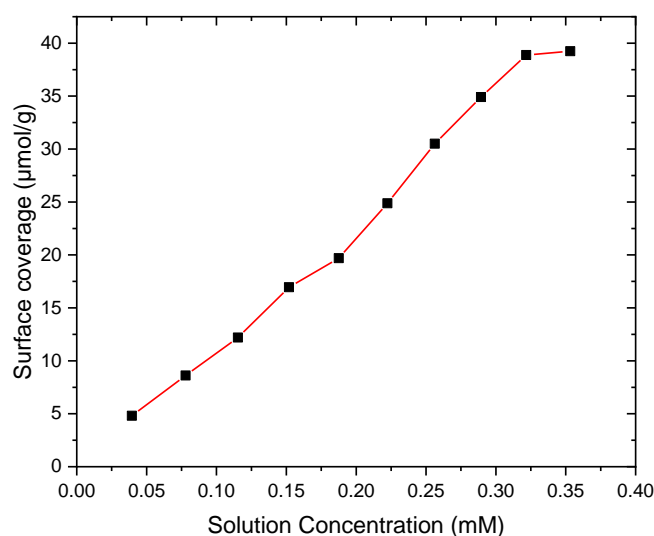


Figure 13 graph showing attained surface coverage against initial concentration of RuBS in solution

2.2.1.3 SBA-15 and MCM-41 as supports

SBA-15 is a highly-ordered mesoporous silica based on uniform hexagonal pores with tuneable pore sizes between 5 and 15 nm.⁴ Its high reported surface area⁵ of 400-900 m² g⁻¹ makes it ideal as a support for adsorbed guests on its surface and its thick framework walls provide it with excellent thermal stability.⁶ These factors make it a suitable support for water disinfection. Its maximum surface coverage per compound and highest singlet oxygen producing activity were measured.

2.2.1.3.1 Surface coverage

The surface coverage of the complex was measured by the same method as used for chromatography grade silica. It was found that the number of moles that bound to the surface of SBA-15 plateaued at around 50 μmol g⁻¹ (Fig. 14), slightly higher than chromatography-grade silica. Assuming the same coverage per unit area by the complex (given that the complex will take up the same amount of space) of 76 nmol cm⁻², this is consistent with a surface area of over 650 m² g⁻¹.

Loading experiments of RuBS onto MCM-41 demonstrated far higher surface coverages. Loadings of $>80 \mu\text{mol g}^{-1}$ were achieved without reaching a plateau. Further experiments are necessary to determine the maximum surface coverage of this material. However, as is seen in chapter 3, the rate of singlet oxygen production by MCM-41 functionalised with RuBS plateaus at around $30 \mu\text{mol g}^{-1}$, making higher surface coverages a waste of costly material.

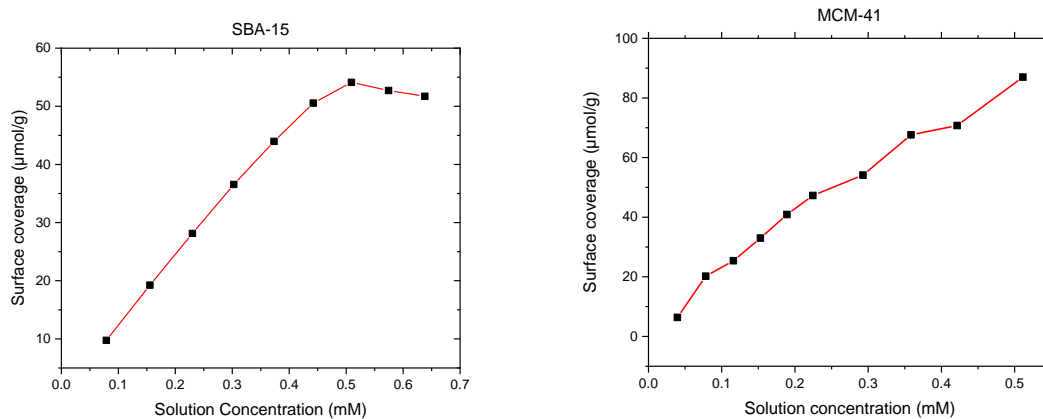


Figure 14 graph showing attained surface coverage against Initial concentration of solution for SBA-15(left) and MCM-41 (right).

2.2.1.3.2 Solid State UV-vis spectroscopy

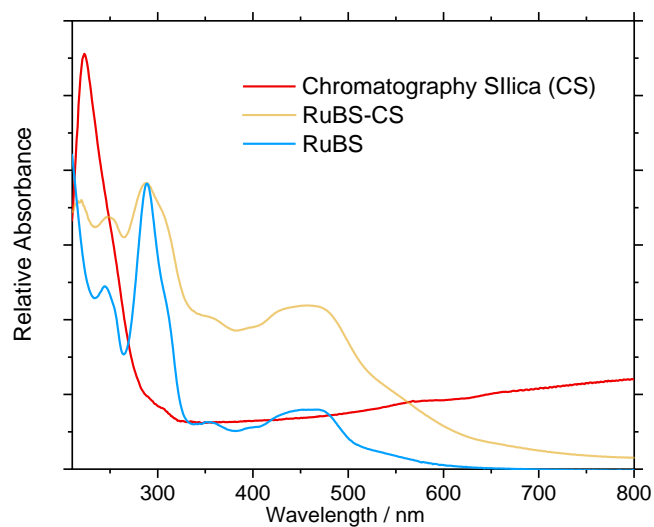


Figure 15 Solid state UV-vis spectrum of Chromatography grade silica (red), RuBS on chromatography grade silica (yellow) and the solution-state UV-vis spectrum of RuBS

The solid-state UV-vis spectrum of the complex RuBS bound to chromatography grade silica (Fig. 15) shows an almost identical profile to the solution-state spectrum of the complex. Although the relative absorbances of the peaks are different, their positions are the same. This indicates the complex is bound to the surface of the material (which was evident from its orange colour).

2.2.1.3.3 Solid State Luminescence

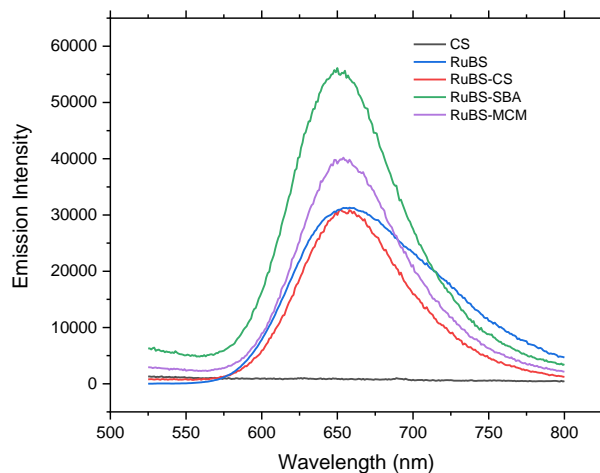


Figure 16 Solid state emission spectra of RuBS bound to the three different types of silica.

The solid-state emission and excitation spectra of the functionalised silica samples were measured by coating the inside of a quartz cuvette with a thin layer of the material, particles of which cling to the quartz surface naturally. Figures 16 and 17 show that the complex and all of the complex-functionalised silicas all have the same emission and excitation peaks. This suggests that immobilisation does not significantly affect the emission properties of the complex. The functionalised MCM-41 did not yield an excitation spectrum, possibly due to the scattering being too high compared to the loading by the complex.

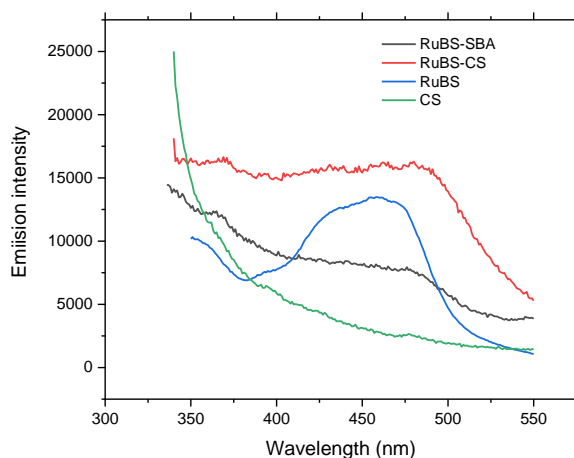


Figure 17 Solid-state excitation spectrum of RuBS immobilised on SBA-15 (black), on Chromatography grade silica (red), unfunctionalised chromatography grade silica (green) and solution-state excitation spectrum of RuBS (blue).

2.2.2 PDMS-ruthenium materials

Polydimethylsiloxane or PDMS (Fig. 18) is a cheap, non-toxic and chemically stable material that can be moulded or set into practically any desired shape. This makes it an ideal support for a photosensitiser such as the Ru/bpy complexes reported here. A common method of functionalisation is the swell-encapsulate-shrink method.^{7,8} While this method is technically simple, it is resource intensive; while the complex is embedded throughout the polymer, only the surface level is active, leaving the complex embedded in the bulk polymer inactive. There is also risk of material leaching from the surface as it is not covalently bonded.

Covalent functionalisation of PDMS can be challenging, with the majority of methods requiring an exceedingly clean surface with exposed surface hydroxyl groups. This can involve harsh conditions such as submerging in piranha solution or treating with an oxygen plasma.⁹ The method developed by Brook et al. consists of a simple and cost-effective way of functionalising PDMS surfaces.¹⁰ The method can be used to produce thiolated surfaces, in this project the procedure has also been successfully modified to produce aminated surfaces.

For the purpose of these experiments, thin film PDMS substrates were produced using a Sylgard 184 elastomer kit. The elastomer was mixed with a curing agent in a 10:1 ratio and the mixture poured into petri dishes, forming a layer around 1 mm in height. These samples were then cured in an oven at 50 C for 48 hours and cut into 1x1x0.1 cm squares before functionalisation

2.2.2.1 Amination route

The surfaces were aminated using (3-aminopropyl)triethoxysilane (APTES) in a modified method by Brook et al.,¹⁰ wherein the PDMS is heated to 50 C for 2h in a methanolic solution of 2% APTES, 1% KOH. They were then washed 3 times by sonication in methanol and dichloromethane. The resulting material was steeped in a solution of 50 mg of 2,2'-bipyridine-4,4'-di(carbonyl chloride) in DCM overnight.

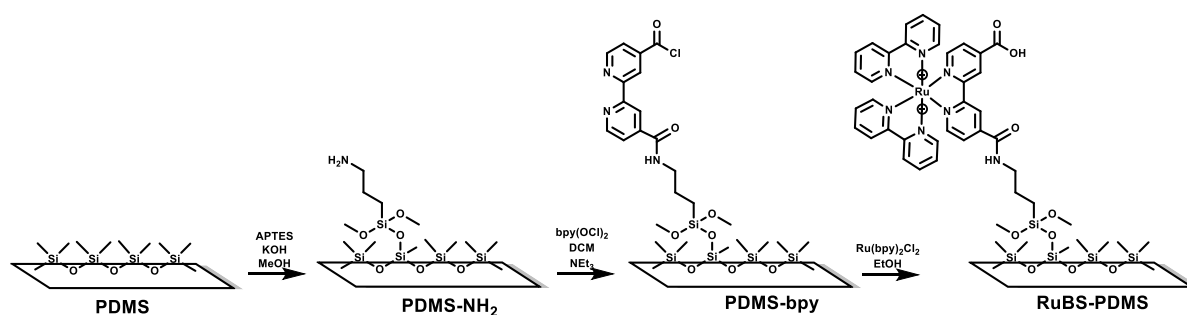


Figure 18 Functionalisation of PDMS via the Amination route.

The functionalised PDMS strips were then washed in DCM for 48 h, changing the solvent every 12 h, before being heated to 70 °C in a solution of $\text{Ru}(\text{bpy})_2\text{Cl}_2$ in EtOH for 1 hour. The strips, now dark red/purple in colour, were sonicated in MeOH for 4 hours. This removed any physisorbed complex, exposing a bright orange colour associated with the covalently attached $\{\text{Ru}(\text{bipy})_3\}^{2+}$ units (Fig. 18).

Attenuated total reflectance FTIR spectra were measured for these PDMS pieces during the first three steps of functionalisation (Fig. 19). The spectra of PDMS-bpy shows a peak at around 1733 cm^{-1} that is distinct from the peak present in the spectra of PDMS-NH₂ and PDMS at 1724 cm^{-1} (this peak is still visible as a shoulder). This fits within the range for the C=O stretch for carboxylic acids. A broad peak at 3390 cm^{-1} is also indicative of a carboxylic acid O-H stretch.

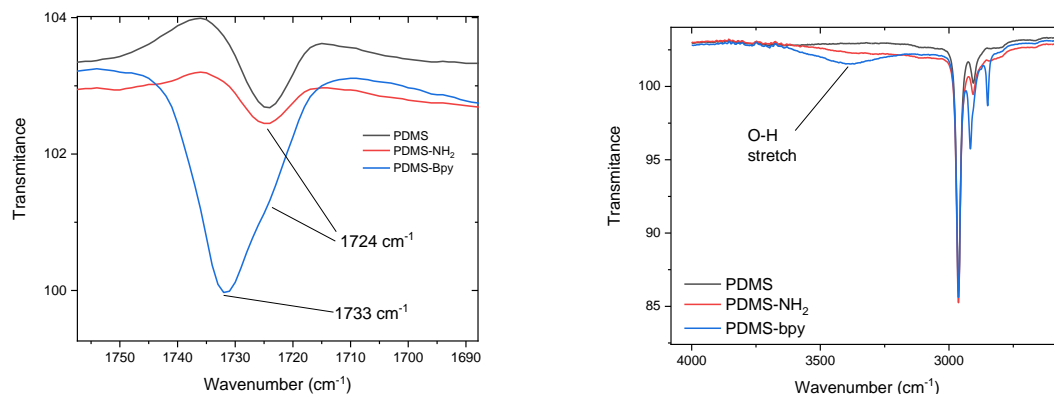


Figure 19 Overlaid ATR-IR spectra of PDMS (black) PDMS-NH₂ (red) and PDMS-bpy (blue).

These results suggest that after attachment of the 2,2'-Bipyridine-4,4'-dicarboxylic acid chloride to form an amide, the unreacted acyl chloride is turned into a carboxylic acid through reaction with water.

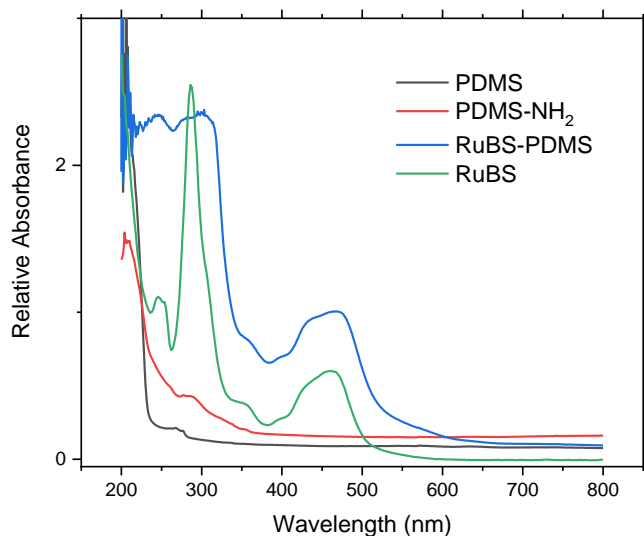


Figure 20 Comparison of solid-state UV-vis spectra of PDMS (black), PDMS functionalised with APTES (Red), PDMS functionalised with the complex RuBS (Blue) and the overlaid spectrum of RuBS in solution (green).

The solid state UV-vis spectrum (Fig. 20) of PDMS-Ru is consistent with the {Ru(BS)}²⁺ complex being on the surface of the support. The entire absorption profile of RuBS in solution is clearly present in the solid-state UV spectrum of PDMS-Ru; in particular the characteristic ¹MLCT absorption band at 455 nm confirms formation of a {Ru(bpy)₃}²⁺ core.

2.2.2.2 Thiol-ene click route

The method by Brook et al. was once again employed to thiolate the surface of PDMS samples. This time the thin films were heated to 50 °C in a methanolic solution of 20% MPS and 1% KOH for 8h. The strips were washed using the same method as above. The strips were then heated in a solution of maleic anhydride in THF with AIBN as a catalyst. The maleic anhydride undergoes addition to the surface *via* a thiol-ene click reaction. Any physisorbed material was cleaned off the surface by washing in THF over 48 hrs, changing the solvent every 12 h.

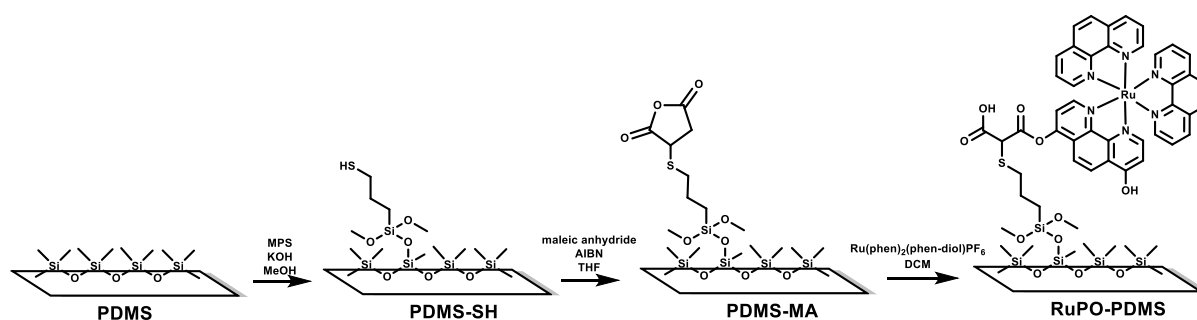


Figure 21 Surface characterisation using the thiol-ene click chemistry route.

The maleic anhydride moiety readily reacts with alcohol groups to form esters, allowing for the facile addition of ligands to the PDMS surface. Bipy and phenanthroline ligands with pendant alcohol moieties that can react with the maleic anhydride are readily available and their respective ruthenium polypyridyl complexes are trivial to synthesise. This represents a facile method for functionalising PDMS surfaces.

ATR-IR spectroscopy performed on PDMS-MA (Fig. 22A) shows the presence of a carbonyl peak (1714 cm^{-1}), indicating that maleic anhydride is present on the surface of the material. Solid-state UV-vis spectra of the material RuPO-PDMS, in which the maleic anhydride has reacted with $[\text{Ru}(\text{phen})_2(\text{phen-diol})]^{2+}$ (Fig. 21) shares a similar profile as the attached photosensitiser (Fig. 22B).

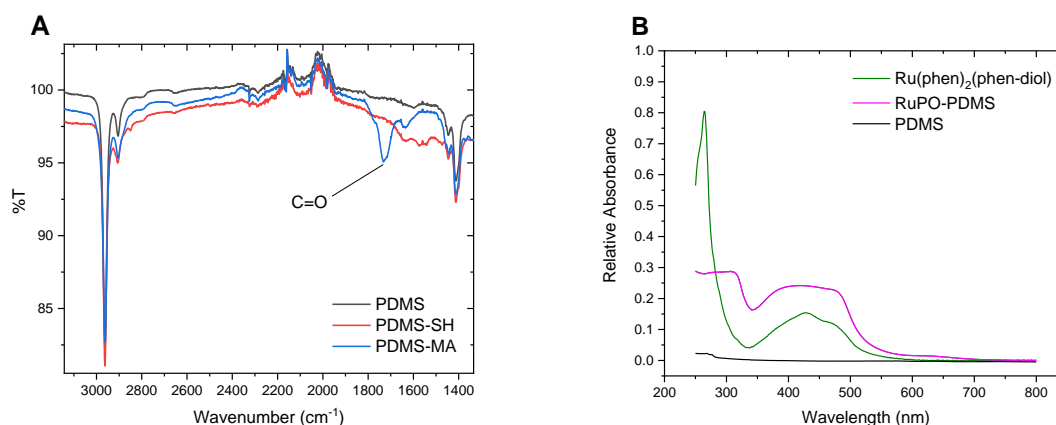


Figure 22 A: Overlay of ATR-IR spectra of PDMS (black), thiolated PDMS (red) and maleic anhydride functionalised PDMS (blue). B Comparison of absorbance spectra of $[Ru(phen)_2(phen-diol)]Cl_2$ in MeOH (green) and solid-state spectra of thiol-route functionalised RuPO-PDMS (magenta) and unfunctionalised PDMS (Black).

2.2.3 Tetrasodium tris(bathophenanthroline disulfonate)ruthenium(II) (Ru-BPS) Supported on Amberlite IRA-900.

Amberlite IRA900 is a macroporous polystyrene cationic exchange resin. It has been successfully used in antimicrobial experiments, supporting an anionic photosensitiser.¹¹ This resin appears to be an attractive support due to its larger bead size (<0.5 mm in diameter). Larger particle sizes allow for easier separation and present a lower respiratory risk. In addition, IRA900 has a strongly cationic surface. Positive surface charges, such as on chitosan, have been shown to interact with bacterial cell walls or membranes, which have a net negative surface charge.¹² The Ru(II) complex chosen to attach to this (Ru-BPS, see Fig. 23) has six pendant, anionic sulfonate groups and should therefore form a strong electrostatic attraction to the Amberlite surface without requiring covalent attachment.

2.2.3.1 Synthesis

RuBPS was synthesised according to a method from the literature¹⁹ in excellent yields (>90%). It was purified on LH-20 Sephadex® with methanol as the eluent. 2 mg of this complex was then dissolved in water and 1 g of Amberlite® IRA900 added. The mixture was stirred

overnight, yielding a clear solution and bright orange beads, indicating that RuBPS had fully adsorbed onto the surface of the Amberlite®. The estimated surface loading is therefore 1.2 $\mu\text{mol g}^{-1}$. This immobilisation consists of a simple counter-ion exchange wherein the RuBPS complex replaces the chloride ions, so the complex / support interaction is electrostatic rather than covalent.

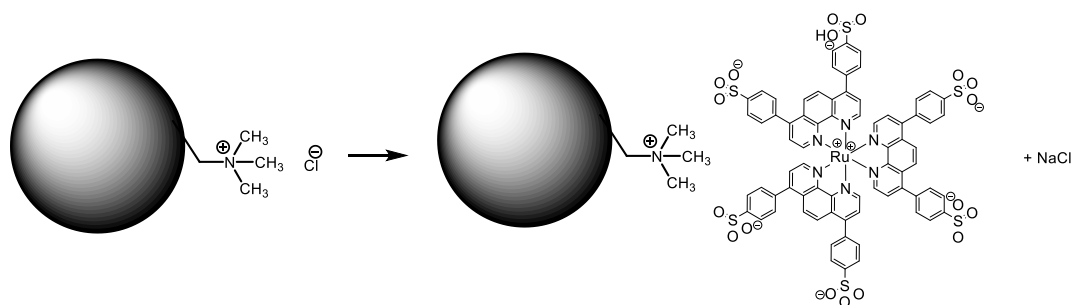


Figure 23 A simplified representation of Amberlite® IRA900 (left) and the subsequent cation exchange for immobilising the complex on the surface.

2.2.3.2 Characterisation

The material was characterised using solid state UV-Vis spectroscopy and luminescence spectroscopy. For this purpose, the dye-supported resin was ground down into a fine powder, as the bead size (0.5 mm) makes it inappropriate for solid-state spectroscopy.

2.2.3.2.1 Solid State UV-vis spectroscopy

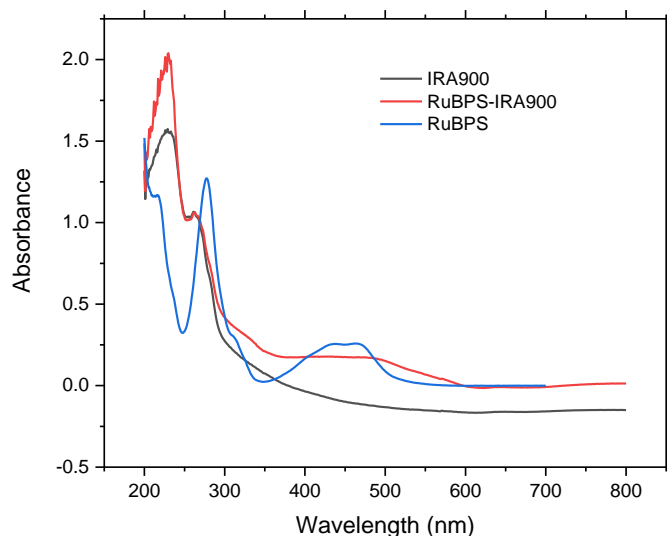


Figure 24 Overlay of solid state UV-vis spectra of the unfunctionalised Amberlite IRA900 (black), IRA900 functionalised with RuBPS (red), and solution state UV-vis spectrum of RuBPS in MeOH (red).

In order to achieve the appropriate consistency for solid state UV-vis spectroscopy, Ru-BPS functionalised Amberlite® beads (IRA900 and Ru-IRA900) were ground up into a fine powder using a mortar and pestle. The solid-state UV-vis spectrum of the complex on Amberlite® IRA900 (Fig. 24) and the solution-state spectrum of the complex in MeOH both have their MLCT absorbance peak at around 460 nm. This confirms that the complex is present on the surface of the material.

2.2.3.2.2 Solid state Luminescence spectroscopy

The emission of Ru-BPS at around 620 nm is clearly visible in the solid state emission spectrum of RuBPS-IRA900 (Fig. 25).

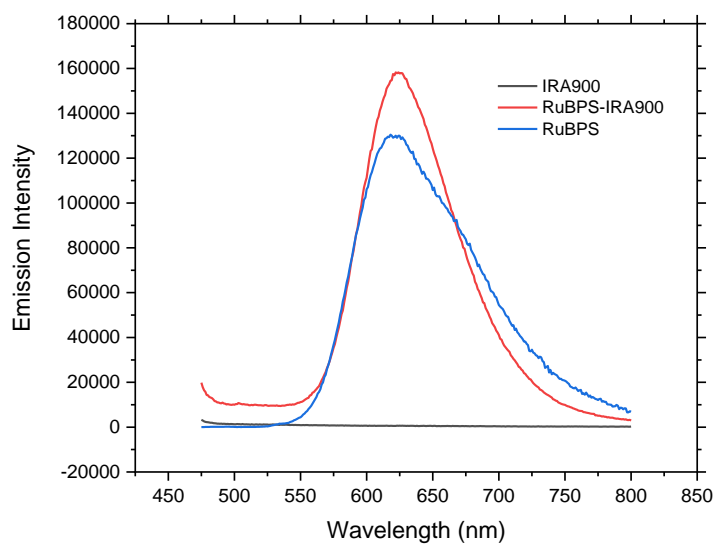
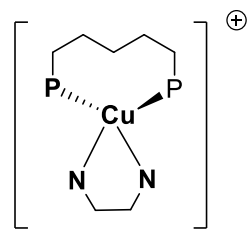


Figure 25 Solid-state Emission Spectrum of the complex supported on IRA900 (red) overlaid with the solution-state emission spectrum of RuBPS and unfunctionalised IRA900 (black).

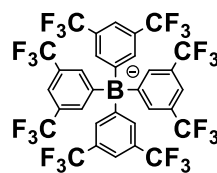
2.3 Copper Complexes

Copper complexes are of interest in the context of this thesis for good reasons: copper is significantly cheaper and more abundant than most transition metals and the complexes it forms can be synthesised in one or two steps at room temperature; and many Cu(I) complexes with diimine-type ligands have $^3\text{MLCT}$ excited-states that can generate $^1\text{O}_2$. Most Cu(I) polypyridyl complexes are however plagued by short excited state lifetimes. This is due to the tetrahedral excited state undergoing a flattening distortion, opening the complex for nucleophilic attack leading to coordination of a fifth ligand at the axial site which deactivates the excited state *via* non-emissive pathways.¹³ Recent studies have involved complexes with improved excited-state lifetimes which could be achieved through use of phenanthroline-xantphos mixed ligand complexes.^{14,15} The complex $[\text{Cu}(\text{xantphos})(\text{dmp})]\text{tfpb}$ (Fig. 26) was found to have a remarkably long excited-state lifetime of up to 30 μs and acted as an effective oxygen gas sensor: quenching of the luminescent $^3\text{MLCT}$ excited state by oxygen is indicative of singlet oxygen generation.

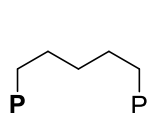
A persistent problem with $[\text{Cu}(\text{NN})(\text{PP})]^+$ photocatalysts, a weak absorbance in the visible region – seems a particularly difficult hurdle to overcome. Even modifications to ligands leading to redshifts in emission from the Cu(I) complexes of just 10 nm are often accompanied by shortening of excited state lifetime.¹⁶ Complications can also arise from ligand exchange in solution, with different ratios of homoleptic/heteroleptic complexes forming, depending on ligand choice.¹⁷ Thus, numerous $[\text{Cu}(\text{NN})(\text{PP})]^+$ complexes and materials have been synthesised and studied with regards to their $^1\text{MLCT}$ absorption band, singlet oxygen generating abilities, and bactericidal activity.



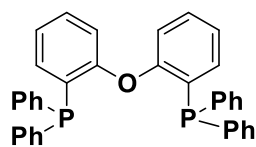
General Structure



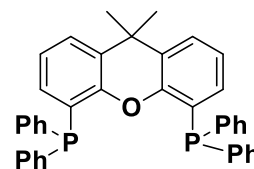
tfpb



=



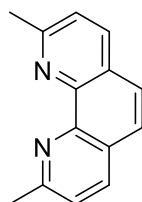
DPEPhos



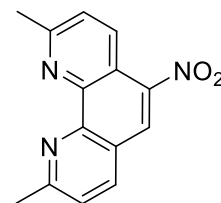
xant



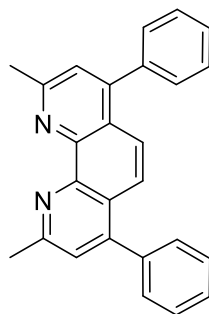
=



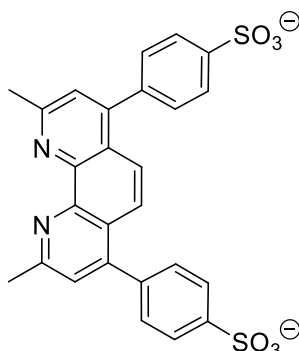
dmp



5N-dmp



BC



BCS

Figure 26 Nomenclatures of ligands attached to copper to form $\text{Cu}(\text{NN})(\text{PP})^+$.

2.3.1 Synthesis

[Cu(dmp)(xantphos)].tfpb was prepared according to the literature¹⁴, and the derivatives aside from the sulfonate complex were prepared under identical conditions. [Cu(NCMe)₄]BF₄ was dissolved in DCM and then equimolar amounts of the xantphos and phenanthroline derivatives were added sequentially, one hour apart. The complex was then precipitated from solution by addition to Et₂O. The reaction produces quantitative yields and a very pure product, however, for spectroscopic purposes both the tetrafluoroborate and tfpb salts were purified by chromatography on Sephadex LH20 in MeOH. The ¹H NMR of the tfpb salt of the complex is consistent with the structure of the complex. The aromatic region of the spectrum has 9 signals, one of them being an overlap of 2 with a sum of the peak integrals of 44, which is consistent with the number of aromatic hydrogen environments and total number of hydrogens on the salt (7 on the complex and 3 on the tfpb salt). There are also two clear singlets each of integration ratio 6 representing the methyl groups on the dmp and xantphos. The Mass Spectrum of the compound was found to be 849.6 for the M⁺ ion which is also consistent with literature values.

The sulfonate complex [Cu(bathocuproine sulfonate)(xantphos)]Na (Cu(BCS)(xant)) was prepared under similar conditions. The starting material [Cu(NCMe)₄]BF₄ was dissolved in MeCN along with xantphos, and the bathophenanthroline-sulfonate ligand in water. The two were combined slowly and stirred for an hour. The majority of the MeCN was then removed (down to 2 mL) under reduced pressure and the remaining solution triturated in Et₂O to afford the complex as a BF₄⁻ salt.

2.3.2 UV-visible and Luminescence spectra and Excited State Lifetime.

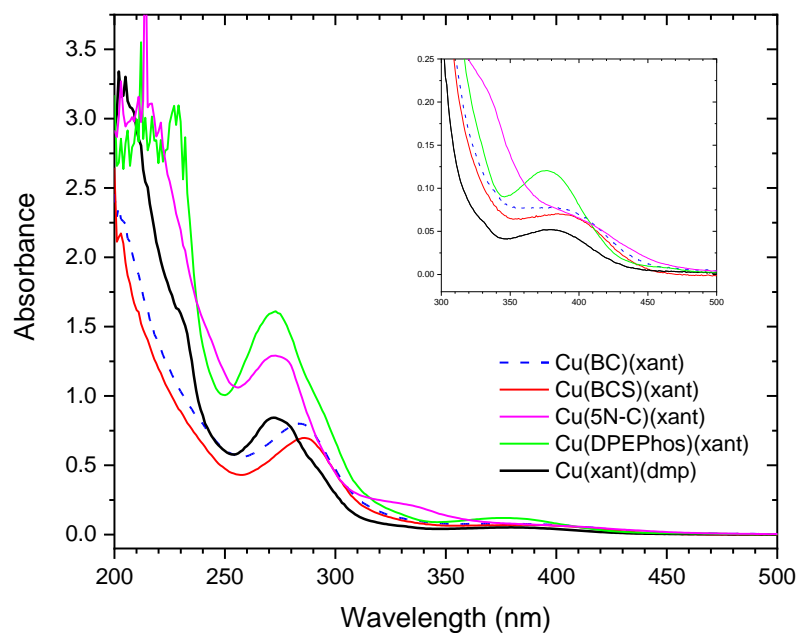


Figure 27 UV-Vis absorption spectra of the Cu(I) complexes in MeCN. (black) Cu(xant)(dmp). (blue dotted) Cu(BC)(xant). (red) Cu(BCS)(xant). (magenta) Cu(5N-C)(xant). (green) Cu(DPEPhos)(xant). Inlet graph is an expansion of the MLCT region around 400 nm.

The solution-state UV-vis spectra of the studied $[\text{Cu}(\text{PP})(\text{NN})]^+$ complexes (Fig. 27) show high-energy, high-intensity absorptions resulting from ligand-ligand $\pi^*-\pi$ transitions. Weak $^1\text{MLCT}$ absorptions due to transitions of an electron from the d^{10} Cu(I) ions to the π^* orbital of the phen-based ligand are present at around 370-400 nm. For uses in solar water disinfection this absorption band would ideally be redshifted further into the visible region. For this reason a number of derivatives have been tested in attempt to red-shift this $^1\text{MLCT}$ absorption band.

Complex	Absorbance		Emission $\lambda_{\text{max}}/\text{nm}$	Lifetime		
	$\lambda_{\text{max}}/\text{nm}$	$\epsilon / \text{M}^{-1} \text{cm}^{-1}$		$\tau_{\text{O}_2} / \text{ns}$	$\tau^{\text{a}} / \text{ns}$	$P_{\text{O}_2}^{\text{b}}$
Cu(dmp)(xant)	378	3820	568	63	112	0.44
Cu(BC)(xant)	390	7650	580	85	312	0.73
Cu(BCS)(xant)	390	7830	580	105	377	0.72
Cu(dmp)(DPEPhos)	353	3333	571	84	1023	0.92
Cu(5NC)(xant)	400	3055	550, 600	2.12	3.50	0.39

Table 4 Table of spectroscopic values for the synthesised $\{\text{Cu}(\text{NN})(\text{PP})\}^{\text{+}}$ complexes. All measurements taken in MeCN. Emission lifetime measurements taken by excitation utilising a 405 nm diode. a) Degassed through bubbling with argon for 30 minutes. b) $P_{\text{O}_2} = 1 - (\tau_{\text{O}_2}/\tau)$

Although only a small red shift of around 10 nm was achieved by the inclusion of phenyl or phenylsulfonate groups at the 4,7-positions on the phenanthroline, their addition did yield a doubling of the absorption intensity at that wavelength. This implies there is an increase in likelihood of excitation to the $^1\text{MLCT}$ excited state. Cu(5NC)(xant) shows an even greater redshift of the $^1\text{MLCT}$ maximum to around 400 nm. The low-energy shoulder on the $^1\text{MLCT}$ peak is also broader, extending to around 500 nm. This is due to the highly π -electron withdrawing nature of the nitro group, which lowers the energy of the LUMO, giving a lower energy $^1\text{MLCT}$ state. The addition of the nitro group did not affect the intensity of the absorption of the $^1\text{MLCT}$ band significantly. The excited state lifetimes of Cu(BC)(xant) and Cu(BCS)(xant) in degassed acetonitrile are also around three times longer than that of Cu(dmp)(xant). This may indicate a decrease in the k_{nr} value, and so phosphorescence quantum yield measurements must be made.

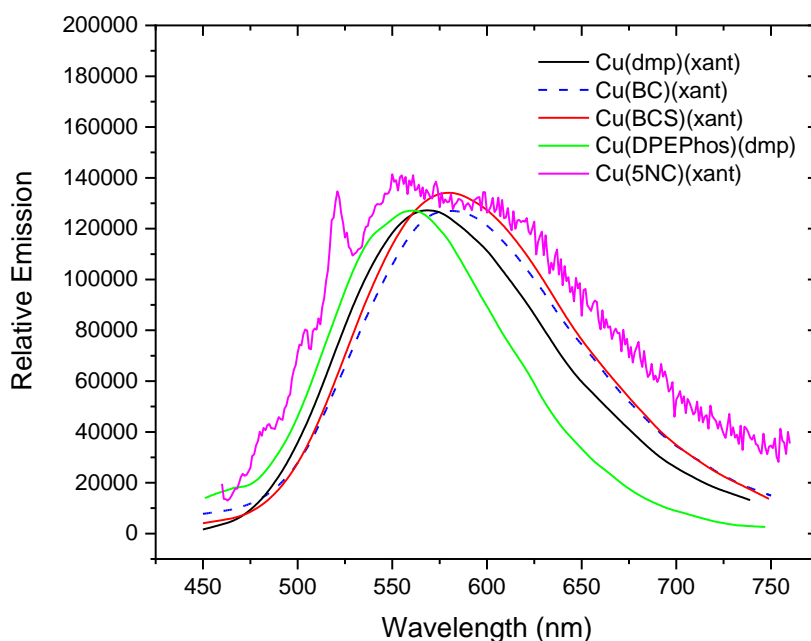


Figure 28 Emission spectra of Cu(I) complexes in MeCN at room temperature. (black) Cu(dmp)(xant), (blue dotted) Cu(BC)(xant), (red) Cu(BCS)(xant), (green) Cu(DPEPhos)(xant), (magenta) Cu(5NC)(xant). Excitation at respective absorbance maxima.

Solution-state emission spectra of the Cu(I) complexes are similar: a broad emission between 570-600 nm. The bathocuproin complexes show an emission around 10 nm longer than Cu(dmp)(xant). The complex [Cu(5NC)(xant)]tfpb showed a very weak, multimodal emission at around 550 and 600 nm (Fig. 28, magenta). Due to the very weak intensity of this emission, this reading was taken at very high concentrations of the compound. Thus, this bimodal emission may arise from the presence of more intensely emitting impurities in the sample. The lifetime of the emission at 550-600 nm is very short compared to the other {Cu(NN)(PP)}⁺ complexes ($\tau = 3.5$ ns). This shortening of the ³MLCT excited state lifetime can be explained by charge localisation on the strongly electron withdrawing NO₂ group, which leads to a charge separated state centred on the nitro group.¹⁸ The lowering in energy of the ¹MLCT absorption also indicates a shortening of the energy gap between the HOMO and the LUMO. Both of these factors should lead to an increase in likelihood of vibrational relaxation.¹⁶

2.4 Copper complexes adsorbed onto solid supports

2.4.1 Silica-bound Cu(xant)(dmp).tfpb (CuXD-CS)

2.4.1.1 Synthesis

Due to the insoluble, hydrophobic nature of [Cu(xant)(dmp)]tfpb, surface loading can be performed without covalently binding to the surface. [Cu(xant)(dmp)]tfpb was successfully attached to the surface of chromatography grade silica (40-60 mesh) utilising a dry-loading method: [Cu(xant)(dmp)]tfpb (20 mg, 0.011 mmol) was dissolved in DCM (5 mL), to which chromatography grade silica (1 g) was added and sonicated for 5 minutes. The solvent was then removed from the slurry utilising a rotary evaporator under reduced pressure. This afforded a pale yellow, free-flowing powder. No compound was found left attached to the reaction vessel which was washed with solvent and the washings tested by UV-vis spectroscopy. This indicates the complex had completely adsorbed onto the surface of the silica. The theoretical surface loading for this compound is $11 \mu\text{mol g}^{-1}$ (assuming total adsorption to the silica as 11 μmol of complex were used per gram of silica). This compound is abbreviated to CuXD-CS.

2.4.1.2 Characterisation

The compound CuXD-CS was characterised via solid state UV-visible spectroscopy and solid-state emission spectroscopy. While these methods cannot be used to quantify the amount of active complex on the surface of the compound, they can confirm the presence of the complex.

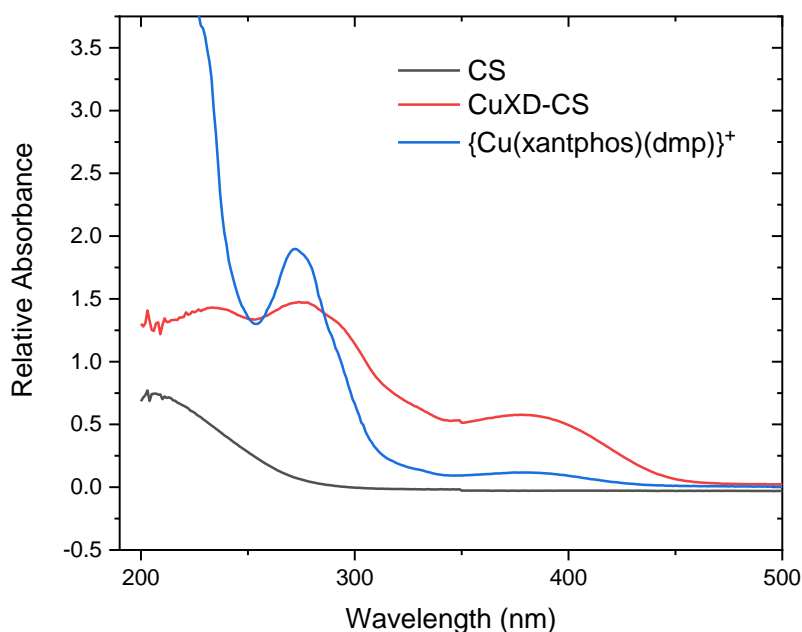


Figure 29 Overlaid UV-Vis absorption spectra of $\{Cu(xant)(dmp)\}^+$ (blue), CuXD-CS (red), CS (black). Spectrum for $\{Cu(xant)(dmp)\}^+$ performed in solution (MeCN). CuXD-CS and CS were performed in solid-state.

Figure 29 shows the solid state UV-Visible absorption spectrum of silica-bound CuXD-CS overlaid on the solution-state UV-Visible absorption spectrum of the complex $[Cu(xant)(dmp)]tfpb$ in solution. It is clear that they share the same profile, with both the MLCT band and the $\pi^*-\pi$ bands overlapping. Unfunctionalised chromatography-grade silica (CS) shows little to no absorption in these regions. The solid-state emission spectrum of CuXD-CS shows a blue shifted emission (544 nm) compared to $[Cu(xant)(dmp)]tfpb$ (569 nm). This may be a case of acetonitrile having an effect on the emission of the complex (solvatochromism) which does not occur in the solid state (rigidochromism). In solvent, the solvent molecules rearrange around the complex to suit the redistributed charge in the excited state, which lowers the 3MLCT state, hence a redshifted emission. This cannot occur in the solid state. It could also indicate changes in state energies due to interactions of the complex with the surface of the support.

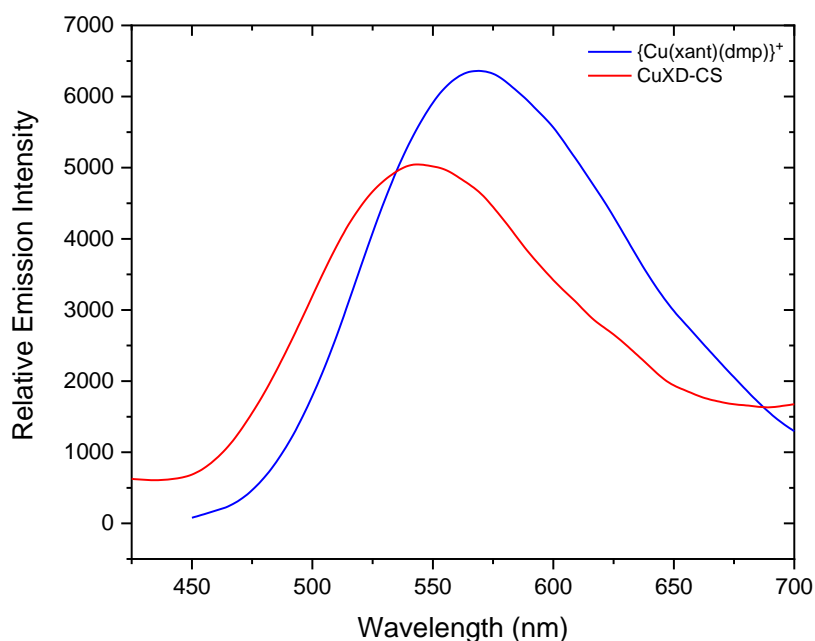


Figure 30 Overlaid emission spectra of $\{\text{Cu}(\text{xant})(\text{dmp})\}^+$ in MeCN (blue) and CuXD-CS (red). CuXD was measured in solution (MeCN), CuXD-CS was measured in the solid-state, both in air. Excitation wavelength 378 nm.

Results for all copper complexes produced from experiments performed together with Martin Appleby (mvappleby1@sheffield.ac.uk).

2.5 Conclusions

Numerous ruthenium polypyridyl complexes were synthesised and characterised through NMR spectroscopy, mass spectrometry and elemental analysis. The complexes exhibited the usual strong ¹MLCT absorptions in the visible region as well as high P_{O₂} values. These complexes have been immobilised to a number of supports utilising various methods of immobilisation: RuBS was covalently bound to silica and PDMS in order to reduce leaching of costly photosensitiser from the surface of the support; and RuBPS was bound electrostatically onto IRA900 a cationic polystyrene-based resin.

A series of Cu^I diimine diphosphine complexes [(Cu(NN)(PP)]⁺ was synthesised based on work by Smith et al.¹⁴ in order to produce a series of less-toxic and more economically viable alternative to the ruthenium polypyridyl complexes for use as singlet oxygen photosensitisers. The phenanthroline ligand on the complex was changed in the hopes of red-shifting the MLCT band of the complex with some success. The original complex, Cu(dmp)(xant).tfpb, was immobilised onto chromatography grade silica by dry loading.

We continue this work by testing all of the above compounds to determine their singlet oxygen generating abilities in the following chapter.

2.6 References

1. WEI, Hui (魏辉) DU, Yan(杜艳) KANG, Jian-Zhen(康建珍) XU, Guo-Bao*(徐国宝) WANG, E.-K. Tris (2 , 2 ' - bipyridyl) Ruthenium (II) Doped Silica Film Modified Indium Tin Oxide Electrode and Its Electrochemiluminescent Properties. *Chinese J. Chem.* **25**, 159–163 (2007).
2. Chen, H., Kuranari, S., Akiyama, T., Zhang, J. & Anpo, M. Synthesis, characterization and catalytic activities of μ -oxo-bridged binuclear iron complexes encapsulated in SBA-15. *J. Catal.* **257**, 215–220 (2008).
3. Kalyanasundaram, K. Photophysics, photochemistry and solar energy conversion with tris(bipyridyl)ruthenium(II) and its analogues. *Coord. Chem. Rev.* **46**, 159–244 (1982).
4. Dongyuan Zhao, Jianglin Feng, Q. H., Nicholas Melosh, Glenn H. Fredrickson, Bradley F. Chmelka, * & Galen D. Stucky*. Triblock Copolymer Syntheses of Mesoporous Silica with Periodic 50 to 300 Angstrom Pores. *Science (80-.)*. **279**, 548–552 (1998).
5. Thielemann, J. P., Girgsdies, F., Schlögl, R. & Hess, C. Pore structure and surface area of silica SBA-15: Influence of washing and scale-up. *Beilstein J. Nanotechnol.* **2**, 110–118 (2011).
6. Cassiers, K. *et al.* A Detailed Study of Thermal, Hydrothermal, and Mechanical Stabilities of a Wide Range of Surfactant Assembled Mesoporous Silicas. (2002). doi:10.1021/cm0112892
7. Ozkan, E., Allan, E. & Parkin, I. P. White-Light-Activated Antibacterial Surfaces Generated by Synergy between Zinc Oxide Nanoparticles and Crystal Violet. *ACS Omega* **3**, 3190–3199 (2018).
8. Manjón, F., Santana-Magaña, M., García-Fresnadillo, D. & Orellana, G. Singlet oxygen sensitizing materials based on porous silicone: photochemical characterization, effect of dye reloading and application to water disinfection with solar reactors. *Photochem. Photobiol. Sci.* **9**, 838–45 (2010).
9. Hu, S. *et al.* Surface modification of poly(dimethylsiloxane) microfluidic devices by ultraviolet polymer grafting. *Anal. Chem.* **74**, 4117–4123 (2002).
10. Zhang, J., Chen, Y. & Brook, M. A. Facile functionalization of PDMS elastomer surfaces using thiol-ene click chemistry. *Langmuir* **29**, 12432–12442 (2013).
11. Felip-León, C. *et al.* Superior performance of macroporous over gel type polystyrene as a support for the development of photo-bactericidal materials. *J. Mater. Chem. B* **5**, 6058–6064 (2017).
12. Alves, E. *et al.* Potential applications of porphyrins in photodynamic inactivation beyond the medical scope. *J. Photochem. Photobiol. C Photochem. Rev.* **22**, 34–57 (2014).
13. Miller, M. T., Gantzel, P. K. & Karpishin, T. B. Structures of the Copper(I) and Copper(II) Complexes of 2,9-Diphenyl-1,10-phenanthroline: Implications for Excited-State Structural Distortion. *Inorg. Chem.* **37**, 2285–2290 (1998).
14. Smith, C. S., Branham, C. W., Marquardt, B. J. & Mann, K. R. Oxygen gas sensing by luminescence quenching in crystals of Cu(xantphos)(phen)⁺ complexes. *J. Am. Chem. Soc.* **132**, 14079–14085 (2010).
15. Cuttell, D. G., Kuang, S. M., Fanwick, P. E., McMillin, D. R. & Walton, R. A. Simple Cu(I) complexes with unprecedented excited-state lifetimes. *J. Am. Chem. Soc.* **124**, 6–7 (2002).

16. Takeda, H., Monma, Y., Sugiyama, H., Uekusa, H. & Ishitani, O. Development of visible-light driven Cu(I) complex photosensitizers for photocatalytic CO₂ reduction. *Front. Chem.* **7**, 1–12 (2019).
17. Leoni, E. *et al.* Heteroleptic Copper(I) Complexes Prepared from Phenanthroline and Bis-Phosphine Ligands: Rationalization of the Photophysical and Electrochemical Properties. *Inorg. Chem.* **57**, 15537–15549 (2018).
18. Preiß, J. *et al.* How does peripheral functionalization of ruthenium(II)-terpyridine complexes affect spatial charge redistribution after photoexcitation at the Franck-Condon point? *ChemPhysChem* **16**, 1395–1404 (2015).
19. Rabilloud, T., Strub, J. M., Luche, S., van Dorsselaer, A. & Lunardi, J. A comparison between Sypro Ruby and ruthenium II tris (bathophenanthroline disulfonate) as fluorescent stains for protein detection in gels. *Proteomics* **1**, 699–704 (2001).

3 Singlet Oxygen Studies

Contents

3	Singlet Oxygen Studies.....	73
3.1	Introduction	75
3.2	Direct detection of singlet oxygen phosphorescence at 1275 nm	77
3.2.1	General Method.....	77
3.2.2	Ruthenium Complexes	80
3.2.3	Copper Complexes	83
3.3	Indirect method of determining $^1\text{O}_2$ quantum yield using a singlet oxygen sensor	84
3.3.1	General Method In Acetonitrile	85
3.3.2	General Method in Water.....	92
3.4	Conclusions	94
3.5	References	96

3.1 Introduction

Singlet oxygen ($^1\text{O}_2$) is the lowest excited state of molecular oxygen, formed by energy transfer to the triplet ground state, $^3\text{O}_2$. In this excited state oxygen is diamagnetic, allowing it to overcome the spin restrictions on redox reactions with most non-radical organic molecules.¹ This increases the reactivity of the molecule making it a strong oxidiser and electrophile and thus a reactive oxygen species (ROS). ROS have a well-documented antimicrobial activity,^{2,3} the most damaging ROS being the hydroxyl radical (HO^\bullet) and $^1\text{O}_2$. While there are many sources of $^1\text{O}_2$ we shall focus on that produced by photosensitisation.

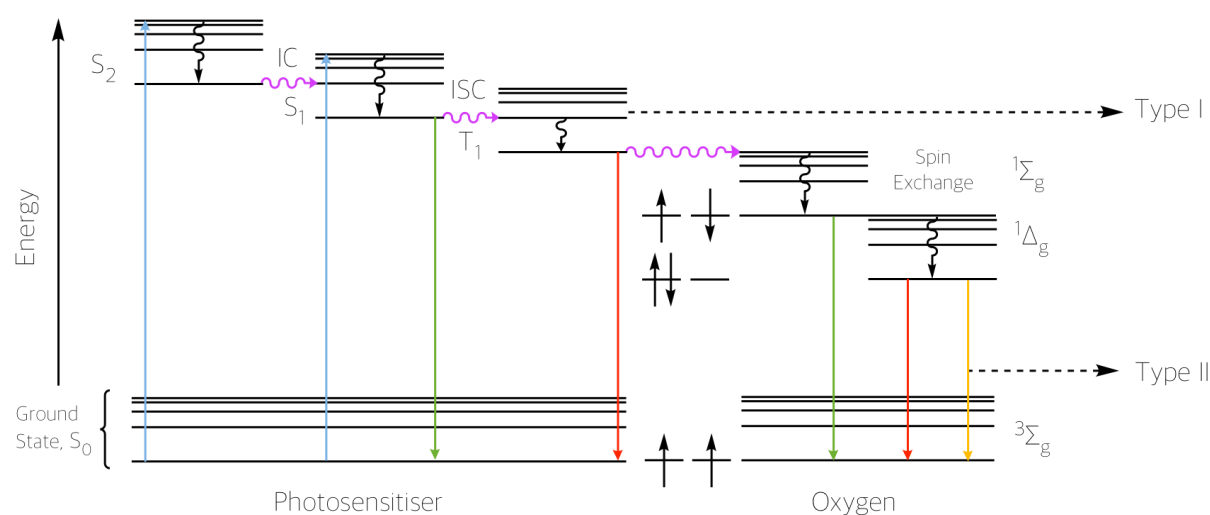


Figure 1 Jablonski diagram showing generation of photosensitiser excited states.

Photosensitised singlet oxygen is produced through energy transfer to triplet molecular oxygen by a triplet- excited state photosensitiser. The photosensitiser generally achieves excitation through one-photon excitation (excluding upconverting complexes) from ground state to a singlet excited state (S_n). This is followed by relaxation to the lowest singlet state (S_1) which then undergoes intersystem crossing to form the triplet excited state (T_1). Due to spin restrictions the T_1 lifetime is far longer than S_1 (μs compared to ns). The T_1 state can react with quenchers in two ways: Type I and Type II mechanisms. In a type I reaction the

photosensitiser reacts directly with the quenching substrate either by electron transfer or hydrogen abstraction, leading to production of radicals or radical ions such as the ROS hydroxide radical (HO^{*}) and superoxide radical anion (O₂^{•-}). Type II on the other hand involves energy transfer from interaction with the excited photosensitiser. These photoprocesses are described in terms of rate constants in chapter 1 (1.2.2.). To recap, singlet oxygen quantum yield (Φ_{Δ}) of a complex can be given as:

$$\Phi_{\Delta} = \Phi_T^{O_2} P_T^{O_2} f_{1O_2}^T \quad (1)$$

Where $\Phi_T^{O_2}$ is the quantum yield of triplet formation, $P_T^{O_2}$ is the proportion of excited triplet state quenched by molecular oxygen and $f_{1O_2}^T$ is the fraction of the molecular oxygen that quenches the excited state that produces singlet oxygen. In this study we are focusing on transition metal coordination complexes, which due to strong spin-orbit coupling, give a $\Phi_T^{O_2}$ of unity. Both $f_{1O_2}^T$ and $P_T^{O_2}$ can be described in terms of the sum of rates of quenching of the triplet state ($k_{TQ}^{O_2}$):

$$P_T^{O_2} = \frac{k_{TQ}^{O_2} [O_2]}{k_{TD} + k_{TQ}^{O_2} [O_2]} \quad (2)$$

$$f_{1O_2}^T = \frac{k_{en}}{k_{TQ}^{O_2}} \quad (3)$$

$P_T^{O_2}$ can be described in terms of excited state lifetimes in degassed (τ_{degas}) and aerated (τ_{O_2}) solutions

$$P_T^{O_2} = 1 - (\tau_{O_2} / \tau_{degas}) \quad (4)$$

This can also be done with $k_{TQ}^{O_2}$ in a Stern-Volmer relationship⁴ from steady state and time-resolved emission measurements:

$$\frac{I_{degas}}{I_{O_2}} = \frac{\tau_{degas}}{\tau_{O_2}} = 1 + k_{TQ}^{O_2} \tau_{degas} [O_2] \quad (5)$$

The rate-limited diffusion control for $k_{TQ}^{O_2}$ is around $10^{10} \text{ s}^{-1}\text{M}^{-1}$. Thus, there are multiple factors that determine a photosensitiser's ability to produce singlet oxygen. Some of these are easily measure or calculated. In this study, the excited state lifetimes in degassed and aerated solvents of each complex has been measured. The amount of singlet oxygen produced can be accurately measured and quantified thanks to singlet oxygen's phosphorescence at approximately 1275 nm.⁵ Through excitation of the photosensitiser in an air-equilibrated solution, the magnitude of the phosphorescence of generated singlet oxygen can be measured and compared to a standard, giving a singlet oxygen quantum yield (ϕ_{1O_2}). $P_T^{O_2}$ and $f_{1O_2}^T$ were calculated for each complex from the obtained lifetimes and singlet oxygen quantum yield.

3.2 Direct detection of singlet oxygen phosphorescence at 1275 nm

3.2.1 General Method

The method used was slightly modified from that reported by McKenzie et al..⁶ Singlet oxygen is detected directly by measurement of singlet oxygen phosphorescence ($\lambda_{em} \sim 1275 \text{ nm}$) following photo excitation of the compound at room temperature in air saturated solutions of methanol or acetonitrile.⁷⁻¹⁰ The third harmonic of a Q-SW Nd:YAG ($\lambda = 355 \text{ nm}$, $\sim 8 \text{ ns}$ pulse length, laser model Ls-1231M from LOTISII) is used to excite the compounds. The time-resolved signal of 1O_2 luminescence at 1275 nm was detected by a liquid-nitrogen cooled InGaAs photodiode of $\varnothing 3 \text{ mm}$ active area (J22D-M204-R03M-60-1.7, Judson Technologies). The output from the photodiode is coupled into a low-noise current amplifier (DLPCA-200, FEMTO Messtechnik GmbH), the amplifier output signal is recorded with a digital oscilloscope

(TDS 3032B Tektronix) and visualised on a computer via Ethernet connection. To selectively detect the $^1\text{O}_2$ emission, a high-contrast bandpass optical filter (1277 nm centre wavelength, 28 nm FWHM, custom-made by Izovac, Belarus) is fixed in front of the InGaAs photodiode. To increase light collection by the detector, a spherical broadband mirror is placed behind the sample to reflect the NIR emission through the sample towards the detector.

The optical densities of any studied compound and the standard are matched at 355 nm. The same solvent must be used for both the studied compound and the standard. The series of experiments is performed at set of different excitation energies ranging from 5 μJ to 100 μJ per pulse, and a kinetic trace collected for each measurement. The presented Φ_Δ values are obtained in low-energy limit, for which the decay of singlet oxygen emission can be mono-exponential (in the case that the compound shows no emission at ~ 1275 nm) or bi-exponential (in the case that the compound shows emission at ~ 1275 nm). The kinetic trace obtained was analysed by a mono- (equation 6) or biexponential (equation 7) decay using OriginPro ExpDecay1 or ExpDecay2 fitting functions respectively.

$$y = A_1 e^{-(x-x_0)/t_1} \quad (6)$$

$$y = A_1 e^{-(x-x_0)/t_1} + A_2 e^{-(x-x_0)/t_2} + y_0 \quad (7)$$

At each excitation power, the amplitude of the decay component (extrapolated to zero time) whose lifetime matches that of the $^1\text{O}_2$ emission in the solvent chosen is used as a measure of intensity of $^1\text{O}_2$ emission.

The quantum yield of singlet oxygen production (Φ_Δ) is determined by comparing the intensity of its emission extrapolated to zero time (the amplitude as described above) for the compounds and that of the standard (perinapthenone, $\Phi_\Delta = 95\%$ (DCM), $\approx 100\%$ (acetonitrile)).¹¹ Emission lifetime for $^1\Delta_g$ sensitised by the compounds and the standard must

be determined to be similar (within the range 70–90 μs usually for acetonitrile), indicating that $^1\Delta_g$ does not react with the photosensitiser in its ground state.

A correction is applied to the calculated initial intensities to adjust for discrepancies in the optical density of the compound and standard solutions at 355 nm. The correction factor takes into account the OD 355 values and produces comparable values:

$$\text{corrected initial amplitude} = \frac{\text{calculated amplitude}}{1 - 10^{-OD_{355}}} \quad (8)$$

Values for Φ_Δ are calculated at each power by the calculation:

$$\frac{\text{corrected initial intensity compound}}{\text{corrected initial intensity standard}} \times \text{standard } \Phi_\Delta \text{ in solvent} = \text{compound } \Phi_\Delta \quad (9)$$

More reliably, the yield of $^1\text{O}_2$ is determined by comparing the slope of a linear plot of initial intensity of emission vs. the light dose absorbed for the standard and the compound. Divergence of the plots of intensity vs laser energy from linearity usually indicates photobleaching of the compound, or a depletion of oxygen due to high efficiency of singlet oxygen production. As such, values at laser powers where divergence has taken place are not included in the final singlet oxygen quantum yield calculations. It is advisable to avoid excitation powers above 100 μJ per pulse as these divergences are more likely to occur.

This method cannot be used for suspensions, when the compound does not dissolve in the solvent of choice. Suspensions cause excessive scattering, making the singlet oxygen emissions undetectable. Φ_Δ for samples in water also cannot be measured on this set-up due to the short lifetime of $^1\text{O}_2$ in water (<10 microseconds), which is shorter than the detector response time.

3.2.2 Ruthenium Complexes

By comparison to perinaphthenone, RuBS shows a two-component decay trace at 1275 nm. This may be due to an emission by the complex itself at 1275 nm. This produces a bi-exponential singlet oxygen decay (Fig. 2). This can likely be expected of all ruthenium complexes herein.

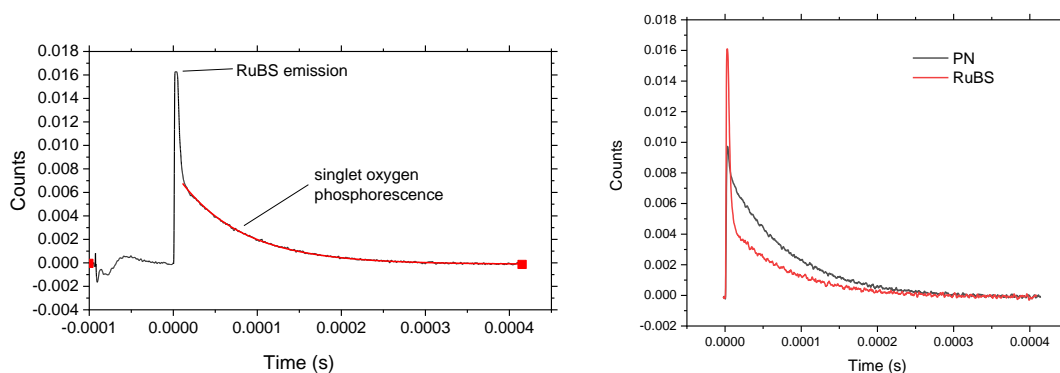


Figure 2 Left: Decay trace of detected emission at 1270 nm of RuBS, Right: Comparison of decay traces of singlet oxygen phosphorescence produced by perinaphthenone (PN) and RuBS

The quantum yield of production of singlet oxygen in acetonitrile with RuBS as a sensitiser was calculated using the above method. The singlet oxygen quantum yield was calculated to be 55% with perinaphthenone as a standard (Fig. 2). This quantum yield is slightly lower than for $\text{Ru}(\text{bpy})_3\text{Cl}_2$ but still falls within the error (Table 1). We would expect a higher singlet oxygen quantum yield from RuBS, due to larger difference between degas and aerated emission lifetimes and greater phosphorescence quantum yield than $\text{Ru}(\text{bpy})_3\text{Cl}_2$. These factors increase the probability of a successful sensitisation encounter between the complex and molecular oxygen. The difference between the two complexes lies in the substituent amide groups on the linking ligand. The effects of these substituents on the electronic properties of the complex are likely numerous. Not only is the complex more likely to undergo relaxation of the excited state via interaction with solvent, but the singlet oxygen

produced is also more likely to interact with its generating molecule(s), in particular with the amide N-H.¹²

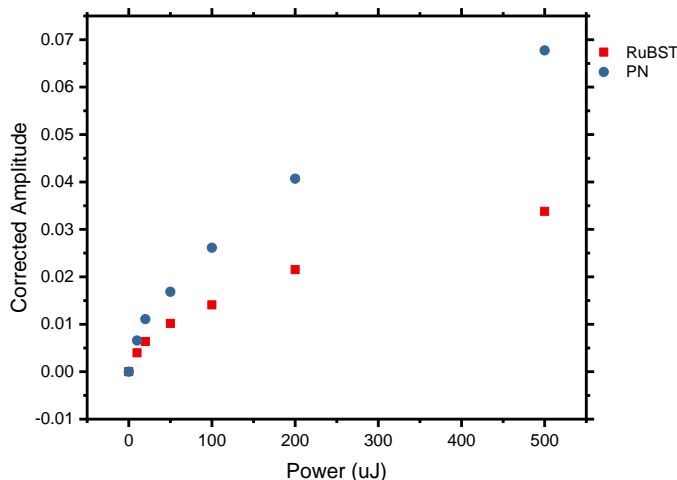


Figure 3 Amplitude of singlet oxygen emission at 1275 nm (extrapolated to zero time) as a function of laser excitation energy at 355 nm with an 8 ns pulse. Performed in acetonitrile.

A plateauing in singlet oxygen production with increase of laser power can be seen in Figure 3. This effect can be explained by two factors: the sample reaches saturation point, the concentration of the solution (OD) being too low to absorb the photons passing through the sample; and the high power causing the sample to degrade along the laser path (as the sample is not stirred and each reading consists of 512 repeat pumps of laser radiation).

Complex	Absorbance		Emission		Lifetime					
	λ_{\max} (nm)	ϵ ($M^{-1}cm^{-1}$)	λ_{\max} (nm)	Φf	τ_{O_2} (μs)	τ_{degas} (μs)	$P_T^{O_2}$	$f_{1O_2}^T$ ^b	$k_{TQ}^{O_2} \times 10^9$ ^c ($M^{-1}s^{-1}$)	Φ_{Δ} ^d
{Ru(bpy) ₃ } ²⁺	450	14600	625	0.062 ^a	0.16	0.87	0.82	0.70	2.11	0.57 ¹³ ± 0.4
RuBS	455	16000	650	0.141	0.35	1.17	0.70	0.78	0.83	0.55 ± 0.03
RuBMS	460	17500	650	0.153	0.334	1	0.67	0.90	0.82	0.60 ± 0.04
RuPS	440	14200	650	0.268	0.307	3.18	0.90	0.97	1.22	0.88 ± 0.03

Table 1 Singlet oxygen quantum yield data for the synthesised Ruthenium Complexes, the data for $\{Ru(bpy)_3\}^{2+}$ are shown for comparison. All measurements performed in spectroscopy grade MeCN. a) Fluorescence quantum yield for reference taken from literature¹⁴. b) calculated assuming the quantum yield for triplet excited state formation is 1 in transition metal complexes. c) $k_{TQ}^{O_2}$ values calculated considering $[O_2]$ in MeCN is 2.42 mM. d) Quantum yields calculated using perinaphthenone as a standard in MeCN, assuming it has a quantum yield of 1.

RuBMS was designed to test whether the amide N-H bond played a large role in singlet oxygen quenching. By changing the amide from a secondary to a tertiary amide, the reactivity towards singlet oxygen should decrease, thereby reducing the amount of generated singlet oxygen quenched by the complex itself.

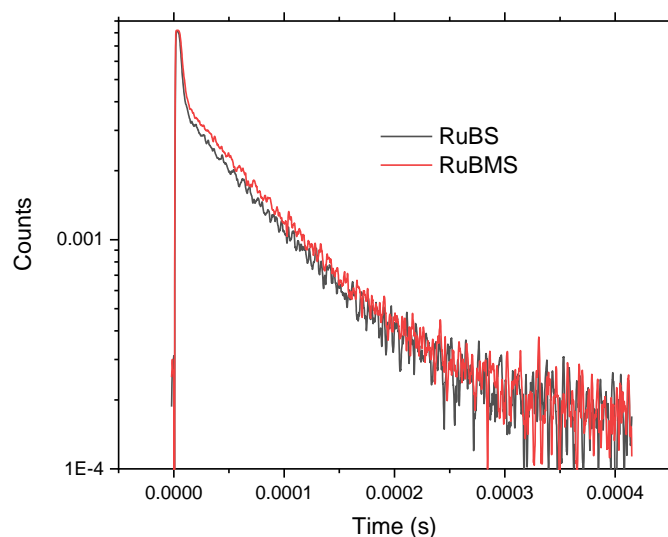


Figure 4 Graph comparing singlet oxygen phosphorescence decay kinetics detected at 1275 nm of RuBS (black) and RuBMS (red) in MeCN. Laser excitation at 355 nm with an 8 ns pulse.

The measured value for the singlet oxygen quantum yield for RuBMS 5% higher than for RuBS, however, they both fall within error. Additionally, by comparing the decay traces of singlet oxygen phosphorescence of RuBS and RuBMS (Figure 4) the lifetimes of the two traces are the same. If the singlet oxygen were being quenched by the amide N-H after generation, the phosphorescence lifetime would be shorter. Thus, N-H may have a small role in reducing singlet oxygen quantum yield but not by a statistically significant amount.

RuPS shows the highest value for Φ_{Δ} , which is consistent with its large $P_T^{O_2}$. This is due to the increased rigidity of the phenanthroline with respect to bipyridine, which makes the molecule less likely to undergo an excited state-relaxing distortion, thus reducing k_{TD} , which in turn increases $P_T^{O_2}$.

3.2.3 Copper Complexes

[Cu(dmp)(xant)]tfpb and [[Cu(dmp)(DPEPhos)]tfpb were reported to have good oxygen sensing abilities in the solid state.¹⁵ Thus their singlet oxygen quantum yields in solution were tested in order to compare their effectiveness as photosensitisers, along with the newly synthesised [Cu(BC)(xant)]⁺ and [Cu(BCS)(xant)]⁺ (Table 2). The singlet oxygen quantum yield for [Cu(dmp)(xant)]⁺ was measured to be 30% \pm 4% in air-equilibrated acetonitrile, utilising PN (Φ_{Δ} =100%) as a standard. Given that [Cu(dmp)(xant)]⁺ has a high proportion of the excited state quenched by molecular oxygen ($P_T^{O_2}$ =0.71), the singlet oxygen quantum yield is relatively low, giving a low fraction of the molecular oxygen that quenches the excited state that produces singlet oxygen ($f_{1O_2}^T$ = 0.42). This implies there may be other reactive oxygen species being produced from the quenching of the [Cu(dmp)(xant)]⁺ excited by ground state oxygen.

Complex	Absorbance		Emission	Lifetime		$P_T^{O_2}$	$f_{1O_2}^T$ ^a	$k_{TQ}^{O_2} \times 10^9$ ^b ($M^{-1}s^{-1}$)	Φ_Δ ^c
	λ_{max} (nm)	ϵ ($M^{-1}cm^{-1}$)	λ_{max} (nm)	τ_{O_2} (ns)	τ_{degas} (ns)				
{Cu(dmp)(xant)} ⁺	378	3820	568	63	220	0.71	0.42	4.72	0.30 ± 0.04
{Cu(BC)(xant)} ⁺	390	7650	580	85	312	0.73	0.56	3.57	0.41 ± 0.03
{Cu(BCS)(xant)} ⁺	390	7830	580	105	377	0.72	0.58	2.86	0.42 ± 0.08
{Cu(dmp)(DPEPhos)} ⁺	353	3333	517	84	1023	0.92	0.44	4.55	0.40 ± 0.09

Table 2 Singlet oxygen quantum yields (ϕ_{1O_2}) in MeCN and relevant spectroscopic data of copper complexes. a) calculated assuming the quantum yield for triplet excited state formation is 1 in transition metal complexes. b) $k_{TQ}^{O_2}$ values calculated considering $[O_2]$ in MeCN is 2.42 mM. c) Quantum yields calculated using perinaphthenone as a standard in MeCN, assuming it has a quantum yield of 1.

The singlet oxygen quantum yield for [Cu(dmp)(DPEPhos)]⁺ is higher, as expected due to its high $P_T^{O_2}$, derived from solution state time-dependent emission studies. Like [Cu(dmp)(xant)]⁺, this quantum yield gives a small $f_{1O_2}^T$ of 0.44, indicating other ROS may be produced under irradiation. While [Cu(dmp)(DPEPhos)]⁺ presents a more efficient photosensitiser of singlet oxygen than [Cu(dmp)(xant)]⁺ it is impaired by a poor absorption in the visible, which limits its use under sunlight.

The complexes made with phenyl groups at the 4,7- positions on the dmp ([Cu(BC)(xant)]⁺, [Cu(BCS)(xant)]⁺) showed a greater singlet oxygen quantum yield, however within error. This may be due to the phenyl groups creating a more rigid ligand, reducing the rate of excited state deactivation by vibrational relaxation. This is also reflected in the increased emission lifetime in degassed solvent. An increased singlet oxygen quantum yield paired with an intense, redshifted MLCT absorption makes these complexes promising candidates for bactericidal studies.

3.3 Indirect method of determining 1O_2 quantum yield using a singlet oxygen sensor

Disinfection of drinking water requires the photosensitiser to be easily removable from solution. Through immobilisation this can become trivial, whilst also allowing reusability of the photosensitiser, and often, improving the photosensitiser's chemical and photostability.¹⁶

Unlike in the method above, for immobilised photosensitisers, singlet oxygen must be measured indirectly, as light scattering makes it impossible to use the direct method of detecting singlet oxygen phosphorescence. Utilising a singlet oxygen probe, one can quantify singlet oxygen produced by an insoluble compound in suspension, or compounds in water. The method relies on activating luminescence of the $^1\text{O}_2$ sensor: a molecule that is not emissive in its native state but undergoes irreversible transformation into an emissive form upon interaction with singlet oxygen. Another mechanism is to measure the changes in the absorption spectra of a known compound which irreversibly reacts with singlet oxygen.

3.3.1 General Method In Acetonitrile

The singlet oxygen generating ability of a compound is measured via the monitoring the rate of deactivation of a singlet oxygen trap. For measurements in MeCN the stock $^1\text{O}_2$ sensor solution is made using 9,10-dimethylanthracene (DMA) (Sigma Aldrich). This compound has a strong absorbance between 300 – 420 nm; upon reaction with singlet oxygen it forms an endoperoxide which no longer absorbs in this region. No appreciable reaction of DMA was observed in the absence of illumination or the PS.¹⁷

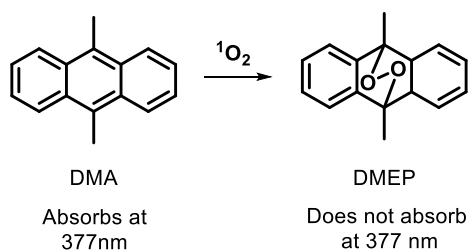


Figure 5 Deactivation of the UV-active singlet oxygen probe DMA to form the endoperoxide DMEP.

5 mg of DMA are dissolved in 10 mL of acetonitrile to give a 2.4 mM solution. 100 μ L of this stock solution then dissolved in 2.4 mL of acetonitrile to give a working concentration of 96 μ M. 5 mg of the PS is added to the cuvette and the mixture stirred whilst being exposed to 455 nm light from a diode (Thorlabs M455L4), set to 1.5 mWcm⁻² and placed 10 cm away from the cell and was shone through a windowed cell holder (1 cm diameter). The absorbance intensity of DMA between 300 – 420 nm is recorded utilising a UV-vis spectrophotometer (Agilent, Varian, or Cary 50 Bio). The rate of deactivation of the probe is measured by plotting the decrease in absorbance at a chosen wavelength against time of exposure.

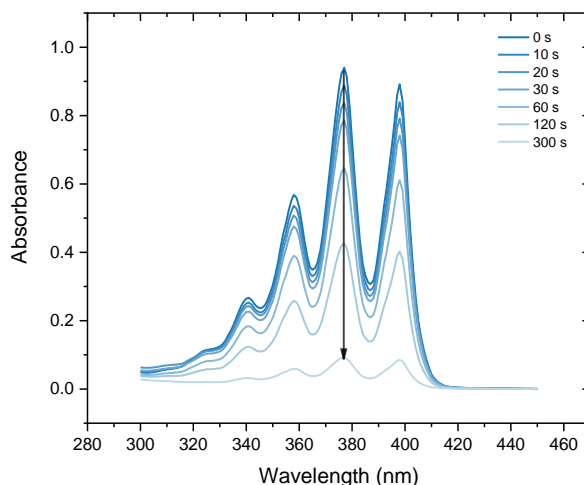


Figure 6 Graph showing destruction of a DMA probe via singlet oxygen production by RuBS immobilised on CS. The black arrow highlights the reduction in absorbance of the probe

Assuming the PS triplet and singlet states are not quenched by the singlet oxygen trap, the reaction can be characterised as a Stern-Volmer relationship (Equation 3).



This represents a second order reaction with two reactant species. The rate of deactivation of DMA can be considered equivalent to the rate of production of singlet oxygen

$$\frac{-d[DMA]}{dt} = \frac{-d[{}^1O_2]}{dt} = k_r^A [DMA][{}^1O_2] \quad (11)$$

However, the production of singlet oxygen is constant over time and is dependent on illumination power (I_a) and singlet oxygen generating ability (Φ_Δ) of the material.

$$\frac{-d[DMA]}{dt} = I_a \Phi_\Delta k_r^A [DMA] \quad (12)$$

Thus the kinetics can be reduced down to a pseudo-first order interaction

$$\frac{-d[DMA]}{dt} = k' [DMA] \quad (13)$$

And the integrated rate law can be considered.

$$[DMA] = [DMA]_0 e^{-k't} \quad (14)$$

$$\ln \frac{[DMA]}{[DMA]_0} = -k't \quad (15)$$

As the concentration of DMA is monitored via the optical density of the solution, we can employ the Beer-Lambert law

$$\ln \frac{A}{A_0} = -k't \quad (16)$$

By plotting the change of concentration as a function of the dose absorbed in the format

$$y = mx + c \quad (17)$$

We can derive a value for the pseudo-first order rate constant ($-k'$) (Figure 7).

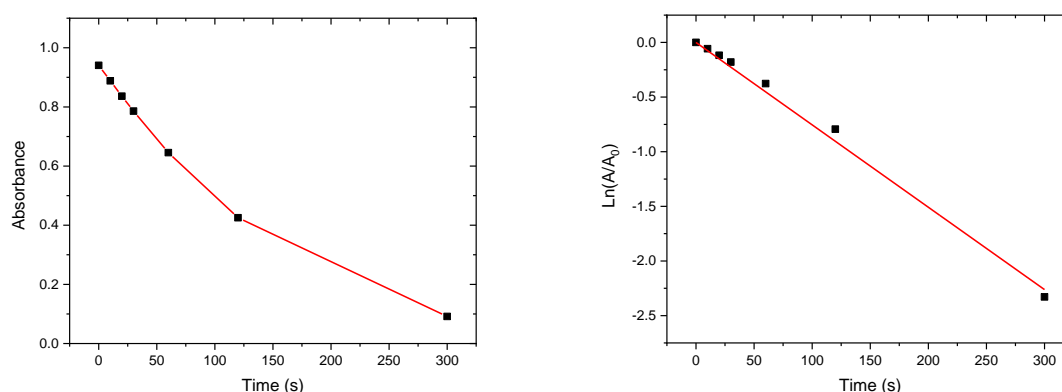


Figure 7 A: Graph showing destruction of the DMA by singlet oxygen through decrease in its absorbance over time. B: Graph plotting the natural logarithm of the absorbance at each exposure time over the absorbance at time zero. We note that the trap does not absorb 455-nm light.

3.3.1.1 RuBS on Silica

From figure 7 we can derive the rate constant for each material. This can give us a quantitative value for the singlet oxygen producing ability, which can be used to compare with other materials tested under the same conditions. By measuring rate of probe destruction with materials of varying surface coverage, it is evident that rate increases with surface coverage (Fig. 8).

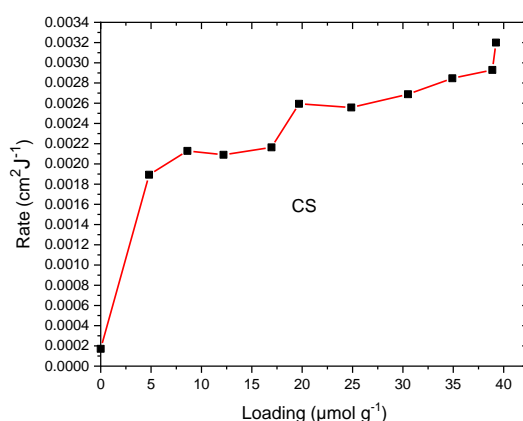


Figure 8 The rate of destruction of DMA against loading of chromatography grade silica (CS) by RuBS.

The first point on the plot is the value for silica with no dye attached, which does produce singlet oxygen at a very small rate. The following point is the lowest surface coverage

produced, which has the highest rate per mole of dye – the higher surface coverages only slightly increase the rate of singlet oxygen production. This may be the consequence of three possible phenomena:

- The coverage of the support by the PS has already passed monolayer coverage. This would mean a certain proportion of the immobilised photosensitiser is no longer in contact with oxygen.
- The material reaching the diffusion rate of oxygen to- or singlet oxygen away from the material.
- Aggregation of the PS on the surface of the support causing. Aggregation-induced self-quenching, which occurs in dye-sensitised solar cells.¹⁸

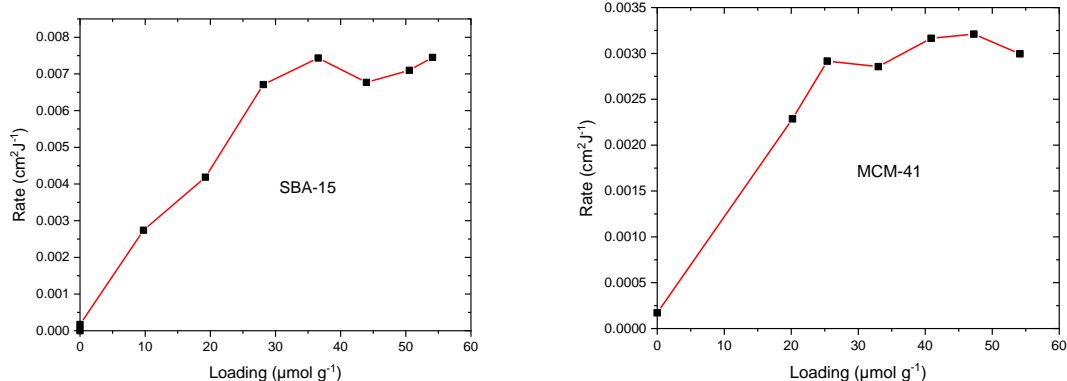


Figure 9 Graphs showing relation between rate of degradation of DMA and surface loading on the silica by the PS (RuBS).

As can be seen by Figure 3.8, the singlet oxygen production rate of both types of mesoporous silica plateaus at around $30 \mu\text{mol g}^{-1}$, with SBA-15 giving over two times the rate the other types of silica. Even at lower surface loadings of $20 \mu\text{mol g}^{-1}$, the SBA-15 material shows twice the rate of singlet oxygen production of the other two materials. The main difference between these supports is their porosity; SBA-15 has a larger pore size compared to MCM-41 (8 nm compared to 4.5 nm), whilst having a comparatively low surface area (450-

550 m²/g compared to around 1000 m²/g). This may mean the singlet oxygen is able to diffuse through the pores more effectively than in MCM-41.

The chromatography-grade silica, with the lowest surface area and no porosity, reaches a plateau on singlet oxygen production at a low loading in comparison to SBA-15 and MCM-41. This is consistent with the theory that multiple layers of PS are forming on the surface of the support.

3.3.1.2 *[Ru(BPS)₃]Na₄ on Amberlite IRA-900 (RuBPS-IRA900)*

Ruthenium tris(disodium bathophenanthroline sulfonate) was supported on Amberlite IRA-900, a macroporous polystyrene anion exchange resin. The resin, in comparison to chromatography-grade silica, is formed of large spherical beads (<0.5 mm in diameter). These beads are very easily removed from solution; however, they have the lowest surface area of the particulate supports and the lowest incident light capture per mole of complex.

A larger sample size of 25 mg was utilised for RuBPS-IRA900 as it was impossible to accurately weigh out 5 mg of the sample. Otherwise the experiments were run under the same conditions as for the silica-based materials. RuBPS-IRA900 shows the lowest OBSERVED rate of singlet oxygen generation among the supported ruthenium polypyridyl-based materials. This comes down to the overall smaller surface area of the material, its opacity and bead weight. The rate of singlet oxygen generation per mole of complex for RuBPS-IRA900 is the highest among the solid-supported photosensitisers, making it the most efficient compound made.

Due to the larger particle size of the material compared to silica, it has a much smaller surface area (22 m² g⁻¹ compared to >400 m² g⁻¹), meaning a smaller proportion of the bound

photosensitiser is being exposed to the light. The opacity of the resin also means that light does not pass through the sample, meaning a shadow is cast onto any particles behind it. As the beads weigh more, it becomes increasingly difficult to create a suspension than with the silica-based samples. However, this setback can be overcome by increasing the scale of the reaction and utilising a more diffuse light source.

Material	$\lambda_{\max}(\text{nm})$	Loading		$k_{\max} (\text{s}^{-1})$	Conc ^c (M)	$k'_M (\text{s}^{-1}\text{M}^{-1})$
		$(\mu\text{molg}^{-1})^a$	Probe ^b			
[Ru(bpy) ₃]Cl ₂	450	-	DMA	2.28E-03	1.75E-06	1.30E+03
RuBS-CS	455	34	DMA	3.20E-03	8.00E-05	4.00E+01
RuBS-SBA	455	36	DMA	7.44E-03	7.44E-05	1.00E+02
RuBS-MCM	455	47	DMA	3.21E-03	9.45E-05	3.40E+01
RuBPS-IRA900	460	1.2	DMA	2.93E-04	1.20E-06	2.44E+02
RuBS-PDMS	455	-	DMA	2.32E-04	-	-

Table 3 Values for rate of DMA destruction by each material. Performed in MeCN under irradiation by a 455 nm diode power density 1.5 mWcm⁻². a) Loading is number of moles of active complex per gram of support. b) Probe concentration of 1 mM. c) "Concentration" represents the number of moles of active complex per litre of reaction medium.

3.3.1.3 RuBS-PDMS

The experiment for the RuBS-bound PDMS film was performed by shining 455 nm diode onto the film from above from 10 cm away, with a stirrer bar on the surface. Although the observed rate of singlet oxygen production is the smallest on this support, it still nearly matches that of the IRA900 sample, meaning it has a high singlet oxygen considering its surface area. A contributing factor to this may be that light is shining on the entire functionalised surface at once. Although the extent of surface functionalisation is unknown, this material will have the greatest efficiency (by mole of functionalised photosensitiser) for singlet oxygen production.

3.3.2 General Method in Water

For the copper compounds, the experiments need to be carried out in water, as acetonitrile strips the complex off the surface. For this, a different probe was used: the commercial probe Singlet Oxygen Sensor Green (SOSG). SOSG is a widely-used water soluble, highly-selective singlet oxygen probe composed of an anthracene moiety connected to a fluorescein moiety.¹⁹ The unreacted probe does not normally emit at 525 nm, as the fluorescein excited state undergoes intramolecular photoelectron transfer quenching from the attached anthracene. The anthracene moiety reacts readily with singlet oxygen producing an endoperoxide (SOSG-EP), which cannot quench the fluorescein moiety, resulting in an emission at 525 nm. There are drawbacks to the use of SOSG in light dependent studies, namely that not only have studies demonstrated that SOSG itself generates singlet oxygen under exposure to 255 and 532 nm light,¹⁹ but that the resulting SOSG-EP produces singlet oxygen with an even greater efficiency.²⁰ Despite this it is one of the few singlet oxygen probes that is suitable for this experiment, given that its absorbance does not overlap with that of the photosensitisers being tested.

For these experiments the same methodology can be used as for the DMA probe by replacing Absorbance of the probe in the kinetics with the Emission Intensity. This can give a relative rate constant. A 405 nm diode was used to illuminate the copper complexes (Thorlabs M405L4), set to 1.5 mW cm⁻² and placed 10 cm away from the cell. A 455 nm diode (Thorlabs M455L4) was used for the [Ru(bpy)₃]Cl₂ standard, set to 1.5 mW cm⁻² and placed 10 cm away from the cell.

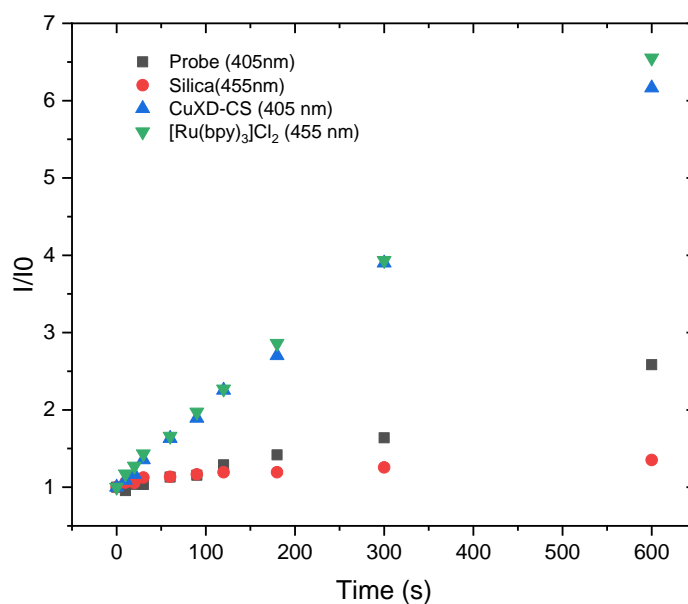


Figure 10 Rates of oxidation of the singlet oxygen probe Singlet oxygen sensor green (SOSG) (Thermofischer) over time in deionised water in the presence of a photosensitising compound under illumination by either 405 or 455 nm light. $[Ru(bpy)_3]Cl_2$ used as a standard for singlet oxygen production.

Figure 10 shows the results of the singlet oxygen generation assay utilising SOSG as a probe to indirectly measure the singlet oxygen generation of $[Cu(xantphos)(dmp)]tfpb$ dry-loaded onto chromatography-grade silica (40-60 mesh) (CuXD-CS) in water. $[Ru(bpy)_3]^{2+}$ in solution was used as a standard. The probe on its own in water as well as the probe and unfunctionalised chromatography grade silica were run as controls. SOSG on its own under illumination by 405 nm light does see an increase in emission. This is due to SOSG itself generating a small amount of singlet oxygen, which it itself then reacts with. The rate of singlet oxygen production also seems to increase, which is consistent with studies reporting that SOSG-EP produces more singlet oxygen than the unreacted probe. The unfunctionalised silica showed a smaller rate of singlet oxygen production, likely due to the silica particles increasing the opacity of the solution.

The estimated rate of singlet oxygen production per mole of complex per litre of solvent of CuXD-CS in water as a suspension under illumination by 405 nm light (1.5 mW cm^{-2}) was calculated to be $1.58 \times 10^2 \text{ s}^{-1} \text{ M}^{-1}$. This is of a similar magnitude to the rates of singlet oxygen production by the ruthenium polypyridyl complexes supported on silica in Table 3.

Material	$\lambda_{\text{max}}(\text{nm})$	Loading		Probe	$k_{\text{max}} (\text{s}^{-1})$	Conc ^c (M)	$k'_M (\text{s}^{-1}\text{M}^{-1})$
		$(\mu\text{molg}^{-1})^a$					
[Ru(bpy) ₃]Cl ₂	450	-		SOSG	9.17E-03	1.50E-06	6.11E+03
CuXD-CS	387	11		SOSG	8.69E-03	5.50E-05	1.58E+02

Table 4 Characterisation and singlet oxygen generation rates utilising the probe Singlet oxygen sensory green. Illuminated utilising a 405 nm and 445 nm diode for CuXD-CS and [Ru(bpy)₃]Cl₂ respectively both at power density 1.5 mWcm^{-2} . a) Loading is number of moles of active complex per gram of support. b) a 1 cm^2 surface was used, under 455 nm irradiation. c) "Concentration" represents the number of moles of active complex per litre of reaction medium

3.4 Conclusions

The singlet oxygen generating abilities of the compounds synthesised and characterised in chapter 2 were successfully quantified through two main methods: direct measurement of singlet oxygen phosphorescence at 1275 nm for compounds in solution and indirect measurement by measuring degradation of a singlet oxygen probe over time for supported compounds.

The compounds in solution all proved to be suitably efficient photosensitisers of singlet oxygen ($0.30 < \Phi_{\Delta} < 0.88$). Immobilisation of RuBS and [Cu(xant)(dmp)]tftp onto chromatography grade silica yielded materials that produce singlet oxygen when illuminated by laser-light near their respective MLCT absorption bands (455 and 405 respectively both with a power density of 1.5 mWcm^{-2}), albeit with a fraction of the efficiency of the homogenous photosensitisers in solution. These compounds are tested for bactericidal efficacy in the following chapter.

RuBS-PDMS showed a relatively high rate of singlet oxygen generation given its low surface area and has a similar rate of degradation of DMA as other film-type photosensitiser by Alvarez et al ($>10^4 \text{ s}^{-1}$).²¹ This may be a promising material for use in a flow system, such as that designed by Fresnadillo et al.²²

RuBPS-IRA900 showed the lowest rate of singlet oxygen generation out of the tested compounds, whilst also having the highest singlet oxygen producing efficiency per mole of active complex. This may be due to its awkward particle size, and may perform better in a scaled-up reaction.

Results for all copper complexes produced from experiments performed together with Martin Appleby (mvappleby1@sheffield.ac.uk).

3.5 References

1. Krumova, K., Cosa, G., Aubry, J. & Kanofsky, J. R. Section I: Fundamentals. *Singlet Oxyg. Appl. Biosci. Nanosci.* 1–4 (2016). doi:10.1039/9781782620389-00001
2. Vatansever, F. *et al.* Antimicrobial strategies centered around reactive oxygen species - bactericidal antibiotics, photodynamic therapy, and beyond. *FEMS Microbiol. Rev.* **37**, 955–989 (2013).
3. Blum, H. F. *Photodynamic action and diseases caused by light.* (1941).
4. Union, I., Pure, O. F. & Chemistry, A. Glossary of terms used in EFTA. *EFTA Bull.* **1**, 15–18 (1985).
5. Schweitzer, C. & Schmidt, R. Physical mechanisms of generation and deactivation of singlet oxygen. *Chem. Rev.* **103**, 1685–1757 (2003).
6. McKenzie, L. K. *et al.* Metal Complexes for Two-Photon Photodynamic Therapy: A Cyclometallated Iridium Complex Induces Two-Photon Photosensitization of Cancer Cells under Near-IR Light. *Chem. - A Eur. J.* **23**, 234–238 (2017).
7. Shavaleev, N. M. *et al.* Deep-red luminescence and efficient singlet oxygen generation by cyclometalated platinum(II) complexes with 8-hydroxyquinolines and quinoline-8-thiol. *Inorg. Chem.* **45**, 9410–9415 (2006).
8. Ogilby, P. R. & Foote, C. S. Chemistry of Singlet Oxygen. 36. Singlet Molecular Oxygen ($^1\Delta_g$) Luminescence in Solution following Pulsed Laser Excitation. Solvent Deuterium Isotope Effects on the Lifetime of Singlet Oxygen. *J. Am. Chem. Soc.* **104**, 2069–2070 (1982).
9. Hurst, J. R., McDonald, J. D. & Schuster, G. B. Lifetime of Singlet Oxygen in Solution Directly Determined by Laser Spectroscopy. *J. Am. Chem. Soc.* **104**, 2065–2067 (1982).
10. Parker, J. G. & Stanbro, W. D. Optical Determination of the Collisional Lifetime of Singlet Molecular Oxygen [$O_2(^1\Delta_g)$] in Acetone and Deuterated Acetone. *J. Am. Chem. Soc.* **104**, 2067–2069 (1982).
11. Schmidt, R., Tanielian, C., Dunsbach, R. & Wolff, C. Phenalenone, a universal reference compound for the determination of quantum yields of singlet oxygen $O_2(^1\Delta_g)$ sensitization. *J. Photochem. Photobiol. A Chem.* (1994). doi:10.1016/1010-6030(93)03746-4
12. Darmanyan, A. P., Jenks, W. S. & Jardon, P. Charge-transfer quenching of singlet oxygen $O_2(^1\Delta_g)$ by amines and aromatic hydrocarbons. *J. Phys. Chem. A* **102**, 7420–7426 (1998).
13. Abdel-shaḍ, A. A., Beer, P. D., Mortimer, J. & Wilkinson, F. Photosensitized generation of singlet oxygen from ruthenium (II) -substituted benzoaza-crown-bipyridine complexes. 3137–3144 (2000).
14. Caspar, J. V. & Meyer, T. J. Photochemistry of $Ru(bpy)_3^{2+}$. Solvent Effects. *J. Am. Chem. Soc.* **105**, 5583–5590 (1983).
15. Smith, C. S., Branham, C. W., Marquardt, B. J. & Mann, K. R. Oxygen gas sensing by luminescence quenching in crystals of $Cu(xantphos)(phen)^+$ complexes. *J. Am. Chem. Soc.* **132**, 14079–14085 (2010).
16. Guo, Y., Rogelj, S. & Zhang, P. Rose Bengal-decorated silica nanoparticles as photosensitizers for inactivation of gram-positive bacteria. *Nanotechnology* **21**, 065102 (2010).

17. Albitar, E., Alfaro, S. & Valenzuela, M. A. Photosensitized oxidation of 9,10-dimethylanthracene with singlet oxygen by using a safranin O/silica composite under visible light. *Photochem. Photobiol. Sci.* **14**, 597–602 (2015).
18. Patwari, J., Sardar, S., Liu, B., Lemmens, P. & Pal, S. K. Three-in-one approach towards efficient organic dye-sensitized solar cells: Aggregation suppression, panchromatic absorption and resonance energy transfer. *Beilstein J. Nanotechnol.* **8**, 1705–1713 (2017).
19. Kim, S., Fujitsuka, M. & Majima, T. Photochemistry of singlet oxygen sensor green. *J. Phys. Chem. B* **117**, 13985–13992 (2013).
20. Gollmer, A. *et al.* Singlet oxygen sensor green®: Photochemical behavior in solution and in a mammalian cell. *Photochem. Photobiol.* **87**, 671–679 (2011).
21. Alvarez, M. G., Gómez, M. L., Mora, S. J., Milanesio, M. E. & Durantini, E. N. Photodynamic inactivation of *Candida albicans* using bridged polysilsesquioxane films doped with porphyrin. *Bioorganic Med. Chem.* **20**, 4032–4039 (2012).
22. García-Fresnadillo, D. Singlet Oxygen Photosensitizing Materials for Point-of-Use Water Disinfection with Solar Reactors. *ChemPhotoChem* **2**, 512–534 (2018).

4 Bacteria Experiments

Contents

4	Bacteria Experiments	98
4.1	Introduction	100
4.2	General Method for the bacterial inactivation assay	102
4.3	Bacterial viability tests on <i>S. aureus</i> and <i>E. coli</i> utilising RuBS-CS under 455 nm light.....	103
4.4	Bacterial viability tests on <i>S. aureus</i> and <i>E. coli</i> utilising CuXD-CS under 405 nm light.	107
4.5	Conclusions and future work	112
4.6	References	114

4.1 Introduction

Singlet oxygen is an electronically excited state of molecular oxygen that can react with a host of biologically relevant molecules.¹ This property makes it an ideal candidate for the killing of microbes, be it in drinking water or in the human body, with no lasting harmful effects. Photodynamic inactivation is the killing of bacteria through photosensitised generation of singlet oxygen and has been in use for over a century.² Even so, the mode by which singlet oxygen actually kills bacteria is not yet fully understood. Inside cells, singlet oxygen causes damage to a multitude of essential parts of the cell including proteins, lipids and DNA,^{3,4} leading to tissue destruction and apoptosis/necrosis.⁵ For use in drinking water disinfection, however, photosensitisers that can be removed from solution after the disinfection must be used, necessitating use of photosensitisers bound to solid supports. In these scenarios the PS cannot accumulate inside the bacteria. The drawback in this case is that singlet oxygen is produced in the bulk solution outside the bacterial cell, potentially reducing the efficacy of bacterial killing. More recent studies have shown that photodynamic effects can be seen with PSs acting from outside the cell, however the efficiency of the PS is reduced by virtue of this.⁶⁻¹⁰

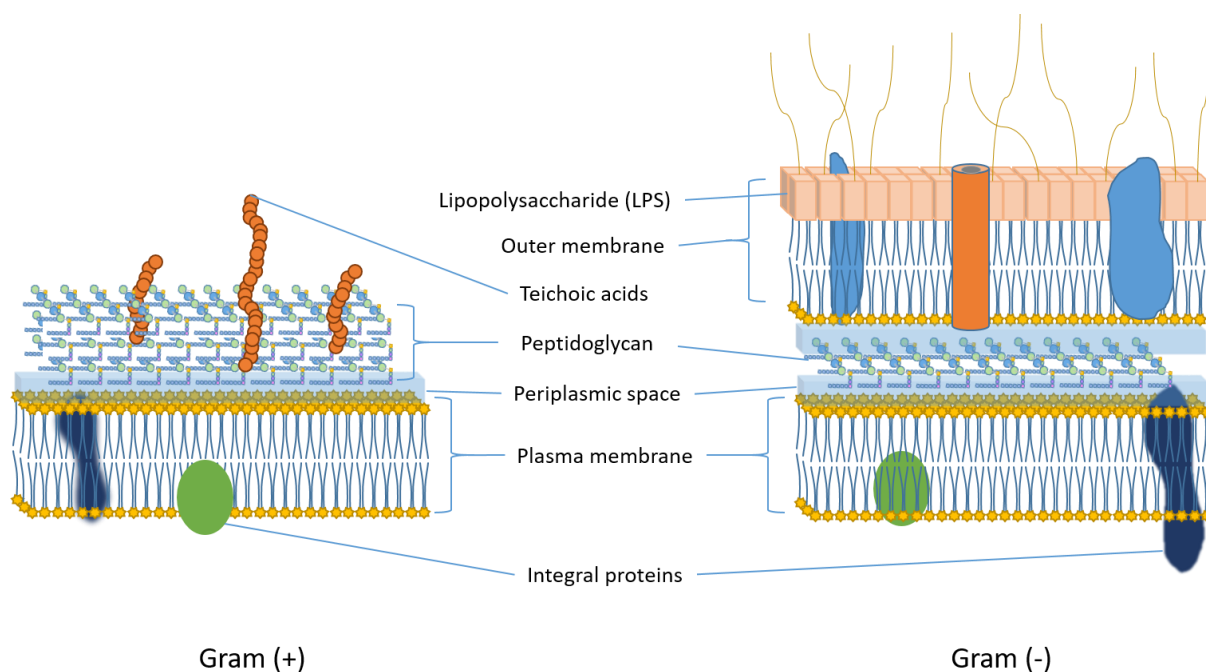


Figure 1 Cell wall structure of Gram positive (+) and Gram negative (-) bacteria.

Bacteria can generally be classified into two large groups: Gram(-) and Gram(+). These names are derived from how they respond to the Gram stain test, which distinguishes the two types of bacteria based on their cell wall composition.¹¹ Gram(+) bacteria possess an inner lipid membrane and a thick layer of relatively porous, mesh-like peptidoglycan on their outer cell wall (Figure 1), which is stained purple by the dye Crystal Violet. Gram(-) bacteria on the other hand possess two lipid membranes sandwiching a thinner peptidoglycan layer, with the outer membrane possessing a lipopolysaccharide (LPS) coat which does not retain crystal violet, and thus tests negative to the Gram stain test. Examples of bacteria Gram(+) are *Staphylococcus (S.) aureus*, *Listeria (L.) monocytogenes* and *Bacillus (B.) anthracis*. Some examples of Gram(-) bacteria are *Escherichia (E.) coli*, *Salmonella* and, *Legionella*. The presence of the additional LPS in Gram(-) bacteria acts as a physical and chemical barrier that allows the bacteria to survive in harsher conditions, such as in mammalian digestive tracts. This also makes penetration of foreign agents far less likely, hindering the accumulation of PS inside the bacteria and making treatment generally more difficult. These factors result in Gram(+) bacteria generally showing higher sensitivity towards photodynamic inactivation compared to Gram(-) bacteria. Owing to its chemical composition, the outer wall holds a net negative charge making Gram(-) bacteria anionic.^{12,13} Gram(+) bacteria also hold a net negative, albeit weaker, charge due to teichoic acids (Figure 1) that stud the peptidoglycan layer

Singlet oxygen possesses a short lifetime (3 μ s) in water,^{14,15} and thus has a very short diffusion distance of *ca.* 200 nm.¹⁶ Therefore, the photosensitiser and the bacteria must be close together for photo-generated singlet oxygen to be able to interact with the bacteria. The net negative surface charge of the bacterial wall may hold the answer to this challenge: through the use of cationic supports, bacteria can be attracted to the active surface of the photosensitising material, bringing it into the effective radius of action of singlet oxygen. This method has been successfully applied in, for example, functionalised cationic exchange resin Amberlite IRA900¹⁷ and cationic porous PDMS functionalised with ruthenium complex photosensitisers¹⁸⁻²⁰. Numerous cationic amphiphilic polymers without a photocatalyst have also had success at killing bacteria without use of photosensitisers.^{21,22}

In this study two potentially antibacterial metal complexes synthesised during this project, RuBS and CuXD, were immobilised onto chromatography grade silica (RuBS-CS and CuXD-CS) and tested for their antibacterial activity. Both materials were found to produce satisfactory quantities of singlet oxygen in solution upon irradiation (Chapter 3).

4.2 General Method for the bacterial inactivation assay

The sample of solid-supported photosensitising complex was thoroughly washed with ethanol or water before being dried in a vacuum oven at 80 °C overnight. A pellet of the wild type bacterial strain (WT) was suspended in phosphate buffered saline (PBS) solution and distributed across the appropriate number of six – well plates in batches of 3 mL (total capacity of each well is 5 mL). For every assay exposed to light, an equivalent dark assay was set up. The desired mass of the sample powder for each well was weighed out and added. The plates were then placed on an agitator with a 450 or 405 nm LED array (built on-site) hanging 10 cm above the base of the plates; with the power arriving at the samples being 2.40 and 17.5 mW cm⁻² respectively. In the course of irradiation, at chosen time intervals a small sample of each assay was removed and immediately serially diluted (dilution by 10 times). Each dilution at chosen interval was performed in triplicate. These samples were then pipetted onto freshly set agar plates and the cultures were incubated at 37 °C overnight before counting final colony-forming units (CFU mL⁻¹).

4.3 Bacterial viability tests on *S. aureus* and *E. coli* utilising RuBS-CS under 455 nm light.

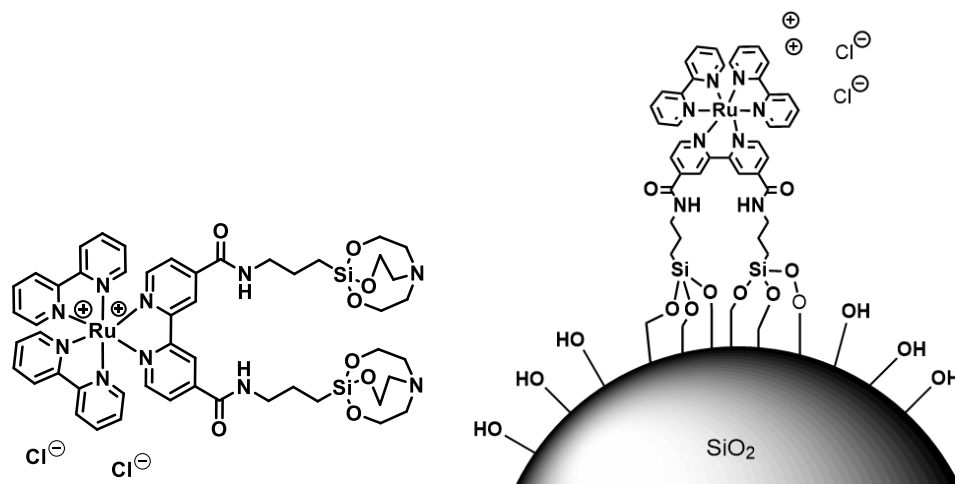


Figure 2 Structures of RuBS (left) and RuBS covalently bound to silica (RuBS-CS) (right)

The complex $[\text{Ru}(\text{bpy})_2(\text{bipy-silatrane})]\text{Cl}_2$ (RuBS, Figure 2) was designed as a photosensitiser with the ability to be covalently bound to the surface of a silica support as a way of reducing leaching and thus increasing the reusability of the photosensitising compound. RuBS was successfully bound to chromatography grade silica (40-60 mesh, Sigma Aldrich) (CS), a cheap, robust powder with high surface area and good chemical and photo-stability (Chapter 2). RuBS has good absorbance in the visible region ($\lambda_{\text{max}} = 455 \text{ nm}$), and has a good singlet oxygen quantum yield (0.55 ± 0.1) in solution, and retains the ability to produce singlet oxygen when immobilised on silica (chapter 3).

Initial bacterial viability assays were performed utilising silica with a surface loading of $20 \mu\text{mol g}^{-1}$ by RuBS. *S. aureus* and *E. coli* were used as common infectious bacteria of the Gram(+) and Gram(-) types, respectively. RuBS-CS showed no killing of either type of bacteria under exposure to 2.5 mW cm^{-2} light, or in the absence of light, over 3 hours. This may be as a result of the dissolution of the silanol groups in water above pH 4 which impart the surface

of the silica with a net negative charge.²²⁻²⁴ This may prevent the bacteria from aggregating close to the surface of the functionalised silica particles.

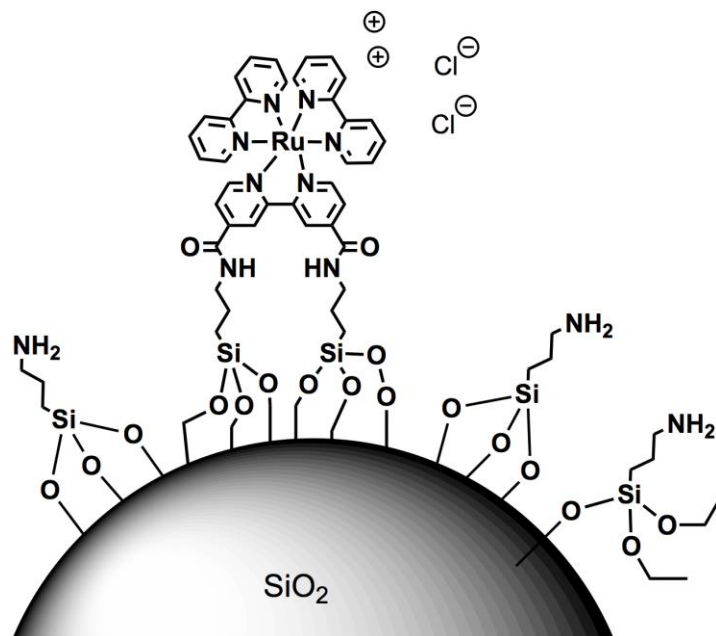


Figure 3 Proposed surface structure of of RuBS-CS-NH₂

The material was thus post-modified with aminopropyl-triethoxysilane (APTES) to make RuBS-CS-NH₂ (Figure 3). APTES functionalisation has found success with TiO₂ and Silica nanoparticles.^{25,26} APTES was covalently grafted to the surface to introduce amine groups that would give the silica surface a less negative surface charge, making it more attractive environment for bacteria and thereby bringing PS and bacteria closer together.

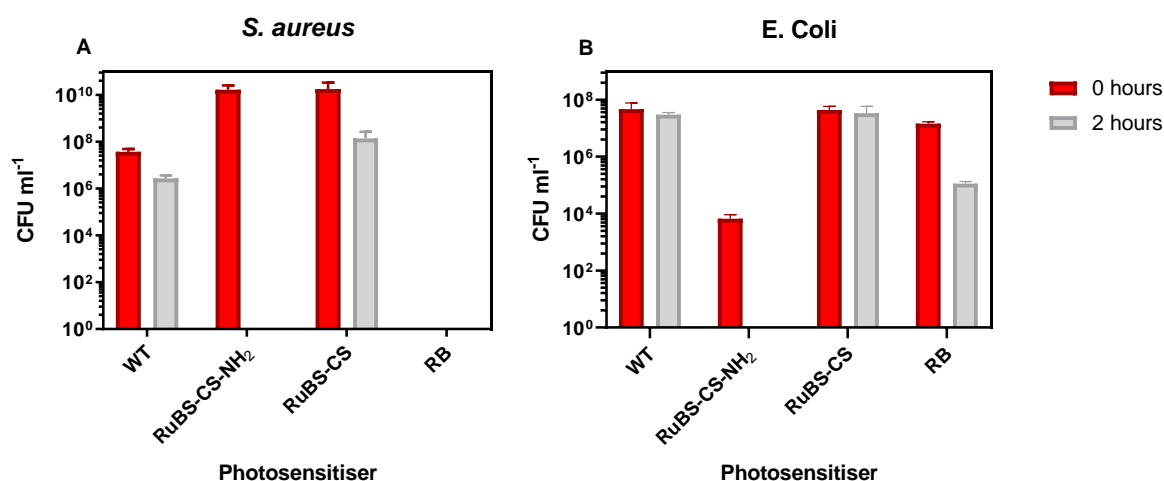


Figure 4 Bacterial viability assays testing the reduction in viability of *S. Aureus* (A) and *E. coli* (B) colonies in the presence of RuBS-CS, RuBS-CS-NH₂ at a concentration of 5 mgmL⁻¹ in NaPhos buffer and Rose Bengal (RB) (50 μM) as a positive control. Viability checked before and after illumination with 2 hours of 455 nm light at 2.4 mW cm⁻². Error bars indicate measurement of each interval was performed in triplicate.

The results are shown in figure 4. Colony forming units (CFUs) are a unit used to estimate viable cells capable of forming a colony. Thus, CFU ml⁻¹ represents the concentration of viable bacteria cells in solution. Wild Type strains of *S. aureus* and *E. coli* in NaPhos buffer were used as controls, represented by WT in Figure 3. Rose Bengal (50 μM) (RB) in solution was utilised as a positive control for photosensitised bactericidal activity, as it has been shown to be an effective antimicrobial photosensitiser for numerous bacterial strains including both *S. aureus* and *E. coli*.^{27–35}

Neither RuBS-CS nor RuBS-CS-NH₂ displayed dark toxicity against *S. aureus* at a concentration of 5 mg mL⁻¹ after 10 minutes of incubation. Irradiation with 455 nm light (2.4 mW cm⁻², 2 hr) without the presence of the photosensitiser caused less than 1-log reduction in *S. aureus* but showed no adverse effects on *E. coli*. Rose Bengal showed abnormally strong dark toxicity in *S. aureus* after 10 minutes of incubation, killing 10-log₁₀ to below the detection limit (2-log₁₀). Other studies have not found RB to show dark toxicity towards *S. aureus*.³⁶ These results may be due to the Rose Bengal deactivating all of the *S. aureus* in the short time

it takes to set up the experiment, under irradiation from laboratory lighting. The way to limit this is by setting these samples up in a dark room.

Illumination of suspensions of *S. aureus* at 455 nm (2.4 mW cm^{-2}) for 2h in the presence of RuBS-CS (5 mg mL^{-1}) led to reduction of colony forming units to 10^{-2} of the original number (2-log_{10} killing). However, the same treatment did not affect the growth of *E. coli*. Overall, RuBS-CS is not a promising antibacterial agent. However RuBS-CS-NH₂ showed much better results: 2 hours of illumination at 455 nm (2.4 mW cm^{-2}) of both solutions of *S. aureus* and of *E. coli* in the presence of RuBS-CS-NH₂ (5 mg mL^{-1}) led to a reduction to below the detection limit (2-log_{10}) by 1 million times (6-log_{10}). The results show a dramatic increase in bactericidal activity upon functionalisation of the photosensitising compound with APTES.

Subsequent batches of the material RuBS-CS-NH₂ did not yield the same results and were unable to reduce the number of colony-forming units at all in the two repeats of the above experiment. The only variable changed between these experiments was the material, which was freshly synthesised for each assay via the same method. We do not have an explanation for this effect, but it may be possible that (despite dark controls remaining healthy) there was something wrong with the batch of bacteria used, or with their incubation conditions, for the experiments which showed dramatic (6-log) killing. This challenging reproducibility led us to move away from Ru-based photosensitisers.

4.4 Bacterial viability tests on *S. aureus* and *E. coli* utilising CuXD-CS under 405 nm light.

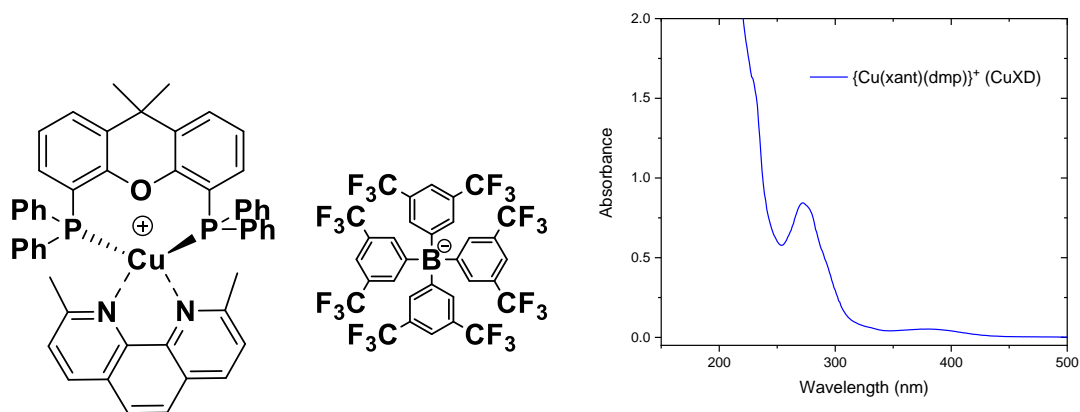


Figure 5 CuXD and its UV-vis absorbance spectrum

$\{Cu(xant)(dmp)\}tfpb$ (CuXD) (Figure 5) is a hydrophobic photosensitiser that was immobilised on chromatography-grade silica (40-60 mesh) (CS) by dry loading (as described in chapter 2 and 5). Both the supported (CuXD-CS) and unsupported (CuXD) compound were tested for bactericidal activity on wild type *S. aureus* and wild type *E. coli*. Assays were performed with varying exposure time, concentration, and both with and in the absence of a support. All illuminations were performed under a 405 nm lamp with power density 17.4 mW cm⁻². This wavelength was chosen as it is close to the complexes' MLCT absorbance maximum of 378 nm (Chapter 2) but still, just, within the visible spectrum. Methylene Blue (MB) was utilised as a positive control for bactericidal activity, numerous studies have shown its photoinactivation of bacteria including *S. aureus* and *E. coli*.²⁴

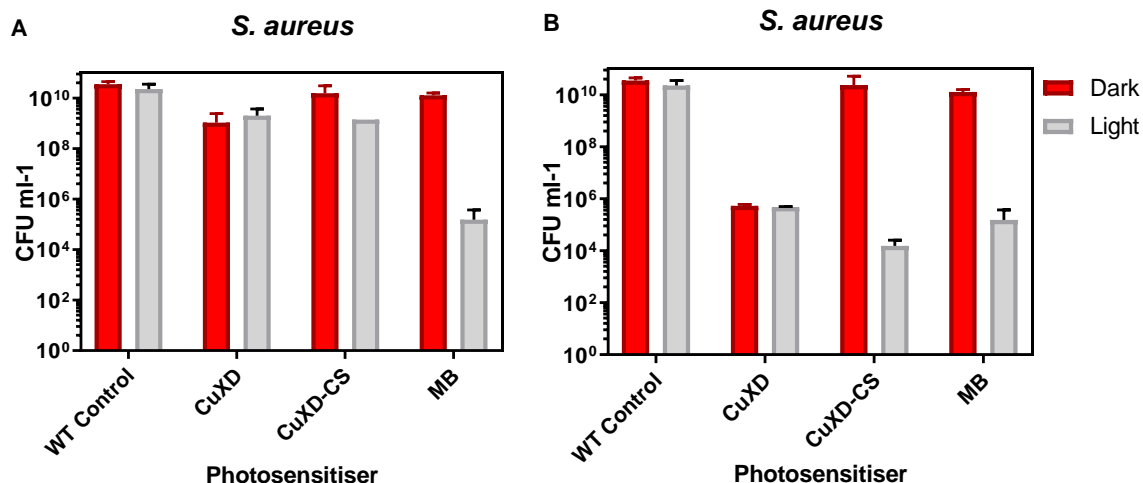


Figure 6 Bacterial assays testing the reduction in viability of *S. Aureus* colonies in the presence of crystals of crystalline *Cu(xant)(dmp).tspb* (CuXD), CuXD-CS and methylene blue (50 μM). In A concentrations of CuXD and CuXD-CS were 1 mg mL^{-1} In B 5 mg mL^{-1} . Cultures were illuminated for 2 hours under 405 nm light at 17.5 mW cm^{-2} . CuXD-CS with a surface loading of 11 $\mu\text{M g}^{-1}$ was used. Error bars indicate measurement of each interval was performed in triplicate.

Figure 6 shows the results of an initial test that was performed to assess whether CuXD-CS showed any bactericidal activity. The experiment involved illuminating the bacterial solutions in the presence of CuXD-CS under illumination by 405 nm light (17.4 mW cm^{-2}) for 2 hours. Methylene blue in solution (50 μM) was utilised as a positive standard. CuXD-CS with a surface loading of 11 $\mu\text{M g}^{-1}$ was used. The tests were performed with mixtures of CuXD or CuXD-CS in NaPhos buffer as suspensions at concentrations of 1 mg mL^{-1} (Fig. 6A) and 5 mg mL^{-1} (Fig. 6B).

CuXD on its own showed considerable dark toxicity towards *S. aureus*. After 2 hours of incubation in the dark the CFU/mL of *S. aureus* was reduced by \log_{10} at concentrations of 1 mg mL^{-1} , and by 4 \log_{10} at 5 mg mL^{-1} . By comparison, *S. aureus* in the presence of the same complex but immobilised on silica (CuXD-CS) showed no dark toxicity at 1 mg mL^{-1} and 5 mg mL^{-1} . Solutions of wild type *S. aureus* without photosensitising compound present, under illumination with 405 nm light, showed no adverse effects. Illumination of the bacterial suspensions in the presence of unsupported CuXD with 405 nm light (17.5 mW cm^{-2}) for 2

hours yielded the same reductions in CFU ml⁻¹ as did the suspensions kept in the dark. This implies no photodynamic bactericidal action is taking place with the unsupported complex.

Solutions of *S. aureus* treated with CuXD-CS showed reductions in CFU ml⁻¹ of 6-log₁₀ at concentration of 1 mg mL⁻¹ and 6 log₁₀ at a concentration of 5 mg mL⁻¹, after 2 hours of exposure to 405 nm light (17.5 mW cm⁻²), thus displaying photodynamic excellent antimicrobial activity.

More preliminary bactericidal assays were performed utilising the supported material CuXD-CS against two organisms, Gram(+) *S. aureus* and Gram(-) *E. coli*, in order to assess the minimum concentration of material required to cause bacteria death after 30 minutes of exposure to 405 nm light. The results (Fig. 7) indicate that suspensions containing 5 mg mL⁻¹ of CuXD-CS successfully reduces *S. Aureus* populations by 3-log₁₀, but that any further addition of CuXD-CS does not increase bacteria death after 30 minutes of illumination. This may be due to the increasing opacity of solution with an increase of the concentration which prevents absorption of light by the PS. Experiments need to be run between 1 and 5 mg mL⁻¹ in order to determine the minimum concentration of compound required in order to see this level of inactivation after 30 minutes.

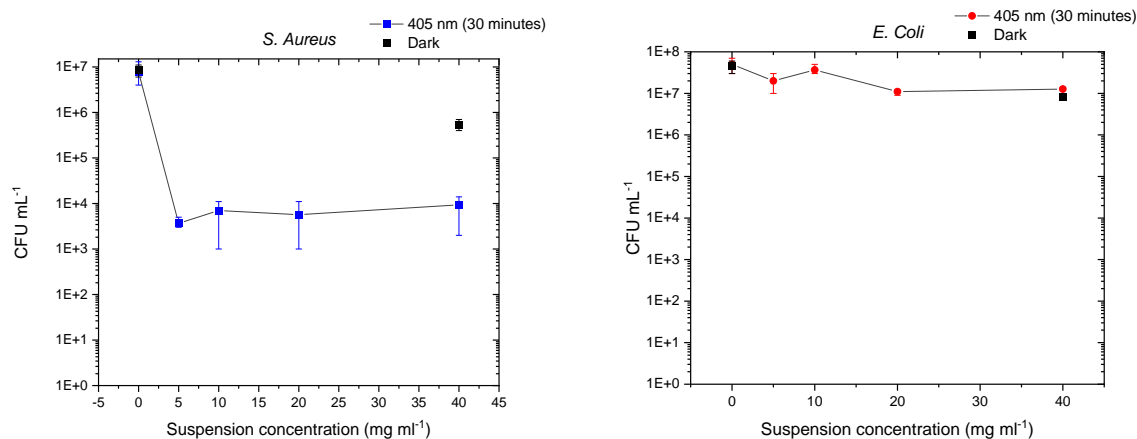


Figure 7 Bacterial inactivation after 30 minutes of exposure at varying concentrations of CuXD-CS in solutions of *S. aureus* (A) and *E. coli* (B) in NaPhos Coloured points show deactivation under illumination by 405 nm light. Black points show deactivation in the presence of CuXD-CS but in the dark. Error bars indicate measurement of each interval was performed in triplicate.

No bacterial killing was seen in the *E. Coli* assays after 30 min exposure. However, some bacterial cell death was achieved at longer exposure times, over 1 hour, (Figure 8 and 9). This need for longer irradiation time to achieve bacterial killing is due to the presence of a different, double, cell wall in Gram negative bacteria *E. coli* compared to single cell-wall in a Gram(+) bacteria such as *S. aureus*.

A small amount of dark toxicity was observed in both experiments (Figure 7 and 9). *S. Aureus* showed 2 log₁₀ of killing in the dark in the presence of 5 mg/mL of CuXD-CS after 2 hours. This may be due to the complex [Cu(xant)(dmp)].tfpb (CuXD) interacting directly with the bacteria. Further tests should be performed on the dark toxicity of the constituent parts of CuXD. Copper and copper alloys are known to be naturally anti-microbial, with reported reduction in viability of *E. coli*^{37,38} and *S. Aureus*³⁹ as well as the influenza A virus.⁴⁰

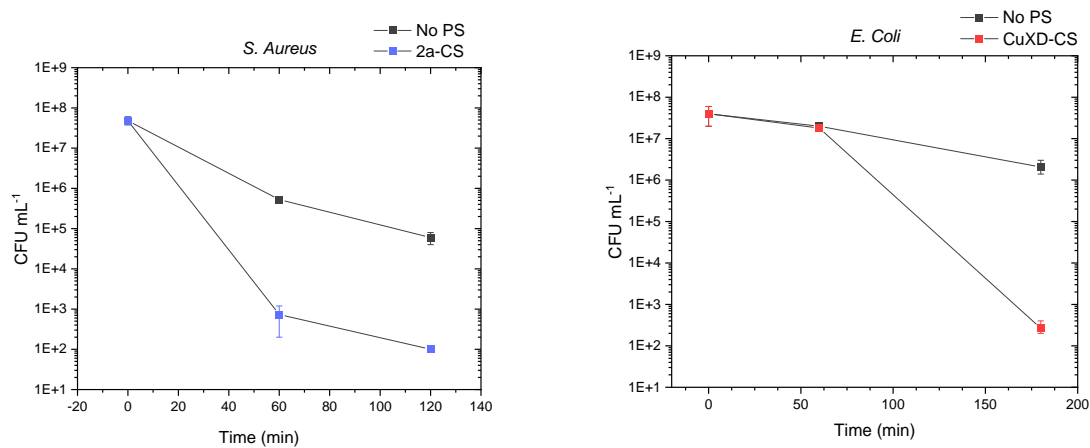


Figure 8 Bacterial inactivation by CuXD-CS (blue) and in absence of photosensitising material (black). Exposed to 400 nm light with power density 17 mW cm⁻². 5 mg of CuXD-CS per mL of NaPhos buffer were used. Error bars indicate measurement of each interval was performed in triplicate.

Both strains of bacteria showed characteristics of deactivation by singlet oxygen.⁴¹ The colonies of *S. Aureus* were successfully reduced to within the detection limit (100 CFU mL⁻¹) after 2 hours of illumination (Figure 9) with reduction in colony count affected after only 20 minutes of irradiation. For *E. Coli*, an appreciable difference in bacterial cell viability was only seen after 60 minutes of exposure, and complete deactivation was achieved after 180 minutes. This is a well-studied phenomenon: in Gram(+) bacteria singlet oxygen immediately causes damage to the cell membrane leading to cell death; with Gram(-) bacteria, singlet oxygen must first destroy the LPS and outer membrane of the cell wall which either leads to the production of substances toxic to the cell or subsequent destruction of the inner cell membrane, which then leads to cell death.⁴¹⁻⁴³

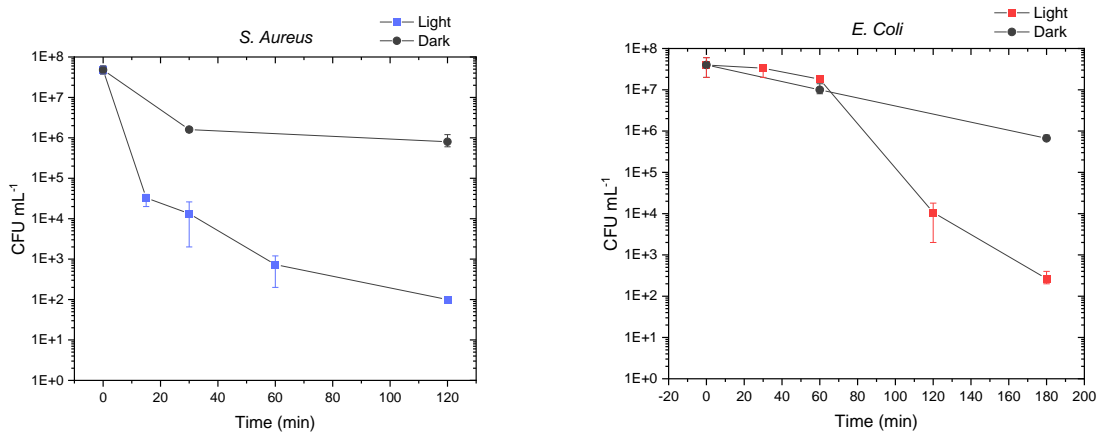


Figure 9 Bacterial inactivation by CuXD-CS under illumination by 405 nm light, power density 17 mW cm^{-2} (coloured points) and in the dark (black points). Error bars indicate measurement of each interval was performed in triplicate.

Bacterial assay experiments performed together with Professor Dave Kelly (d.kelly@sheffield.ac.uk) and Peter G Walker (pgwalker1@sheffield.co.uk).

Results for all copper complexes produced from experiments performed together with Martin Appleby (mvappleby1@sheffield.ac.uk).

4.5 Conclusions and future work

Preliminary tests showed that both of the synthesised photosensitising compounds, $[\text{Ru}(\text{bpy})_2(\text{bpy-Silatrane})]\text{Cl}_2\text{-CS-NH}_2$ and $[\text{Cu}(\text{xant})(\text{dmp})]\text{tfpb-CS}$ successfully deactivated both Gram(+) and Gram(-) strains of bacteria under illumination. RuBS-CS-NH₃ showed promising results initially, showing complete reduction in colonies after 2 hours of illumination with a relatively low-power lamp (2.4 mW cm^{-2}). However, two repeats of this experiment performed with new batches of prepared material showed little to no reduction in colonies with illumination. In the future, experiments with higher power density may be undertaken to investigate if reduction in colony formation can be achieved with more consistency.

The results for CuXD-CS were more promising and yielded consistent results albeit requiring a far higher power density of light (17 mW cm^{-2}) at 405 nm. CuXD-CS displayed inconsistent amount of dark toxicity, showing no adverse effects in one experiment and reducing 2-log_{10} CFU of both *S. aureus* and *E. coli* in another experiment (using 5 mg mL^{-1} of compound and 2 hours incubation time for both experiments). Further tests need to be performed to resolve these inconsistencies. A minimum concentration of CuXD-CS in NaPhos buffer of 5 mg mL^{-1} was necessary to achieve reduction in *S. aureus* colonies after 30 minutes of irradiation. Increasing further the concentration of CuXD-CS had no effect on the efficiency of treatment. Experiments at lower concentrations of CuXD-CS are required in order to determine the minimum active concentration of the photosensitising compound. Experiments at lower surface loadings could also be performed to determine whether even less material can be used to achieve the same killing.

Overall, the results show that CuXD-CS can be a viable candidate for solar water disinfection. Experiments to determine leaching of photosensitiser from the surface of the silica over time, as well as photodecomposition of the photosensitiser must be performed to ensure that use of the compound is safe and economically viable.

4.6 References

1. Foote, C. S. & Clennan, E. L. Properties and Reactions of Singlet Dioxygen. in *Active Oxygen in Chemistry* (eds. Foote, C. S., Valentine, J. S., Greenberg, A. & Liebman, J. F.) 105–140 (Springer Netherlands, 1995). doi:10.1007/978-94-007-0874-7_4
2. Spikes, J. D. The origin and meaning of the term ‘photodynamic’ (as used in ‘photodynamic therapy’, for example). *J. Photochem. Photobiol. B Biol.* **9**, 369–371 (1991).
3. Ravanat, J. L., Di Mascio, P., Martinez, G. R., Medeiros, M. H. G. & Cadet, J. Singlet oxygen induces oxidation of cellular DNA. *J. Biol. Chem.* **275**, 40601–40604 (2000).
4. Zhang, J. *et al.* Synthesis and antibacterial study of 10, 15, 20-triphenyl-5-{4-hydroxy-3-(trimethylammonium)methyl}phenylporphyrin as models for combination of porphyrin and alkylating agent. *Bioorganic Med. Chem. Lett.* **13**, 1097–1100 (2003).
5. Berg, K. *et al.* Photochemical internalization (PCI): A technology for drug delivery. *Methods in Molecular Biology* **635**, (2010).
6. Kim, H. S. *et al.* Antibacterial application of covalently immobilized photosensitizers on a surface. *Environ. Res.* **172**, 34–42 (2019).
7. Cahan, R., Schwartz, R., Langzam, Y. & Nitzan, Y. Light-activated antibacterial surfaces comprise photosensitizers. *Photochem. Photobiol.* **87**, 1379–1386 (2011).
8. García-Fresnadillo, D. Singlet Oxygen Photosensitizing Materials for Point-of-Use Water Disinfection with Solar Reactors. *ChemPhotoChem* **2**, 512–534 (2018).
9. Valkov, A., Raik, K. A., Mualem-Sinai, Y., Nakonechny, F. & Nisnevitch, M. Water disinfection by immobilized photosensitizers. *Water (Switzerland)* **11**, (2018).
10. Coronel, A. *et al.* Photodynamic action of methylene blue subjected to aromatic-aromatic interactions with poly(sodium 4-styrenesulfonate) in solution and supported in solid, highly porous alginate sponges. *Dye. Pigment.* **147**, 455–464 (2017).
11. Beveridge, T. J. & Davies, J. A. Cellular responses of *Bacillus subtilis* and *Escherichia coli* to the Gram stain. *J. Bacteriol.* **156**, 846–858 (1983).
12. Ferris, F. G. & Beveridge, T. J. Functions of Bacterial Cell Surface Structures. *Bioscience* **35**, 172–177 (1985).
13. James, A. M. The electrical properties and topochemistry of bacterial cells. *Adv. Colloid Interface Sci.* **15**, 171–221 (1982).
14. MOAN, J. & BERG, K. the Photodegradation of Porphyrins in Cells Can Be Used To Estimate the Lifetime of Singlet Oxygen. *Photochem. Photobiol.* **53**, 549–553 (1991).
15. Hatz, S., Lambert, J. D. C. & Ogilby, P. R. Measuring the lifetime of singlet oxygen in a single cell: Addressing the issue of cell viability. *Photochem. Photobiol. Sci.* **6**, 1106–1116 (2007).
16. Baier, J., Maier, M., Engl, R., Landthaler, M. & Bäumlner, W. Time-resolved investigations of singlet oxygen luminescence in water, in phosphatidylcholine, and in aqueous suspensions of phosphatidylcholine or HT29 cells. *J. Phys. Chem. B* **109**, 3041–3046 (2005).
17. Felip-León, C. *et al.* Superior performance of macroporous over gel type polystyrene as a support for the development of photo-bactericidal materials. *J. Mater. Chem. B* **5**, 6058–6064 (2017).

18. Gutierrez, M. *et al.* Singlet Oxygen ($^1\Delta_g$) Production by Ruthenium (II) Complexes in Microheterogenous Systems. *J.Phys. Chem* **107**, 3397–3403 (2003).
19. Manjón, F., Villén, L., García-fresnadillo, D. & Orellana, G. On the Factors Influencing the Performance of Solar Reactors for Water Disinfection with Photosensitized Singlet Oxygen. *Environ. Sci. Technol.* **42**, 301–307 (2008).
20. Garcia-Fresnadillo, D., Georgiadoub, Y., Orellana ', G., Braunb), A. M. & Oliverosb, E. 06. Singlet-Oxygen (1Ag) Production by Rutheniurn(I1) Complexes Containing Polyazaheterocyclic Ligands in Methanol and in Water. *Helv. Chim. ACTA* ~ **79**, (1996).
21. Louzao, I., Sui, C., Winzer, K., Fernandez-Trillo, F. & Alexander, C. Cationic polymer mediated bacterial clustering: Cell-adhesive properties of homo- and copolymers. *Eur. J. Pharm. Biopharm.* **95**, 47–62 (2015).
22. Haruko Takahashi, Enrico T. Nadres, and K. K. Cationic Amphiphilic Polymers with Antimicrobial Activity for Oral Care Applications: Eradication of *S. mutans* Biofilm Haruko. *Biomacromolecules* **18**, 257–265 (2017).
23. Seil, J. T. & Webster, T. J. Antimicrobial applications of nanotechnology: Methods and literature. *Int. J. Nanomedicine* **7**, 2767–2781 (2012).
24. Vecchio, D. *et al.* Bacterial photodynamic inactivation mediated by methylene blue and red light is enhanced by synergistic effect of potassium iodide. *Antimicrob. Agents Chemother.* **59**, 5203–5212 (2015).
25. Youssef, Z. *et al.* Titania and silica nanoparticles coupled to Chlorin e6 for anti-cancer photodynamic therapy. *Photodiagnosis Photodyn. Ther.* **22**, 115–126 (2018).
26. Rokicka-Konieczna, P., Wanag, A., Sienkiewicz, A., Kusiak-Nejman, E. & Morawski, A. W. Antibacterial effect of TiO₂ nanoparticles modified with APTES. *Catal. Commun.* **134**, 0–3 (2020).
27. Cooper, A. T. & Goswami, D. Y. Evaluation of Methylene Blue and Rose Bengal for Dye Sensitized Solar Water Treatment. *J. Sol. Energy Eng.* **124**, 305 (2002).
28. Dahl, T. A., Midden, W. R. & Neckers, D. C. Comparison of Photodynamic Action By Rose Bengal in Gram Positive and Gram Negative Bacteria. *Photochem. Photobiol.* **48**, 607–612 (1988).
29. Shrestha, A., Hamblin, M. R. & Kishen, A. Photoactivated rose bengal functionalized chitosan nanoparticles produce antibacterial/biofilm activity and stabilize dentin-collagen. *Nanomedicine Nanotechnology, Biol. Med.* **10**, 491–501 (2014).
30. Shrestha, A., Hamblin, M. R. & Kishen, A. Characterization of a conjugate between rose bengal and chitosan for targeted antibiofilm and tissue stabilization effects as a potential treatment of infected dentin. *Antimicrob. Agents Chemother.* **56**, 4876–4884 (2012).
31. Pessoni, L., Lacombe, S., Billon, L., Brown, R. & Save, M. Photoactive, porous honeycomb films prepared from rose bengal-grafted polystyrene. *Langmuir* **29**, 10264–10271 (2013).
32. Guo, Y., Rogelj, S. & Zhang, P. Rose Bengal-decorated silica nanoparticles as photosensitizers for inactivation of gram-positive bacteria. *Nanotechnology* **21**, 065102 (2010).
33. Decraene, V., Pratten, J. & Wilson, M. Cellulose acetate containing toluidine blue and rose bengal is an effective antimicrobial coating when exposed to white light. *Appl. Environ. Microbiol.* **72**, 4436–4439 (2006).

34. Moczek, Ł. & Nowakowska, M. Novel water-soluble photosensitizers from chitosan. *Biomacromolecules* **8**, 433–438 (2007).
35. Jemli, M., Alouini, Z., Sabbahi, S. & Gueddari, M. Destruction of fecal bacteria in wastewater by three photosensitizers. *J. Environ. Monit.* **4**, 511–516 (2002).
36. Sabbahi, S., Ben Ayed, L. & Jemli, M. Staphylococcus aureus photodynamic inactivation mechanisms by rose bengal: use of antioxidants and spectroscopic study. *Appl. Water Sci.* **8**, 1–9 (2018).
37. Michels, H. T., Wilks, S. A., Noyce, J. O. & Keevil, C. W. Copper alloys for human infectious disease control. *Mater. Sci. Technol.* **1**, 3–13 (2005).
38. Wilks, S. A., Michels, H. & Keevil, C. W. The survival of Escherichia coli O157 on a range of metal surfaces. *Int. J. Food Microbiol.* **105**, 445–454 (2005).
39. Michels, H. T., Noyce, J. O. & Keevil, C. W. Effects of temperature and humidity on the efficacy of methicillin-resistant Staphylococcus aureus challenged antimicrobial materials containing silver and copper. *Lett. Appl. Microbiol.* **49**, 191–195 (2009).
40. Noyce, J. O., Michels, H. & Keevil, C. W. Inactivation of influenza A virus on copper versus stainless steel surfaces. *Appl. Environ. Microbiol.* **73**, 2748–2750 (2007).
41. Dahl, T. A., Midden, W. R. & Hartman, P. E. Comparison of killing of gram-negative and gram-positive bacteria by pure singlet oxygen. *J. Bacteriol.* **171**, 2188–2194 (1989).
42. Castano, A. P., Demidova, T. N. & Hamblin, M. Mechanisms in photodynamic therapy: part one. *Photodiagnosis Photodyn Ther* **1**, 279–293 (2004).
43. Dahl, T. A., RobertMiddenand, W. & Hartman, P. E. Pure Singlet Oxygen Cytotoxicity for Bacteria. *Photochem. Photobiol.* **46**, 345–352 (1987).

5 Experimental

Contents

5	Experimental	117
5.1	Experimental Methods	120
5.1.1	NMR Spectroscopy	120
5.1.2	Mass Spectrometry	120
5.1.3	Fourier-Transform Infrared Spectroscopy	120
5.1.4	UV-visible Absorption Spectroscopy	120
5.1.5	Emission Spectroscopy	121
5.1.6	X-ray photoelectron spectroscopy	121
5.2	Materials	122
5.3	Ruthenium Complexes	122
5.3.1	cis-Bis(2,2'-bipyridine)dichlororuthenium(II)	122
5.3.2	cis-Bis(1,10-phenanthroline)dichlororuthenium(II)	122
5.3.3	2,2'-Bipyridine-4,4'-dicarboxylic acid (dcbpy)	123
5.3.4	2,2'-bipyridyl-4,4'-dicarboxylic acid bis-[(3-triethoxysilylpropyl)amide] (bpy-sil)	123
5.3.5	bis-(2,2'-bipyridine)ruthenium(II) [2,2'-bipyridyl-4,4'-dicarboxylic acid bis-[(3-triethoxysilylpropyl)amide] dichloride, (Ru(bpy-sil))	124
5.3.6	1-(3'-amino)propylsilatrane	125
5.3.7	N-Methylaminopropyltrimethoxysilatrane	125
5.3.8	2,2'-Bipyridine-4,4'-dicarboxylic acid bis[(3-silatranylpropyl) amide] (bipy-silatrane)	126
5.3.9	2,2'-Bipyridine-4,4'-dicarboxylic acid bis[(3-silatranylpropyl) N-methyl amide] (bipy-Me-silatrane)	127
5.3.10	2,2'-bipyridyl-4,4'-dicarboxylic acid bis-[(3-Silatrane-propyl)amide] bis-(2,2'-bipyridine) ruthenium(II) dichloride (RuBS)	127
5.3.11	Phenanthroline-4,7-dicarboxylic acid	128
5.3.12	1,10-Phenanthroline-4,7-dicarboxylic acid bis[(3-silatranylpropyl) amide]	129
5.3.13	1,10-Phenanthroline-4,7-dicarboxylic acid bis[(3-silatranylpropyl) amide] bis-1,10-Phenanthroline Ruthenium(II) dichloride (RuPS).	130
5.3.14	RuBS-CS	130
5.3.15	Preparation of PDMS compounds	131
5.4	Copper Complexes	133
5.4.1	[Cu(dmp)(Xantphos)]tfpb	133
5.4.2	[Cu(bathocuproine)(xantphos)]tfpb	134
5.4.3	Na[Cu(bathocuproine-disulfonate)(xantphos)]	135
5.4.4	[Cu(DPEPhos)(dmp)]tfpb	135

5.4.5	5-Nitrocuproine	136
5.4.6	[Cu(5-Nitrocuproine)(xantphos)]tfpb	137
5.5	Other metal complexes	137
5.5.1	Ir(fppy) ₂ (bpy-silatrane)	137
5.6	References	139

5.1 Experimental Methods

5.1.1 NMR Spectroscopy

All one dimensional ^1H NMR spectra were recorded using a 400 MHz Bruker Avance 400 spectrometer. Spectra were recorded in spectroscopic grade deuterated chloroform, methanol or DMSO and calibrated against the residual protonated solvent peak.¹

5.1.2 Mass Spectrometry

All experiments were performed by the University of Sheffield mass spectrometry service. Electron impact (EI) mass spectra were recorded using a Waters LCT time-of-flight (TOF) mass analyser. Positive-ion electrospray (ES^+) mass spectra were recorded on a VG AutoSpec magnetic sector instrument.

5.1.3 Fourier-Transform Infrared Spectroscopy

Infra-red spectra were recorded in a DCM solution, using a Perkin Elmer Spectrum One FTIR instrument at a 4 cm^{-1} resolution in demountable solution cells with sodium chloride windows. Solid-state infra-red spectra were recorded using a Perkin Elmer Spectrum Two FT-IR Spectrometer fitted with an attenuated total reflectance (ATR) module.

5.1.4 UV-visible Absorption Spectroscopy

Solution-based UV-Vis spectra were recorded on a Cary 50 Bio instrument, with the samples in solution in a quartz cuvette, with a 1 cm path length. Solid State UV-Vis spectra were measured with a Varian Cary 5000 spectrophotometer using a Praying Mantis™ Diffuse Reflectance Accessory to hold the solid samples.

5.1.5 Emission Spectroscopy

Emission spectra were obtained from a Horiba Jobin-Yvon Fluoromax-4 spectrofluorimeter. Analyte solutions were contained within quartz cuvettes of 1 cm path length.

5.1.6 X-ray photoelectron spectroscopy

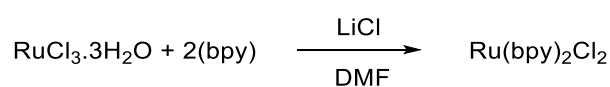
The analyses were carried out using a Kratos Supra instrument with the monochromated aluminium source, with two analysis points per sample. Survey scans were collected between 1200 to 0 eV binding energy, at 160 eV pass energy and 1.0 eV intervals. In addition, high-resolution O(1s), Ag(3d), N(1s), C(1s), F(1s) and Si(2p) spectra were collected over an appropriate energy range at 20 eV pass energy and 0.1 eV intervals. The analysis area was 700 μm x 300 μm . The data collected were calibrated in intensity using a transmission function characteristic of the instrument (determined using software from NPL) to make the values instrument-independent. The data can then be quantified using theoretical Scofield relative sensitivity factors. The data were calibrated for binding energy by making the main carbon C(1s) peak at 285.0 eV, and correcting all data for each sample analysis accordingly.

5.2 Materials

All organic and inorganic reagents were purchased from either Sigma-Aldrich or Alfa Aesar and used as received. Dry solvents were produced from an in-house Grubbs solvent drying system.

5.3 Ruthenium Complexes

5.3.1 cis-Bis(2,2'-bipyridine)dichlororuthenium(II)

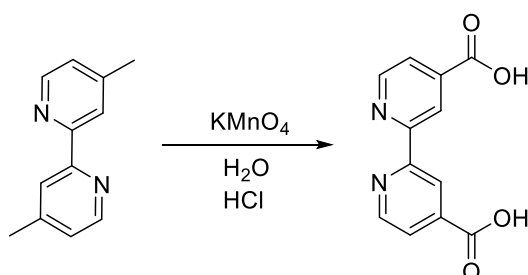


Ruthenium trichloride hydrate (7.8 g, 38 mmol), 2,2-bipyridyl (11.9 g, 76 mmol) and lithium chloride (8.4 g, 200 mmol) were refluxed in DMF (50 mL) for 8 hours. The solution was then cooled to room temperature before adding acetone (250 mL). This mixture was then cooled to 0 °C overnight and the resulting purple crystals were filtered and washed with acetone, water and diethyl ether to give a purple/brown solid. This was then heated in 400 ml of 1:1 EtOH water to give a deep purple/red solution and filtered while hot. EtOH was evaporated from solution in the presence of LiCl (20 g) and the product left to recrystallize out at room temperature. The resulting black crystals were washed with water and EtOH and dried under vacuum (12.1 g, 68% yield).

5.3.2 cis-Bis(1,10-phenanthroline)dichlororuthenium(II)

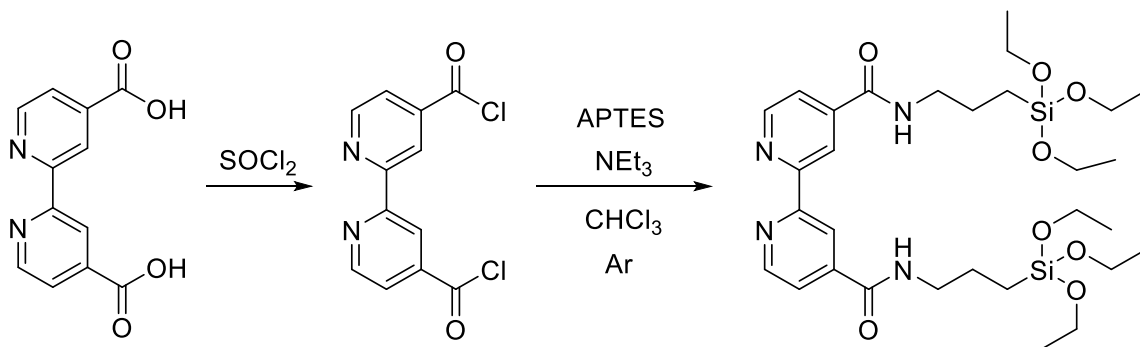
Synthesis and purification for this compound the same as for above, but replacing 2,2-bipyridyl with 1,10-phenanthroline. (65 % yield).

5.3.3 2,2'-Bipyridine-4,4'-dicarboxylic acid (dcbpy)



4,4'-dimethyl-2,2'-bipyridine (2 g, 10.9 mmol) and potassium permanganate (6.5 g, 41.1 mmol) were dissolved in water and refluxed for 12 hours. A brown precipitate was then filtered off from the cooled reaction mixture to leave a yellowish solution. Any remaining starting material was extracted from the solution by washing with diethyl ether. The product was precipitated from solution by trituration with hydrochloric acid and filtered, washed with water, and dried to give an off-white powder (1.32 g, 50% yield). *m/z* (ESI) 244.1 (100 %, M⁺).

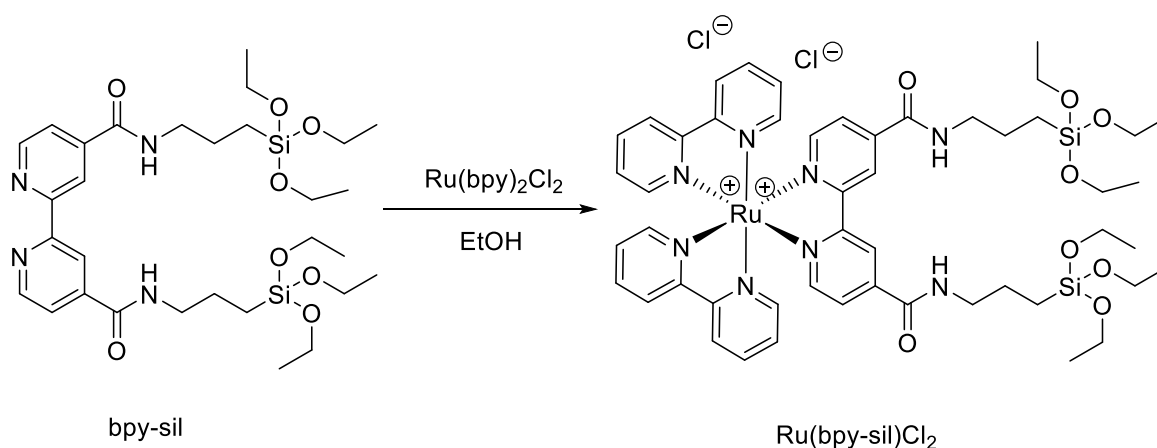
5.3.4 2,2'-bipyridyl-4,4'-dicarboxylic acid bis-[(3-triethoxysilylpropyl)amide] (bpy-sil)



2,2'-bipyridyl-4,4'-dicarboxylic acid (0.35 g, 1.43 mmol) was dissolved in excess thionyl chloride (10 mL, 138 mmol) and refluxed overnight until the mixture turned clear yellow. The solvent was then removed under reduced pressure to give an air-sensitive yellow-white powder. This was immediately dissolved in chloroform (20 mL) and was added dropwise over an hour to a stirred solution of 3-aminopropyltriethoxysilane (APTES) (0.6 mL, 3 mmol) and

triethylamine (0.54 mL, 3 mmol) in dry chloroform (10 mL). The reaction mixture was stirred overnight under an inert argon atmosphere before removing the solvent under reduced pressure. The resulting white powder was dissolved in toluene and the undissolved triethylammonium chloride filtered off before removing the solvent under reduced pressure to give an off-white waxy, air-sensitive solid (0.63 g, 68% yield). ^1H NMR: δ_{H} (400 MHz; CDCl_3 ; Me_4Si) 8.82 (d, $J = 5.0$ Hz, 2H), 8.74 (s, 2H), 7.85 (dd, $J = 5.0, 1.6$ Hz, 2H), 7.02 (d, $J = 4.0$ Hz, 2H), 3.97 – 3.79 (m, 12H), 3.13 (qd, $J = 7.3, 4.8$ Hz, 4H), 1.87 – 1.78 (m, 4H), 1.24 (t, $J = 7.0$ Hz, 18H), 0.81 – 0.70 (m, 4H). m/z (ESI) 651.3 (100 %, M^+).

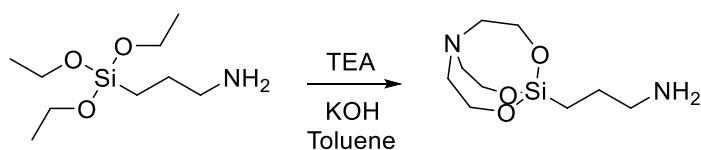
5.3.5 bis-(2,2'-bipyridine)ruthenium(II) [2,2'-bipyridyl-4,4'-dicarboxylic acid bis-[(3-triethoxysilylpropyl)amide] dichloride, ($\text{Ru}(\text{bpy-sil})$)



Bpy-sil (115 mg, 0.177 mmol) and $\text{Ru}(\text{bpy})_2\text{Cl}_2$ (84 mg, 0.174 mmol) were dissolved in absolute ethanol (10 mL) under an inert argon atmosphere and refluxed for 8 hours. After cooling the solvent was removed under reduced pressure. The resulting dark red crystals were dissolved in a minimum amount of methanol and purified by passing through a Sephadex LH-20 column in methanol (0.61 mg, 32 %). ^1H NMR (400 MHz, CDCl_3) δ 10.70 (s, 2H, ArH), 9.63 (t, $J = 5.8$ Hz, 2H, ArH), 9.00 – 8.86 (m, 4H, ArH), 8.82 (d, $J = 5.0$ Hz, 1H, ArH), 8.17 (dd, $J = 16.3, 8.1$ Hz, 4H, 2 ArH), 8.11 – 8.05 (m, 2H, ArH), 7.78 (d, $J = 5.4$ Hz, 1H), 7.68 (d, $J = 5.8$ Hz, 1H),

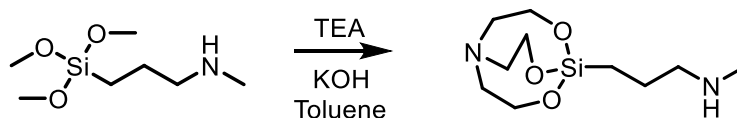
7.59 (t, $J = 7.9$ Hz, 2H), 7.50 – 7.41 (m, 2H, NH), 3.91 – 3.78 (m, 12H, OCH_2CH_3), 3.62 – 3.46 (m, 4H, $\text{NHCH}_2\text{CH}_2\text{CH}_2$), 1.86 (ddd, $J = 30.1, 15.4, 7.5$ Hz, 4H, $\text{NHCH}_2\text{CH}_2\text{CH}_2$), 1.32 – 1.12 (m, 18H, OCH_2CH_3), 0.81 – 0.65 (m, 4H, $\text{NHCH}_2\text{CH}_2\text{CH}_2$); $\nu_{\text{max}}/\text{cm}^{-1}$ 773 (SiC), 1069 (SiO), 1099 (SiC), 1542 (CONH), 1638 (ArCONH), 2922 (NH); $\lambda_{\text{max}}(\text{MeOH})/\text{nm}$ ($\epsilon/\text{dm}^3 \text{ mol}^{-1} \text{ cm}^{-1}$) 289 (5547), 244 (3550), 466 (1156). m/z (ESI) 532.2 (100 %, $\{\text{M} - 2\text{Cl}\}^{2+}$).

5.3.6 1-(3'-amino)propylsilatrane



A mixture of APTES (8.84 g, 40 mmol) and triethanolamine (TEA) (5.69 g, 40 mmol) in toluene (10 mL) was heated to reflux in a Dean-Stark apparatus with a catalytic amount of potassium hydroxide. The ethanol was removed as it was evolved throughout the reaction. The resulting white crystalline solid was washed with n-hexane and dried in air to afford a white sticky powder (5.00 g, 54 %). ^1H NMR (400 MHz, CDCl_3) δ 3.77 (t, $J = 5.8$ Hz, 1H), 2.81 (t, $J = 5.8$ Hz, 1H), 2.64 (q, $J = 7.2$ Hz, 1H), 1.59 – 1.45 (m, 1H), 0.48 – 0.31 (m, 1H); m/z (ESI) 233.1 (100 %, M^+).

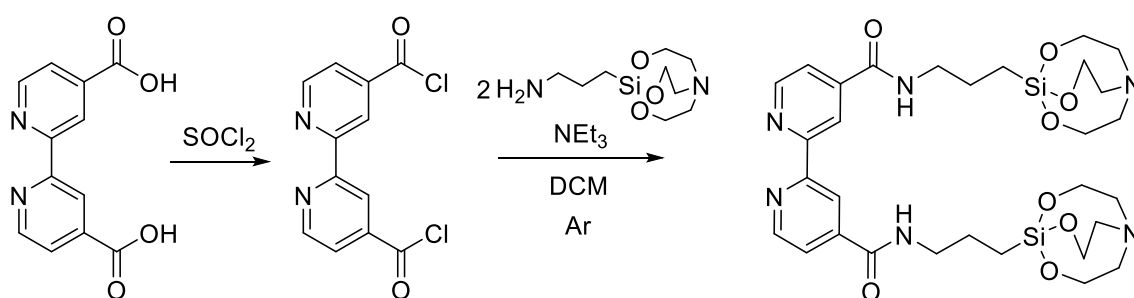
5.3.7 N-Methylaminopropyltrimethoxysilatrane



A mixture of *N*-Methyl-aminopropyltrimethoxysilane (7.7 g, 40 mmol) and triethanolamine (TEA) (5.69 g, 40 mmol) in toluene (10 mL) was heated to reflux in a Dean-Stark apparatus with a catalytic amount of potassium hydroxide. The ethanol was removed as it was evolved throughout the reaction. The resulting yellow oil was used without further

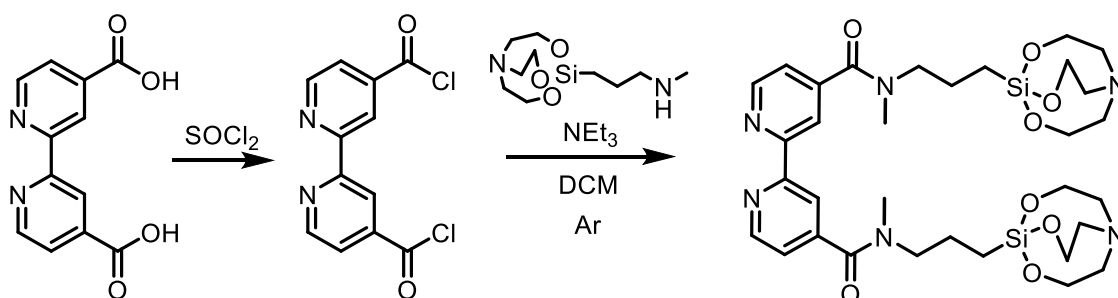
purification (6.3 g, 63%). $^1\text{H NMR}$ (400 MHz, CDCl_3) δ 7.27 – 7.08 (m, 1H), 3.74 (t, $J = 5.8$ Hz, 6H), 2.78 (t, $J = 5.8$ Hz, 6H), 2.55 – 2.44 (m, 2H), 2.37 (s, 3H), 1.65 – 1.46 (m, 2H), 0.44 – 0.28 (m, 2H).); m/z (ESI) 246.4 (100 %, M^+). Elemental Analysis Molecular formula: $\text{C}_{10}\text{H}_{22}\text{N}_2\text{O}_3\text{Si}$ Predicted Results C 48.75%, H 9.00%, N 11.37% Found: C 48.53%, H 9.18%, N 11.32%.

5.3.8 2,2'-Bipyridine-4,4'-dicarboxylic acid bis[(3-silatranylpropyl) amide] (bipy-silatrane)



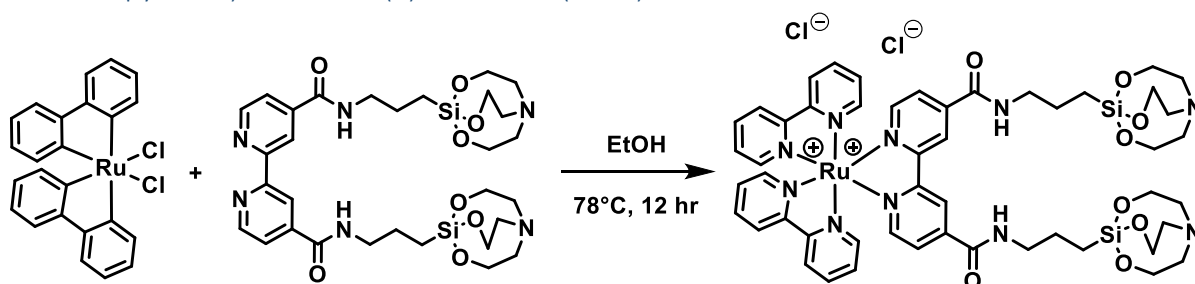
2,2'-Bipyridine-4,4'-dicarboxylic acid (dcbpy) (0.350 g, 1.25 mmol) was dissolved in excess thionyl chloride (10 mL, 86.6 mmol) and refluxed overnight under argon. The unreacted thionyl chloride was removed *in vacuo* before dissolving the residue in DCM (10 mL) and filtering. The filtrate was collected and added dropwise to a stirred mixture of 1-(3'-amino)propylsilatrane (0.609 g, 2.625 mmol) and triethylamine (0.6 mL, 4.3 mmol) in DCM under argon over the course of an hour. This mixture was stirred at room temperature for 3 hours under argon. The mixture was then cooled to 0 °C overnight. The mixture was then filtered and washed with cold DCM to afford a pale pink precipitate (0.81 g, 96 %). $^1\text{H NMR}$ (400 MHz, CDCl_3) δ 8.77 (dd, $J = 5.0, 0.6$ Hz, 1H), 8.71 (s, 1H), 7.84 (dd, $J = 5.0, 1.7$ Hz, 1H), 7.59 (s, 1H), 3.79 (t, $J = 5.8$ Hz, 6H), 3.51 (dd, $J = 12.2, 5.8$ Hz, 2H), 2.82 (t, $J = 5.8$ Hz, 6H), 1.93 – 1.71 (m, 3H), 0.59 (t, $J = 7.3$ Hz, 2H). m/z (ESI) 673.4 (100 %, M^+). Elemental Analysis Molecular formula: $\text{C}_{30}\text{H}_{44}\text{N}_6\text{O}_8\text{Si}_2$ Predicted Results C 53.55%, H 6.59%, N 12.49% Found: C 52.93%, H 6.78%, N 12.32%.

5.3.9 2,2'-Bipyridine-4,4'-dicarboxylic acid bis[(3-silatranylpropyl) N-methyl amide] (bipy-Me-silatrane)



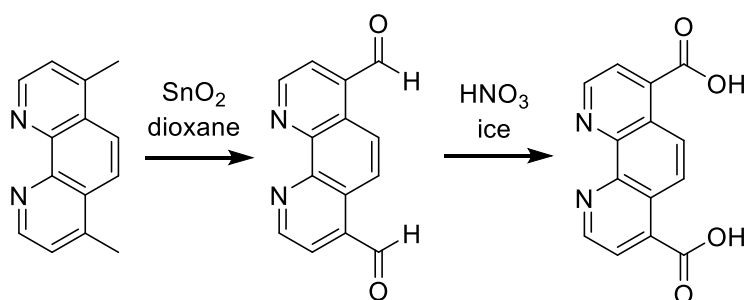
Dcbpy (0.350 g, 1.25 mmol) was dissolved in excess thionyl chloride (10 mL, 86.6 mmol) and refluxed overnight under argon. The unreacted thionyl chloride was removed *in vacuo* before dissolving the residue in DCM (10 mL) and filtering. The filtrate was collected and added dropwise to a stirred mixture of N-Methylaminopropyltrimethoxysilatrane (0.64 g, 2.6 mmol) and triethylamine (0.6 mL, 4.3 mmol) in DCM under argon over the course of an hour. This mixture was stirred at room temperature for 3 hours under argon. The mixture was then cooled to 0 °C overnight. The mixture was then filtered and washed with cold DCM to afford a yellowish white precipitate (0.6 g, 96 %). ^1H NMR (400 MHz, DMSO) δ 8.78 (d, $J = 4.9$ Hz, 2H), 8.29 (s, 2H), 7.43 (dd, $J = 24.9, 4.8$ Hz, 2H), 3.63 (t, $J = 5.8$ Hz, 4H), 3.43 (t, $J = 5.7$ Hz, 6H), 3.17 (d, $J = 5.0$ Hz, 3H), 2.98 (d, $J = 13.9$ Hz, 1H), 2.81 (t, $J = 5.8$ Hz, 2H), 2.66 (t, $J = 5.8$ Hz, 4H). m/z (ESI) 701.3 (100 %, MH^+).

5.3.10 2,2'-bipyridyl-4,4'-dicarboxylic acid bis-[(3-Silatrane-propyl)amide] bis-(2,2'-bipyridine) ruthenium(II) dichloride (RuBS)



Bpy-silatrane (0.130 g, 0.193 mmol) and Ru(bpy)₂Cl₂ (84 mg, 0.174 mmol) were dissolved in absolute ethanol (20 mL) under an inert argon atmosphere and refluxed for 8 hours to produce a clear red solution. After cooling the solvent was removed under reduced pressure. The resulting dark red crystals were dissolved in a minimum amount of methanol and purified by passing through a Sephadex LH-20 column in methanol (0.61 mg, 32 %) followed by evaporation of the solvent. The resulting crystalline solid is hygroscopic. ¹H NMR (400 MHz, MeOD): δ 9.15 (d, J = 1.5 Hz, 2H), 8.75 (dd, J = 8.2, 2.7 Hz, 4H), 8.26 – 8.08 (m, 4H), 8.00 (d, J = 5.9 Hz, 2H), 7.85 (dd, J = 5.9, 2.0 Hz, 6H), 7.61 – 7.41 (m, 4H), 3.75 (t, J = 5.9 Hz, 12H), 3.42 – 3.37 (m, 4H), 2.90 (t, J = 5.9 Hz, 12H), 1.80 – 1.62 (m, 4H), 0.48 – 0.26 (m, 4H). *m/z* (ESI) 543.4 (100 %, {M – 2Cl}²⁺). Elemental Analysis Chemical formula: C₅₀H₆₀N₁₀O₈RuSi₂Cl₂·10H₂O Predicted Results C 44.90%, H 6.03%, N 10.47%. Found: C 45.76%, H 5.65%, N 10.64%.

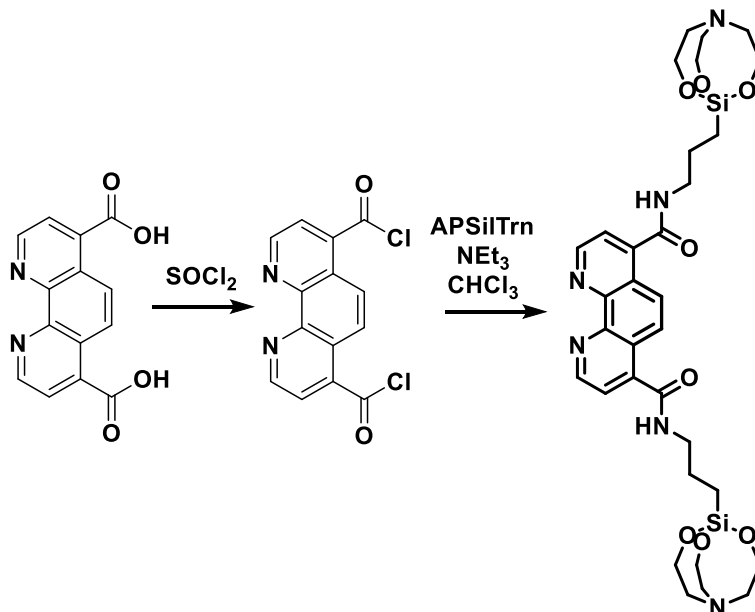
5.3.11 Phenanthroline-4,7-dicarboxylic acid



4,7-Dimethylphenanthroline (1g, 4.8 mmol) and SnO₂ (2.4 g, 21.6 mmol) were refluxed in dioxane with 4% water (60 ml) overnight before hot filtering through celite. The filtrate was left to reach room temperature and the resulting precipitate was filtered to afford the dialdehyde, a pale orange powder. This crude material was used quantitatively to produce the diacid by refluxing it in 70% nitric acid (10 mL) overnight. The reaction mixture was poured into ice (20 g) and left until the ice had melted. The resulting precipitate was filtered off and washed with methanol to afford the diacid as pale yellow crystals (0.54 g, 0.20 mmol, 41%

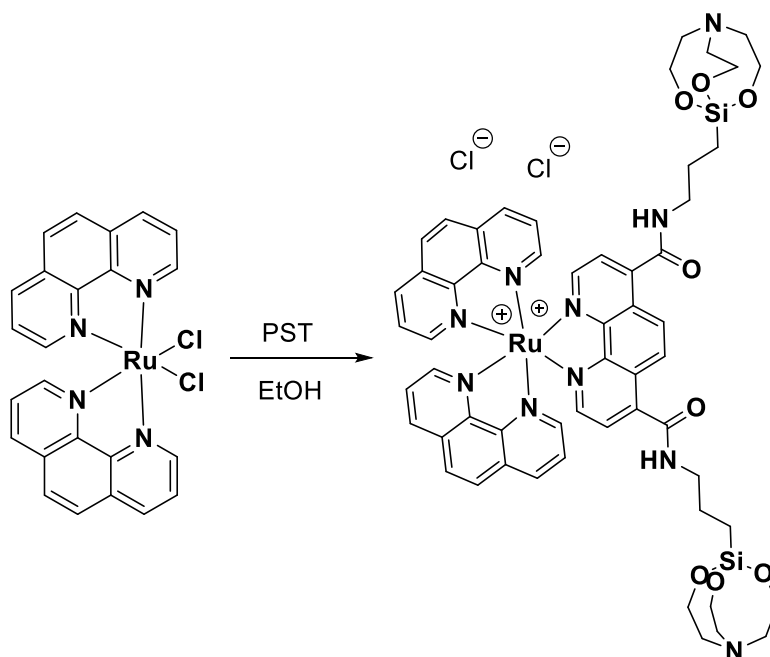
yield). $^1\text{H NMR}$ (400 MHz, DMSO) δ 9.27 (d, $J = 4.5$ Hz, 2H), 8.78 (s, 2H), 8.17 (d, $J = 4.5$ Hz, 2H). m/z (ESI) 269.1 (100%, M^+).

5.3.12 1,10-Phenanthroline-4,7-dicarboxylic acid bis[(3-silatranylpropyl) amide]



Phenanthroline-4,7-dicarboxylic acid (0.1 g, 0.373 mmol) was refluxed in thionyl chloride (6 mL) overnight to afford a bright yellow solution. The thionyl chloride was distilled off and the resulting yellow solid dissolved in acetonitrile (20 mL). This was added to a stirred solution of APSilTrn (0.173 g, 0.745 mmol) and NEt_3 (0.238 mL, 1.12 mmol) in chloroform (10 mL) over 1 hour, turning the solution a pale pink colour. The reaction mixture was stirred under nitrogen at room temperature overnight. The solvent was removed to afford a waxy yellowish solid. This was then washed with methanol to give the product as a white powder (60 mg, 0.086 mmol, 23%). $^1\text{H NMR}$: (400 MHz, DMSO) δ 9.16 (d, $J = 4.4$ Hz, 1H), 8.75 (t, $J = 5.6$ Hz, 1H), 8.14 (s, 1H), 7.73 (d, $J = 4.4$ Hz, 1H), 3.62 (t, $J = 5.8$ Hz, 6H), 3.24 (dd, $J = 13.5, 7.1$ Hz, 2H), 2.80 (t, $J = 5.8$ Hz, 6H), 1.71 – 1.45 (m, 2H), 0.43 – 0.07 (m, 2H). m/z (ESI) 697.3 (100%, M^+). Elemental Analysis Molecular Formula: $\text{C}_{32}\text{H}_{44}\text{N}_6\text{O}_8\text{Si}_2$ Predicted Results: C: 55.15%; H: 6.36%; N: 12.06% Found: C: 55.13%; H: 6.39%; N: 12.01%.

5.3.13 1,10-Phenanthroline-4,7-dicarboxylic acid bis[(3-silatranylpropyl) amide] bis-1,10-Phenanthroline Ruthenium(II) dichloride (RuPS).



Ru(phen)₂Cl₂ (35 mg, 0.065 mmol) and 1,10-Phenanthroline-4,7-dicarboxylic acid bis[(3-silatranylpropyl) amide] (50 mg, 0.072 mmol) were dissolved in ethanol (20 mL) and refluxed overnight to give a clear dark-red solution. The solvent was removed under reduced pressure and the complex was re-dissolved in 1 mL of MeOH, before purifying on Sephadex LH-20 in MeOH. The solvent was evaporated to afford deep red crystals (50 mg, 62%). ¹H NMR (400 MHz, CDCl₃) δ 8.75 (s, 2H), 8.63 (s, 2H), 8.61 (d, J = 5.1 Hz, 2H), 8.47 (t, J = 8.3 Hz, 4H), 8.40 (d, J = 5.0 Hz, 2H), 8.33 (d, J = 5.3 Hz, 2H), 7.96 – 7.85 (m, 4H), 7.82 (dd, J = 8.1, 5.4 Hz, 2H), 7.72 (dt, J = 7.3, 3.6 Hz, 2H), 7.55 (dd, J = 5.7, 3.3 Hz, 2H), 3.82 – 3.64 (m, 12H), 3.58 – 3.37 (m, 4H), 2.80 (t, J = 5.8 Hz, 12H), 1.85 – 1.71 (m, 4H), 0.62 – 0.42 (m, 4H). *m/z* (ESI) 597.2 (100%, M²⁺). Elemental Analysis Chemical Formula: C₅₆H₆₀Cl₂N₁₀O₈RuSi₂•5H₂O Predicted Results: C, 50.98; H, 5.35; N, 10.62; Found: C, 50.99; H, 5.37; N, 10.60

5.3.14 RuBS-CS

Chromatography grade silica (1 g) was suspended in a solution of RuBS (20 mg, ??) in MeCN. The suspension was stirred at room temperature for 3 hours before filtering to afford a dark orange powder. The powder was washed 3 times each with methanol, chloroform and diethyl ether respectively before drying under vacuum at 80 °C. $\nu_{\max}/\text{cm}^{-1}$ 797 (Si-OH), 1068 (Si-OCH₂CH₃), 1542 (CON-H); UV-visible λ_{\max} (solid state)/nm 289, 244, 466.

5.3.15 Preparation of PDMS compounds

PDMS was prepared from a Dow Corning Sylgard 184 elastomer kit, as per the instructions provided by the manufacturer. The elastomer and the curing agent were mixed in a 10:1 ratio and mixed for 5 minutes. The mixture was then poured into 9 cm petri dishes to between 1-2 mm in depth. The elastomer was then allowed to cure at 50 °C for 48 h.

5.3.15.1 PDMS-NH₂

This was prepared using a modified method by Brook et al.² The elastomer was steeped in a 30 mL solution of methanol, KOH and APTES (100:1:1 w/w) for 8 h at 50 °C. The polymer was then sonicated in fresh methanol for 30 minutes to remove any non-covalently bound reagents and washed with DCM.

5.3.15.2 PDMS-bpy

PDMS-NH₂ was steeped in 30mL of a solution of triethylamine (2 mL) in DCM for 30 minutes in order to ensure that the pendant NH₂ groups were not protonated, before addition of a solution of 2,2'-Bipyridine-4,4'-di(carbonylchloride) (0.1 g) in DCM (5 mL), this was then left to steep at room temperature overnight. The polymer was then sonicated in DCM for 30 minutes to remove any unbound reagents.

5.3.15.3 PDMS-Ru(bpy)₃

PDMS-bpy was steeped in a solution of Ru(bpy)₂Cl₂ (5 mg) in ethanol (30 mL) and heated to 75 °C for 48 h. The resulting red elastomer was sonicated in fresh ethanol for 4 h to remove physisorbed material. Any unbound Ru(bpy)₂Cl₂ is easily recovered through removal of solvent from the reaction mixture. UV-visible λ_{max} (solid state)/nm 289, 244, 466.

5.3.15.4 PDMS-SH

This was prepared using a modified method by Brook et al.² The elastomer was steeped in a 30 mL solution of methanol, KOH and 3-mercaptopropyl-trimethoxysilane (100:1:20 w/w) for 8 h at 50 °C. The polymer was then sonicated in fresh methanol for 30 minutes to remove any non-covalently bound reagents and washed with DCM.

5.3.15.5 PDMS-MA

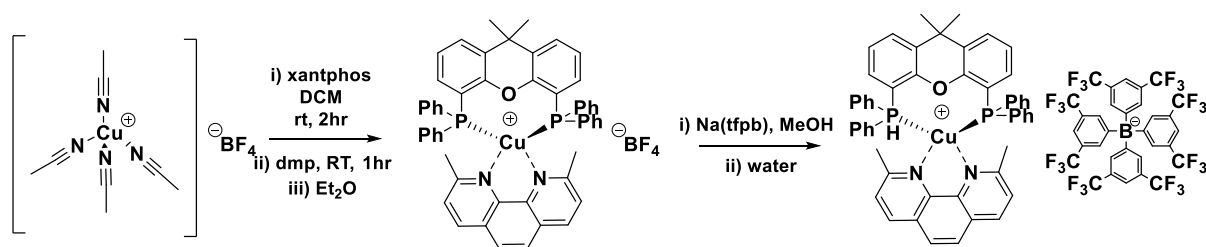
PDMS-SH was steeped in THF overnight, followed by heating to reflux in a solution of maleic anhydride (4g, excess) and AIBN (cat.) in DCM for 36 hours. The resulting polymer was washed in THF for 48 hours, refreshing the solvent every 12 hours.

5.3.15.6 PDMS-S-Ru

[Ru(phen)₂(phen-diol)](PF₆)₂ (2 mg) was dissolved in DCM and 4, 1x1 cm squares of PDMS-MA were steeped in the solution for 24 hours before filtering and washing with DCM for 48 hours.

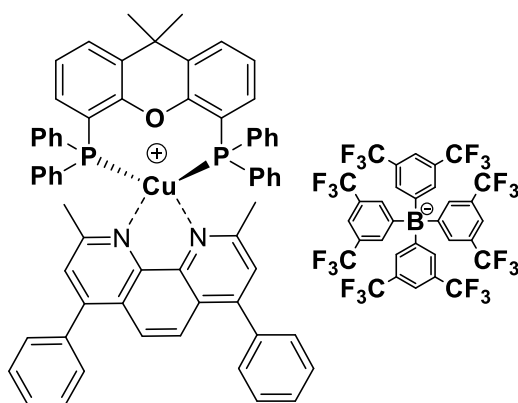
5.4 Copper Complexes

5.4.1 [Cu(dmp)(Xantphos)]tfpb



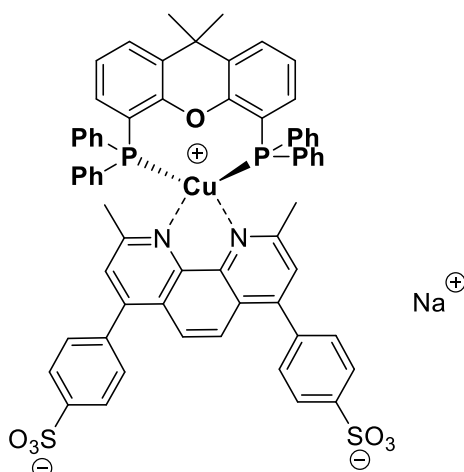
Cu(NCCH₃)₄.BF₄ (50 mg, 0.16 mmol) and xantphos (92 mg, 0.16 mmol) were dissolved in DCM (20 mL) and stirred at rt for 2 hours. 2,9-dimethyl-1,10-phenanthroline (dmp) (33 mg, 0.16 mmol) was then added, causing the solution to immediately turn bright yellow. The solution was stirred at rt for 1 hour before removing all but 1 mL of solvent under reduced pressure. The product was then precipitated by trituration with diethyl ether, and separated *via* vacuum filtration. The resulting bright-yellow powder was dissolved in the minimum amount of MeOH and Sodium tetrakis[3,5-bis(trifluoromethyl)phenyl]borate (tfpb) (0.164 g, 0.185 mmol) added. The solution was stirred for 1 hour at rt and then triturated with water to give bright yellow crystals (0.114 g, 0.146 mmol). ¹H NMR (400 MHz, CDCl₃) δ 8.17 (d, J = 8.2 Hz, 2H), 7.74 s, 8H), 7.70 (s, 2H), 7.65 (dd, J = 7.8, 1.1 Hz, 2H), 7.51 (s, 4H), 7.41 (d, J = 8.3 Hz, 2H), 7.26 – 7.13 (m, 6H), 7.09 – 6.95 (m, 16H), 6.95 – 6.84 (m, 2H), 2.25 (s, 6H), 1.74 (d, J = 7.1 Hz, 6H). m/z (ES⁺) 849.6 (100 %, M⁺).

5.4.2 [Cu(bathocuproine)(xantphos)]tfpb



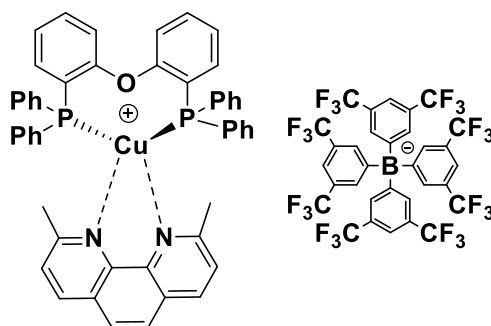
The method for this synthesis is the same as for [Cu(dmp)(Xantphos)]tfpb but bathocuproine (2,9-dimethyl-4,7-diphenyl-1,10-phenanthroline) was used instead of dmp. Cu(NCCH₃)₄.BF₄ (50 mg, 0.16 mmol) and xantphos (92 mg, 0.16 mmol) were dissolved in DCM (20 mL) and stirred at rt for 2 hours. Bathocuproine (58 mg, 0.16 mmol) was then added, causing the solution to immediately turn bright yellow. The solution was stirred at rt for 1 hour before removing all but 1 mL of solvent under reduced pressure. The product was then precipitated out by trituration with diethyl ether and separated *via* vacuum filtration. The resulting bright-yellow powder was dissolved in the minimum amount of MeOH and Sodium tetrakis[3,5-bis(trifluoromethyl)phenyl]borate (tfpb) (0.164 g, 0.185 mmol) was added. The solution was stirred for 1 hour at rt and then trituated with water to give bright yellow crystals (0.114g, 0.146 mmol). ¹H NMR (400 MHz, CDCl₃): δ 7.80 (s, 2H), 7.69 (d, J = 7.3 Hz, 2H), 7.58 (t, J = 6.8 Hz, 8H), 7.49 (d, J = 9.5 Hz, 6H), 7.24 (t, J = 7.8 Hz, 4H), 7.18 – 7.04 (m, 16H), 6.99 (d, J = 3.4 Hz, 2H), 2.35 (s, 6H), 1.78 (s, 6H). m/z (ES+) 1001.3 (100 %, M⁺). Elemental Analysis Chemical Formula: C₆₅H₅₂BCuF₄N₂OP₂ Predicted Results: C, 71.66; H, 4.81; N, 2.57; Found: C, 71.60; H, 4.95; N, 2.35.

5.4.3 Na[Cu(bathocuproine-disulfonate)(xantphos)]



Cu(NCCH₃)₄.BF₄ (50 mg, 0.16 mmol) and xantphos (92 mg, 0.16 mmol) were dissolved in MeCN (20 mL) and stirred at rt for 2 hours. Disodium bathocuproinedisulfonate (90 mg, 0.16 mmol) was added and the reaction mixture stirred at 30 °C overnight. The solvent was removed under reduced pressure. The resulting dark yellow powder was dissolved in MeOH and purified on Sephadex LH-20 to give a bright yellow solid (60 mg, 32% yield). ¹H NMR (400 MHz, CDCl₃): δ 8.02 (d, J = 8.8 Hz, 2H), 7.99 (d, J = 8.6 Hz, 2H), 7.96 (d, J = 6.7 Hz, 2H), 7.72 (s, 2H), 7.60 (d, J = 6.9 Hz, 4H), 7.32 (d, J = 5.0 Hz, 3H), 7.22 – 7.05 (m, 6H), 7.05 – 6.77 (m, 20H), 2.18 (s, 6H), 1.66 (s, 6H). m/z (ES⁺) 1159.0 (100 %, M⁺).

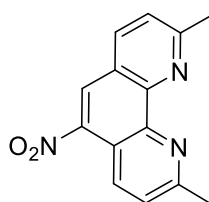
5.4.4 [Cu(DPEPhos)(dmp)]tfpb



Cu(NCCH₃)₄.BF₄ (50 mg, 0.16 mmol) and DPEPhos (92 mg, 0.16 mmol) were dissolved in DCM (20 mL) and the solution was stirred at rt for 2 hours. 2,9-dimethyl-1,10-

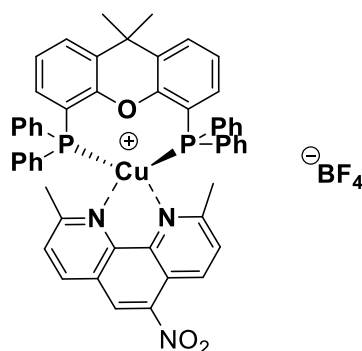
phenanthroline (33 mg, 0.16 mmol) was then added, causing the solution to immediately turn bright yellow. The solution was stirred at rt for 1 hour before removing all but 1 mL of solvent under reduced pressure. The product was then precipitated out by trituration with diethyl ether and separated *via* vacuum filtration. The resulting bright-yellow powder was dissolved in the minimum amount of MeOH and Sodium tetrakis[3,5-bis(trifluoromethyl)phenyl]borate (tfpb) (0.164 g, 0.185 mmol) was added. The solution was stirred for 1 hour at room temperature and then triturated with water to give bright yellow crystals. ^1H NMR (400 MHz, CDCl_3): δ 8.41 (d, $J = 8.3$ Hz, 2H), 7.88 (s, 2H), 7.62 (d, $J = 8.3$ Hz, 2H), 7.40 – 7.32 (m, 2H), 7.21 (dd, $J = 12.4, 4.9$ Hz, 6H), 7.05 (t, $J = 7.6$ Hz, 8H), 7.01 – 6.93 (m, 10H), 2.46 (s, 6H). m/z (ES+) 809.2 (100 %, M^+).

5.4.5 5-Nitrocuproine



2,9-dimethyl-1,10-phenanthroline (0.5 g, 2.4 mmol) was dissolved in HNO_3 (5 ml, 70%) and H_2SO_4 (10 mL, 95%) and heated to 115 °C for 1 hr before pouring into ice (100 g). After the ice had melted the solution was brought to pH 8 using concentrated NaOH solution and the resulting precipitate was filtered off and washed with water to yield a grey solid (0.2 g, 32%). ^1H NMR (400 MHz, CDCl_3): δ 8.96 (d, $J = 8.7$ Hz, 1H), 8.64 (s, 1H), 8.31 (d, $J = 8.2$ Hz, 1H), 7.68 (dd, $J = 17.6, 8.5$ Hz, 2H), 3.03 (d, $J = 6.6$ Hz, 6H). m/z (ES+) 253.1 (M^+).

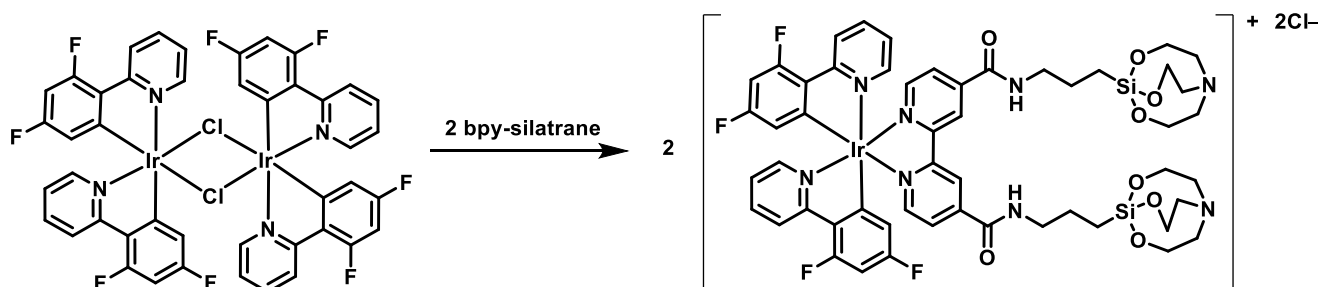
5.4.6 [Cu(5-Nitrocuproine)(xantphos)]tfpb



Cu(NCCH₃)₄.BF₄ (50 mg, 0.16 mmol) and xantphos (92 mg, 0.16 mmol) were dissolved in DCM (20 mL) and the solution was stirred at rt for 2 hours. 5-Nitrocuproine (40 mg, 0.16 mmol) was then added, causing the solution to immediately turn orange. The solution was stirred at rt for 1 hour before removing all but 1 mL of solvent under reduced pressure. The product was then precipitated by trituration with diethyl ether and separated *via* vacuum filtration. ¹H NMR (400 MHz, CDCl₃): δ 8.94 (d, J = 11.3 Hz, 1H), 8.53 (s, 1H), 8.23 (d, J = 8.3 Hz, 1H), 7.73 (s, 8H), 7.66 (d, J = 7.6 Hz, 2H), 7.61 (d, J = 8.8 Hz, 1H), 7.50 (s, 4H), 7.45 (d, J = 8.3 Hz, 1H), 7.28 – 7.16 (m, 6H), 7.09 – 6.99 (m, 14H), 6.97 (dt, J = 7.3, 3.8 Hz, 2H), 2.36 (s, 3H), 2.31 (s, 3H), 1.73 (d, J = 8.7 Hz, 6H). m/z (ES⁺) 849.2 (M⁺).

5.5 Other metal complexes

5.5.1 Ir(fppy)₂(bpy-silatrane)



Ir₂(fppy)₄Cl₂³ (68.7 mg, 51 μmol) and bpy-silatrane (71 mg, 100 μmol) were dissolved in DMF (20 mL), heated to 90 °C and stirred for 24 hours under argon. After

cooling the solvent was removed under reduced pressure. The resulting dark yellow powder was purified using size exclusion column chromatography on Sephadex LH-20 in methanol to afford a bright yellow powder (40 mg, 59 %). ^1H NMR (400 MHz, CDCl_3) δ 10.51 (s, 1H), 9.53 (d, $J = 5.9$ Hz, 1H), 8.36 (d, $J = 8.7$ Hz, 2H), 8.15 (dd, $J = 5.6, 1.5$ Hz, 2H), 7.98 (d, $J = 5.6$ Hz, 1H), 7.86 (t, $J = 7.2$ Hz, 2H), 7.44 (d, $J = 4.9$ Hz, 2H), 7.07 (dd, $J = 9.7, 3.7$ Hz, 2H), 6.69 – 6.56 (m, 2H), 5.72 (dd, $J = 8.2, 2.3$ Hz, 2H), 3.76 (dd, $J = 11.8, 6.1$ Hz, 9H), 3.52 (d, $J = 9.8$ Hz, 5H), 2.79 (t, $J = 5.8$ Hz, 8H), 1.97 – 1.82 (m, 6H), 0.59 – 0.43 (m, 3H). m/z (ESI) 1245.3 (100 %, M^+).

5.6 References

1. Gottlieb, H. E., Kotlyar, V. & Nudelman, A. NMR Chemical Shifts of Common Laboratory Solvents as Trace Impurities In the course of the routine use of NMR as an aid for organic chemistry , a day-to-day problem is the identification of signals deriving from common contaminants literature , but the. *J. Org. Chem.* **62**, 7512–7515 (1997).
2. Zhang, J., Chen, Y. & Brook, M. A. Facile Functionalization of PDMS Elastomer Surfaces Using Thiol – Ene Click Chemistry. (2013). doi:10.1021/la403425d
3. Baggaley, E. *et al.* Combined Two-Photon Excitation and d - f Energy Transfer in a Water-Soluble Ir III / Eu III Dyad : Two Luminescence Components from One Molecule for Cellular Imaging. 8898–8903 (2014). doi:10.1002/chem.201403618

6 Conclusions and Future Work

Contents

6	Conclusions and Future Work	140
6.1	Aims.....	142
6.2	Ruthenium-based Photosensitising Materials	142
6.3	Copper-based Photosensitising Materials	142
6.4	Summary	145
6.5	Final Words.....	146
6.6	References.....	148

6.1 Aims

This research aimed to synthesise and characterise a transition metal complex-based photosensitising compound supported on silica that could successfully reduce bacterial populations, as well as to measure its ability to produce singlet oxygen.

6.2 Ruthenium-based Photosensitising Materials

A ruthenium complex, $[\text{Ru}(\text{bpy})_2(\text{bpy-silatrane})]\text{Cl}_2$ (RuBS) was successfully covalently immobilised onto various types of silica and characterised by UV-vis and luminescence spectroscopy. The singlet oxygen generation of the free complex in acetonitrile was determined ($\Phi_{1O_2} = 0.55$) and the compound immobilised onto chromatography grade silica (RuBS-CS) was also found to produce singlet oxygen, albeit with poorer efficiency.

RuBS-CS was unable to reduce colonies of *S. aureus* or *E. coli* after 2 hours of irradiation by 455 nm light (2.4 mWcm^{-2}). The composite material was then post-functionalised using 3-amino(propyltriethoxysilane) to produce RuBS-CS-NH₂, which was able to reduce colonies by 6 log₁₀ after 2 hours of illumination at concentrations of 5 mg of compound per mL of NaPhos buffer. These results, however, were not reproducible with newly synthesised batches of RuBS-CS-NH₂.

A number of other ruthenium polypyridyl-based immobilised photosensitisers have been made and their singlet oxygen generating abilities verified. However these compounds have not been tested for bactericidal efficacy.

6.3 Copper-based Photosensitising Materials

$[\text{Cu}(\text{xantphos})(2,9\text{-dimethyl-1,10-phenanthroline})]\text{tfpb}$ (CuXD) was found to produce singlet oxygen in acetonitrile with a singlet oxygen quantum yield of 30% ($\Phi_{1O_2} = 0.30$). This was determined via observation of singlet oxygen phosphorescence at 1270 nm. When

immobilised onto chromatography silica, Cu-XD-CS was found to produce singlet oxygen in water using a singlet oxygen probe to indirectly measure the singlet oxygen generated. CuXD-CS reduced CFU_{mL}⁻¹ in *S. aureus* and *E. coli* by 99.99999% (6 log₁₀) after exposure to 405 nm light (17.5 mWcm⁻²) for 2 and 3 hours respectively in concentrations of 5 mgmL⁻¹ in NaPhos buffer.

Further experiments need to be run to determine the optimum working concentrations and conditions for bactericidal activity of the compound. An experiment testing whether chromatography grade silica (40-60 mesh) on its own shows bactericidal activity upon illumination with 405 nm light is necessary as a control. Using a quencher such as sodium azide, a known singlet oxygen quencher,^{1,2} to test whether it is the singlet oxygen produced that is killing the bacteria and not another process, such as the photosensitiser interacting directly with the bacteria. Live/dead staining can also be performed to determine whether or not the bacteria in the viability assays are being killed due to membrane damage.³ The compound may also generate other reactive oxygen species (ROS) such as the hydroxyl radical and superoxide radical. The generation of these species should be tested utilising the appropriate probes.⁴ Such as 2,2'-di-p-nitrophenyl-5,5'-diphenyl-(3,3'-dimethoxy)-4,4'-bisphenyleneditetrazolium chloride (NBT) or luminol for the superoxide anion,

The leaching rate of the complex from the surface of the silica, as well as photobleaching rate of the complex is paramount for determining commercial viability. Utilising a solar simulator or white light, increasing the scale of the bacterial inactivation assays and disinfecting actual wastewater are also necessary to evaluate the feasibility of the compounds for real-world use.

Counter ion effect on bactericidal activity should also be tested, not only to see if the current salt, tetrakis[3, 5-bis(trifluoromethyl)phenyl]borate (tfpb) enhances antibacterial activity but if a cheaper counterion can be used.

In these works the salt [Cu(xantphos)(2,9-dimethyl-1,10-phenanthroline)]tfpb was used, which is soluble in polar organic solvents. In addition, a water-soluble complex should be synthesised, so that the bactericidal activity of the complex in solution may be assessed. A water soluble salt of CuXD may be difficult to synthesise, as the ligands on the complex are very bulky and non-polar.

Numerous other heteroleptic copper diamine diphosphine complexes, {Cu(NN)(PP)}⁺, were synthesised and characterised in hopes of producing a singlet oxygen generating complex similar to CuXD but with an MLCT absorption band further in the visible spectrum. [Cu(xant)(bathocuproine)]tfpb and [Cu(xant)(bathocuproinesulfonate)]Na were successfully synthesised and were found to have an MLCT absorption band that is redshifted by 10 nm with respect to CuXD. While this represents a very small change in absorbance the molar extinction coefficient of the MLCT band (390 nm) increased by a factor of 3. The newly synthesised compounds also gave a higher singlet oxygen quantum yield ($\Phi_{^1O_2} = 0.4$). Future work will see these complexes adsorbed onto silica and used in bactericidal assays as for CuXD-CS.

Although CuXD-CS certifies itself a promising compound based on preliminary antibacterial tests, it is unlikely that the photosensitiser will be used in this form. This is due to the practical difficulties associated with utilising a free-flowing fine-meshed powder such as chromatography silica (easy to lose compound when handled manually, risk of inhalation leading to silicosis). It may be advisable to mechanically fix the CuXD-CS powder onto a flat surface, such as a polymer or glass. Due to the hydrophobicity of [Cu(dmp)(xant)]tfpb, the

complex can be easily immobilised on surfaces by “painting” surfaces with the complex in acetonitrile or dichloromethane. Research is underway of creating thin films onto glass by spin coating.

6.4 Summary

A breakdown of what has been achieved throughout this work:

- Ruthenium polypyridyl complexes RuBS, RuBMS, RuPS successfully synthesised and characterised using ^1H NMR, ESI Mass Spectrometry, Elemental Analysis, UV-visible spectrometry, fluorescence spectrometry and time-resolved emission spectrometry.
- The singlet oxygen quantum yields for the above compounds in acetonitrile were measured through detection of singlet oxygen phosphorescence at 1275 nm.
- RuBS was successfully immobilised covalently onto three types of silica: Chromatography grade silica (40-60 mesh), SBA-15 (8 nm pore diameter), MCM-41. These immobilised compounds were characterised using solid-state UV-visible spectroscopy, solid-state emission spectroscopy and ATR-FTIR spectroscopy. The singlet oxygen generating ability of these materials was measured indirectly using a singlet oxygen probe.
- Two PDMS-based photosensitising materials we synthesised, Ru-N-PDMS and Ru-S-PDMS and were characterised by UV-visible and ATR FTIR spectroscopy.
- A ruthenium polypyridyl complex RuBPS was ionically bound to Amberlite® IRA-900 and characterised by UV-visible and emission spectroscopy.
- The singlet oxygen generating ability of Ru-N-PDMS and Ru(BPS)-IRA900 were measured utilising a singlet oxygen probe (DMA).

- RuBS immobilised on chromatography grade silica was found to not reduce colonies of *S. aureus* or *E. coli* under illumination by 455 nm light (2.4 mWcm^{-2}) after 2 hours of illumination.
- [Cu(dmp)(xant)]tfpb (CuXD) was synthesised according to literature, characterised and its singlet oxygen quantum yield in acetonitrile measured through detection of singlet oxygen phosphorescence at 1275 nm.
- CuXD was immobilised onto chromatography grade silica through dry loading (CuXD-CS) and characterised using solid-state UV-visible spectroscopy, solid-state emission spectroscopy.
- The above compound was found to successfully deactivate colonies of both *S. aureus* and *E. coli* by 6 log₁₀ after 2 hours of illumination.
- New complexes [Cu(BC)(xant)]tfpb, [Cu(BCS)(xant)]Na and [Cu(5NC)(xant)]tfpb were synthesised and characterised ¹H NMR, ESI Mass Spectrometry, Elemental Analysis, UV-visible spectrometry, fluorescence spectrometry and time-resolved emission spectrometry.
- The singlet oxygen quantum yields of the above complexes was measured in acetonitrile through detection of singlet oxygen phosphorescence at 1275 nm.

6.5 Final Words

The research project presented herein is still in its nascent stages. Nevertheless, some of the outcomes have been promising. The most promising of these is the potential of the use of Copper (I) photosensitisers as disinfecting agents. The field of transition metal photosensitisers for water disinfection is mainly guided by the work performed by Fresnadillo et al,⁵⁻¹³ with most of the photosensitisers being ruthenium-based. Whilst ruthenium complexes often yield highly efficient and robust photocomplexes, the prospect of replacing

ruthenium complexes (which suffer from increasing costs, low earth abundance and energy intensive syntheses) could present economically and environmentally advantageous.

The bactericidal activity of CuXD-CS was indeed promising. However, there are still a litany of tests required to determine its suitability as a point-of-use method for water treatment. Ultimately, the composite material must be applied to a practical setup such as a solar reactor or SODIS-style vessel. Designing one of these systems may still yet present the largest hurdle towards production of a sustainable model for water disinfection in rural areas. Research on graphitic carbon nitride as a photocatalyst by Zeng et al. should be a model for this area of research, providing data on durability, reusability and showing effective application of the active material in both vessel and reactor set ups.¹⁴ Whilst the research by Zeng et al. is excellent there is still assessment of costing and sustainability and ease of use for the technology and uptake statistics also need to be studied. Indeed, the scope of this study is relatively narrow compared to the necessary research required to produce an effective POU water disinfection technology, but you have to start somewhere.

6.6 References

1. Sabbahi, S., Ben Ayed, L. & Jemli, M. Staphylococcus aureus photodynamic inactivation mechanisms by rose bengal: use of antioxidants and spectroscopic study. *Appl. Water Sci.* **8**, 1–9 (2018).
2. Linetsky, M. & Ortwerth, B. J. Quantitation of the singlet oxygen produced by UVA irradiation of human lens proteins. *Photochem Photobiol* **65**, 522–529 (1997).
3. Hatz, S., Lambert, J. D. C. & Ogilby, P. R. Measuring the lifetime of singlet oxygen in a single cell: Addressing the issue of cell viability. *Photochem. Photobiol. Sci.* **6**, 1106–1116 (2007).
4. Gomes, A., Fernandes, E. & Lima, L. F. C. Fluorescence probes used for detection of reactive oxygen species. *J. Biochem. Biophys. Methods* **65**, 45–80 (2005).
5. García-Fresnadillo, D. Singlet Oxygen Photosensitizing Materials for Point-of-Use Water Disinfection with Solar Reactors. *ChemPhotoChem* **2**, 512–534 (2018).
6. Díez-Mato, E., Cortezón-Tamarit, F. C., Bogialli, S., García-Fresnadillo, D. & Marazuela, M. D. Phototransformation of model micropollutants in water samples by photocatalytic singlet oxygen production in heterogeneous medium. *Applied Catalysis B: Environmental* **160–161**, 445–455 (2014).
7. Garcia-Fresnadillo, D., Georgiadoub, Y., Orellana ', G., Braunb), A. M. & Oliverosb, E. 06. Singlet-Oxygen ('Ag) Production by Rutheniurn(I1) Complexes Containing Polyazaheterocyclic Ligands in Methanol and in Water. *HELVETICA CHIMICA ACTA* ~ **79**, (1996).
8. Manjón, F., Santana-Magaña, M., García-Fresnadillo, D. & Orellana, G. Are silicone-supported [C60]-fullerenes an alternative to Ru(ii) polypyridyls for photodynamic solar water disinfection? *Photochemical & photobiological sciences : Official journal of the European Photochemistry Association and the European Society for Photobiology* **13**, 397–406 (2014).
9. Garcia-Fresnadillo, D., Georgiadou, Y., Orellana, G., Braun, A. M. & Oliveros, E. Singlet-Oxygen production by Ruthenium(II) Complexes Containing Polyazaheterocyclic Ligands in Methanol and Water. *Helvetica Chimica Acta* **79**, 1222–1238 (1996).
10. Villén, L., Manjón, F., García-Fresnadillo, D. & Orellana, G. Solar water disinfection by photocatalytic singlet oxygen production in heterogeneous medium. *Applied Catalysis B: Environmental* **69**, 1–9 (2006).
11. Manjón, F., Villén, L., García-fresnadillo, D. & Orellana, G. On the Factors Influencing the Performance of Solar Reactors for Water Disinfection with Photosensitized Singlet Oxygen. *Environ. Sci. Technol.* **42**, 301–307 (2008).

12. Manjón, F., Santana-Magaña, M., García-Fresnadillo, D. & Orellana, G. Singlet oxygen sensitizing materials based on porous silicone: photochemical characterization, effect of dye reloading and application to water disinfection with solar reactors. *Photochemical & photobiological sciences : Official journal of the European Photochemistry Association and the European Society for Photobiology* **9**, 838–45 (2010).
13. Jimenez-Hernandez, M. E., Manjon, F., Garcia-Fresnadillo, D. & Orellana, G. Solar water disinfection by singlet oxygen photogenerated with polymer-supported Ru(II) sensitizers. *Solar Energy* **80**, 1382–1387 (2006).
14. Zeng, X. et al. Cooperatively modulating reactive oxygen species generation and bacteria-photocatalyst contact over graphitic carbon nitride by polyethylenimine for rapid water disinfection. *Applied Catalysis B: Environmental* **274**, 119095 (2020).

Appendix

1 Chapter 2: Synthesis and characterisation

1.1 Molar Extinction coefficients

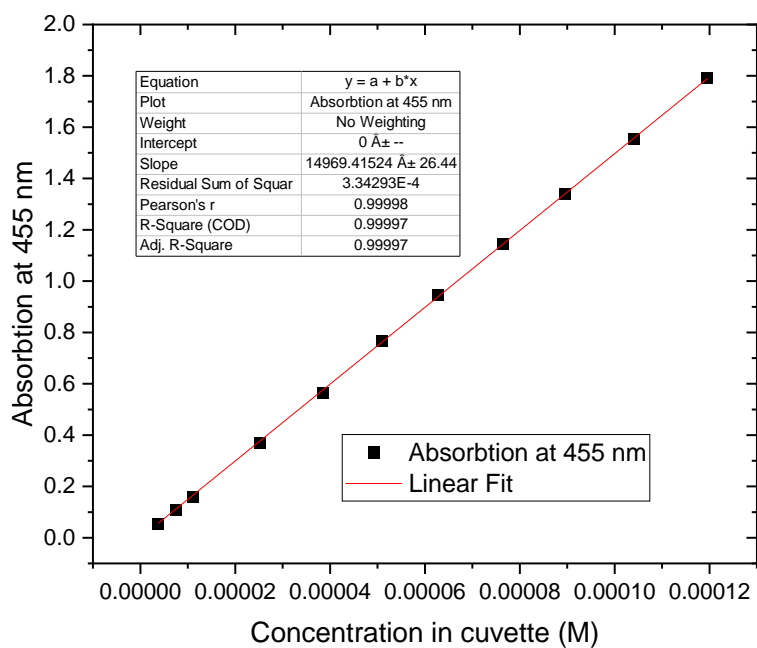


Figure 1 RuBS molar extinction coefficient

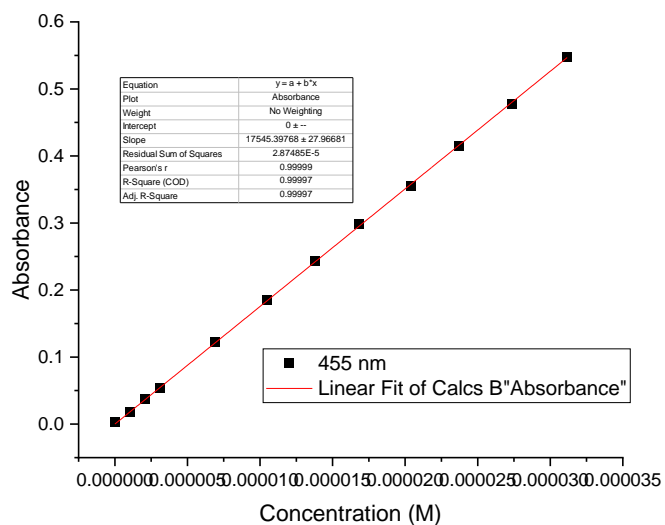


Figure 2 RuBMS molar extinction coefficient plot

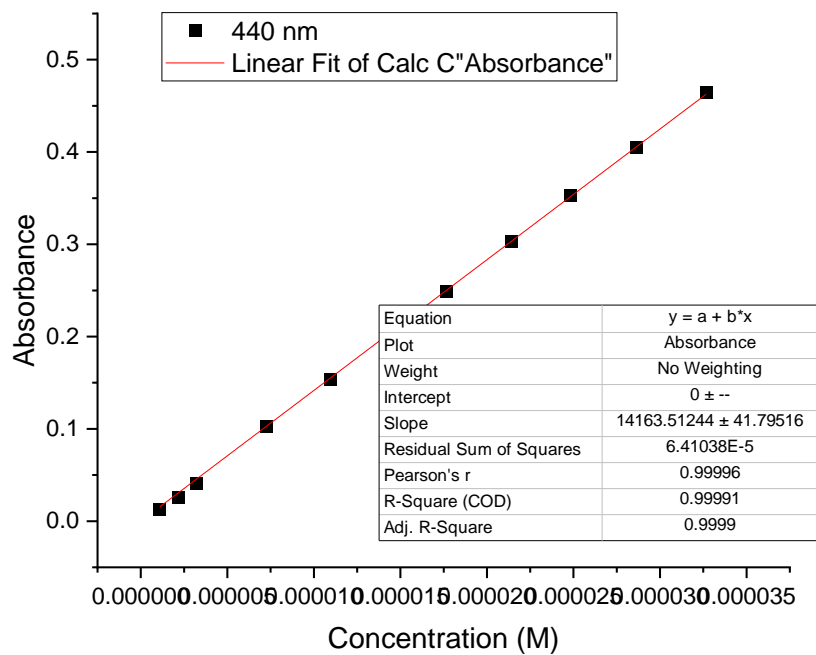


Figure 3 RuPS molar extinction coefficient plot

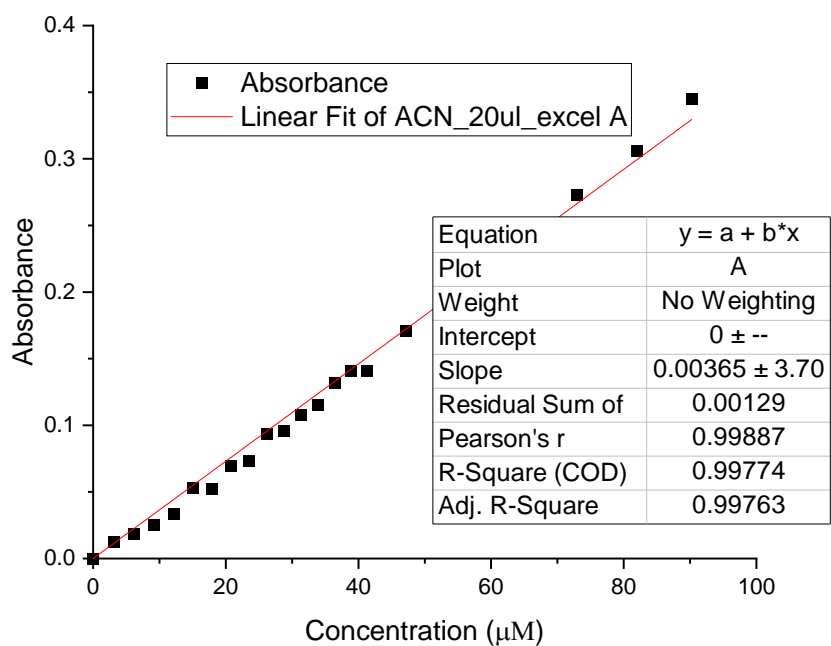


Figure 4 Cu(xant)(dmp) molar extinction coefficient

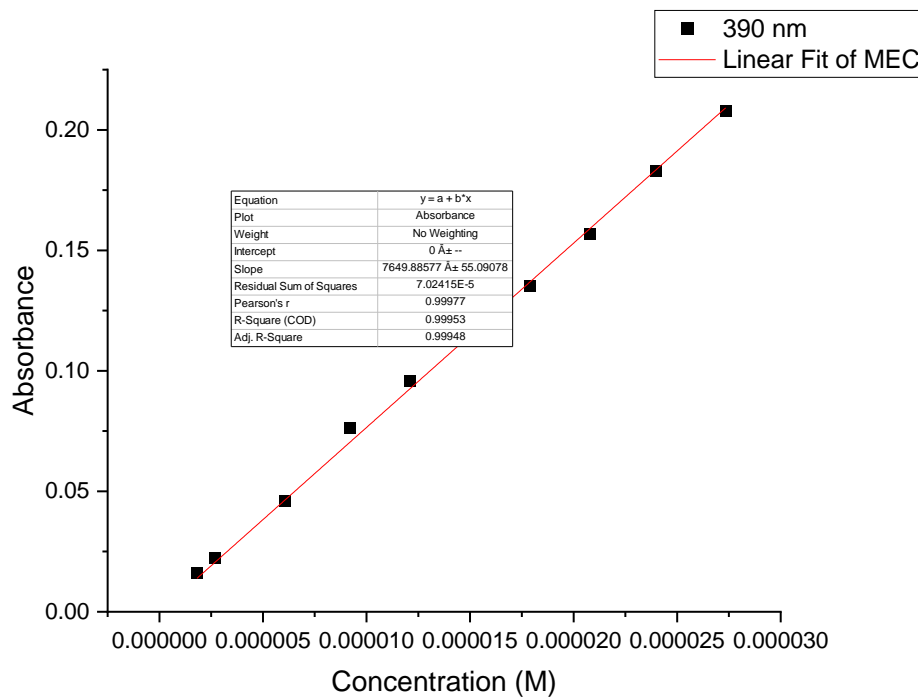


Figure 5 Cu(BC)(xant) molar extinction coefficient plot

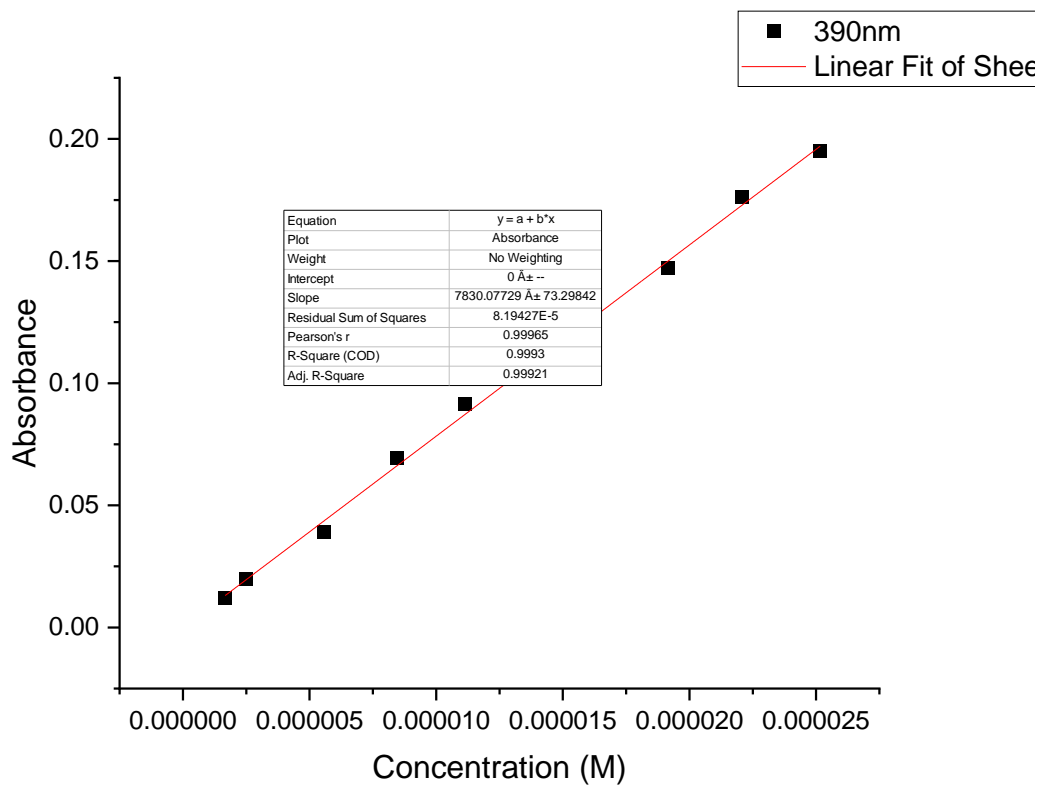


Figure 6 Cu(BCS)(xant) molar extinction coefficient plot

1.2 Lifetimes

1.2.1 Cu(DPEPhos)(dmp).tfpb

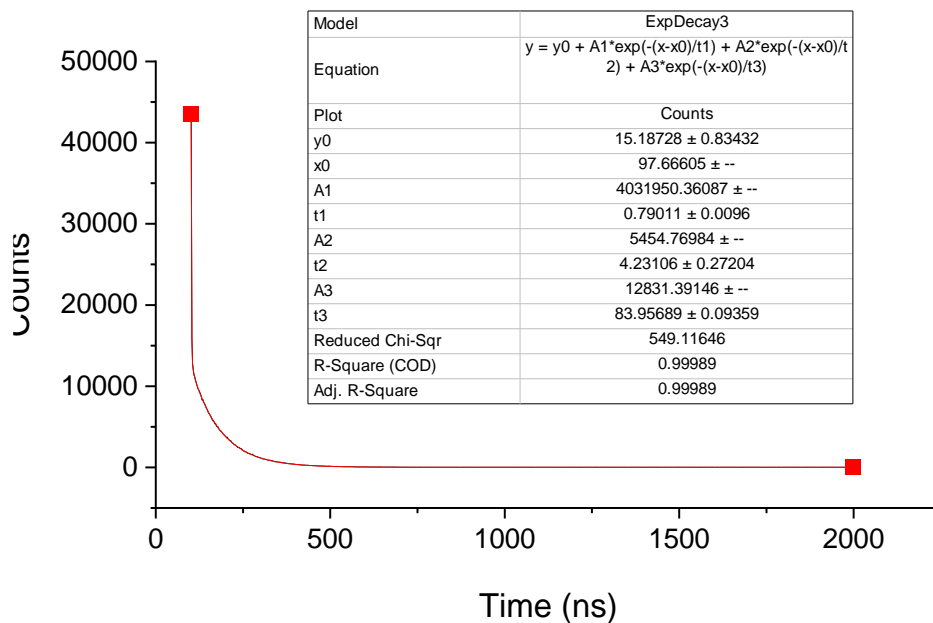


Figure 7 air equilibrated lifetime

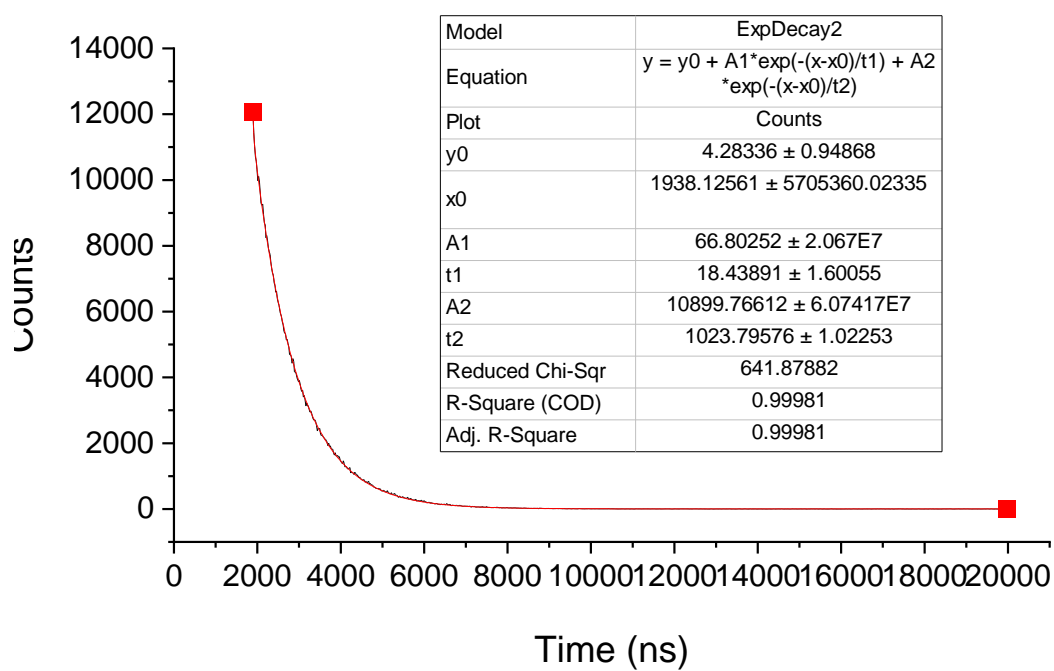


Figure 8 Degassed lifetime

2 Chapter 3: Singlet Oxygen Studies

2.1 Direct detection of singlet oxygen phosphorescence at 1275 nm

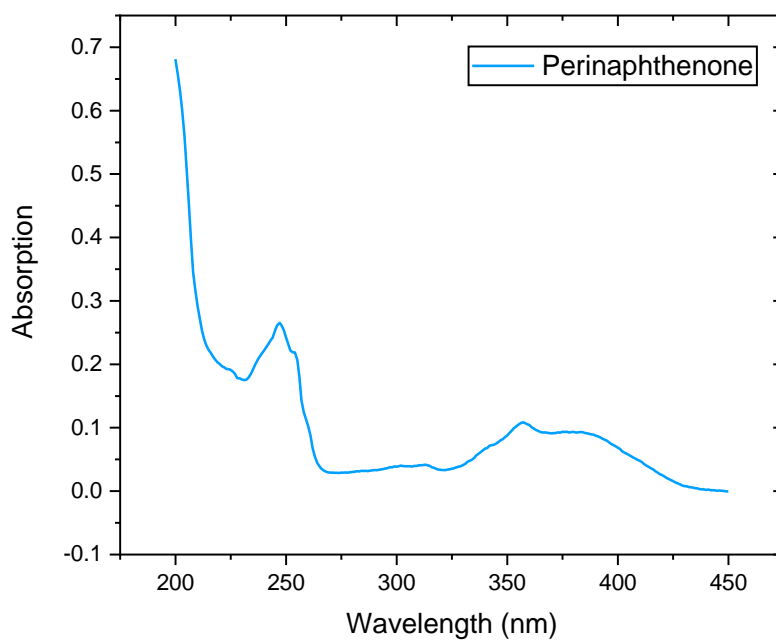


Figure 9 Perinaphthenone absorption spectrum

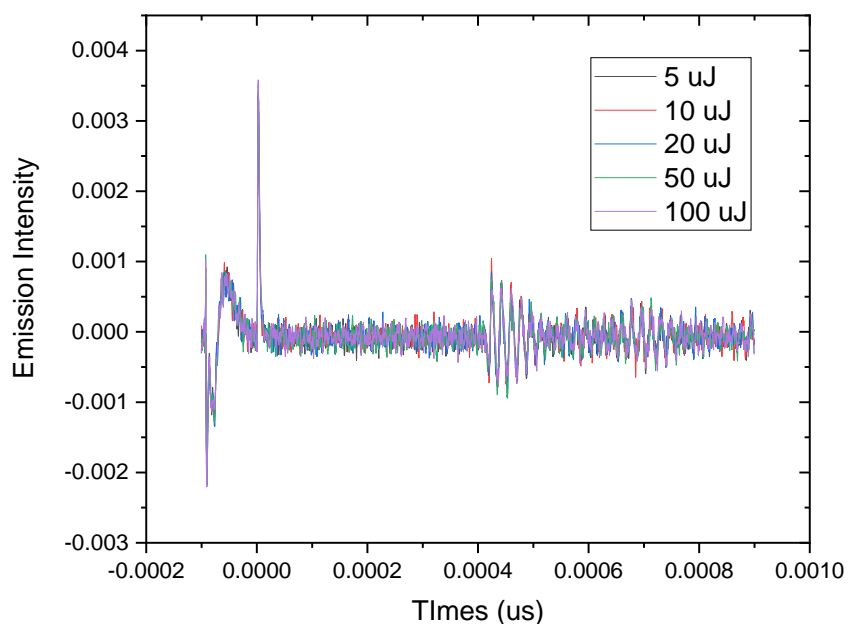


Figure 10 Overlaid decay traces of acetonitrile illuminated with 355 nm light, detection at 1275 nm at various power settings.

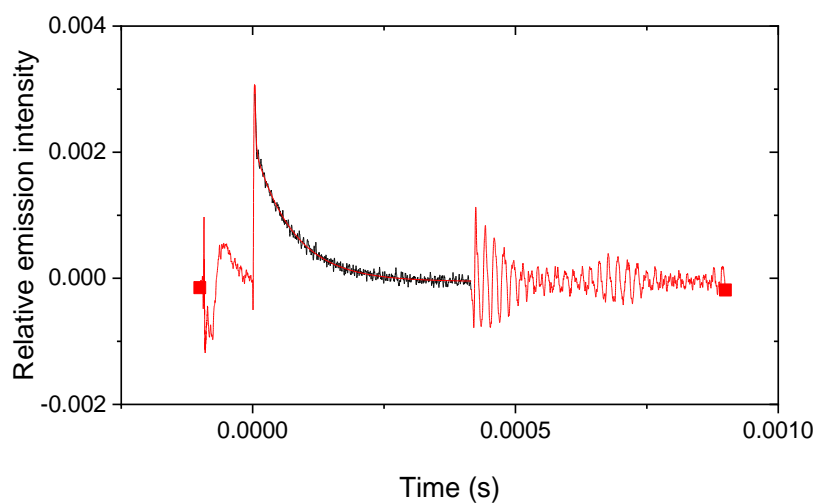


Figure 11 Singlet oxygen phosphorescence decay curve at 1275 nm. Produced by shining 355 nm light set to 20 μJ per pulse at a sample of Cu(xant)(dmp).tfpb in MeCN at an optical density of 0.2.

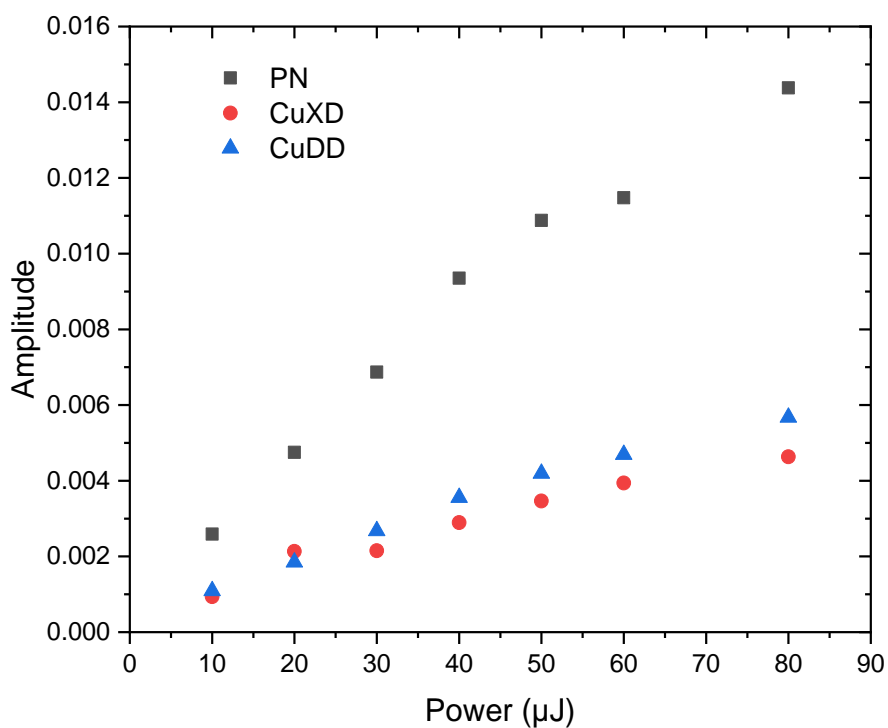
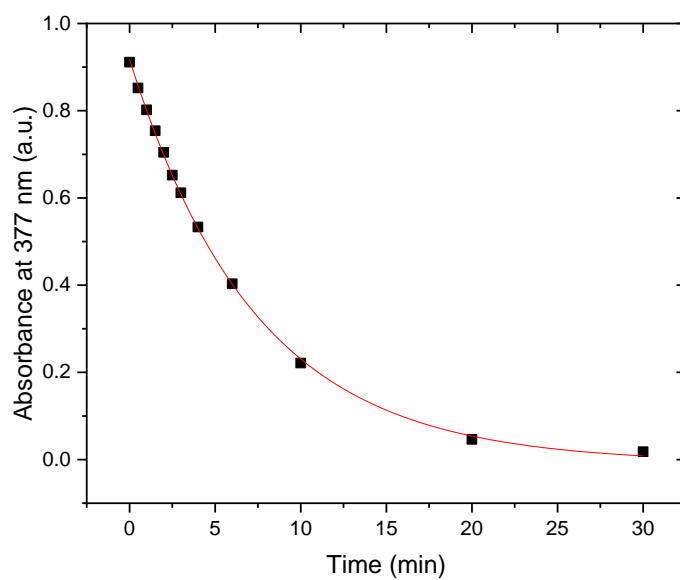
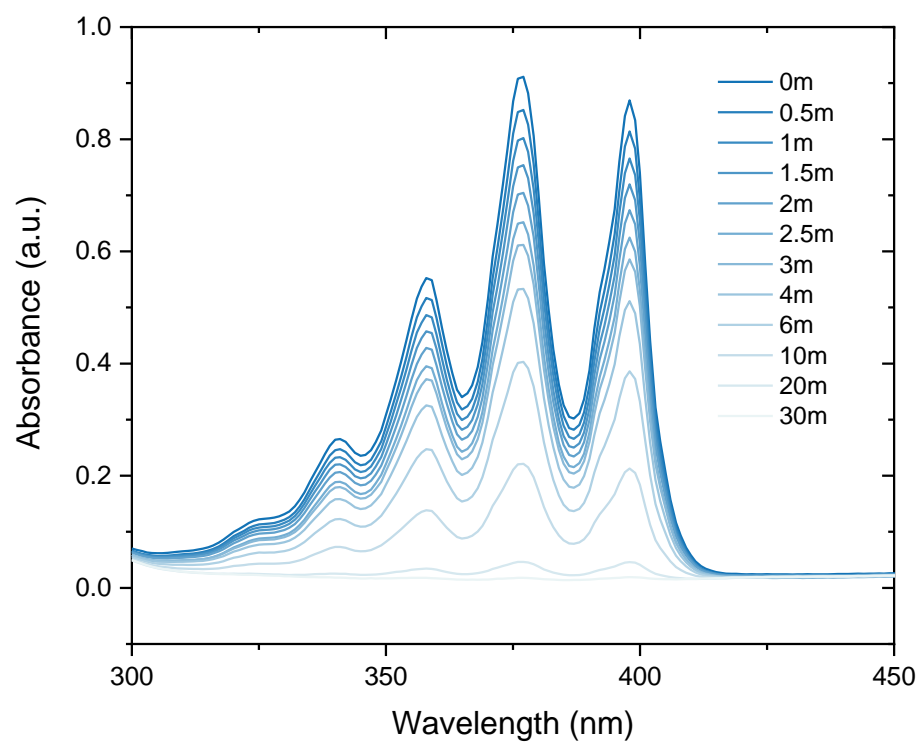
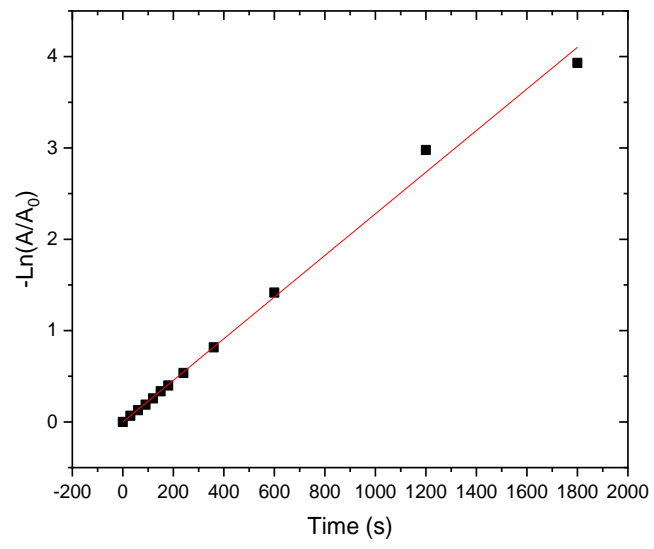


Figure 12 Amplitude of singlet oxygen phosphorescence intensity measured at 1275 nm compared to energy of 355 nm. PN is the standard perinphthenone, CuXD is Cu(xant)(dmp).tfpb and CuDD is Cu(DPEPhos)(dmp).tfpb. All performed in MeCN at an OD of 0.2 ± 0.01 .

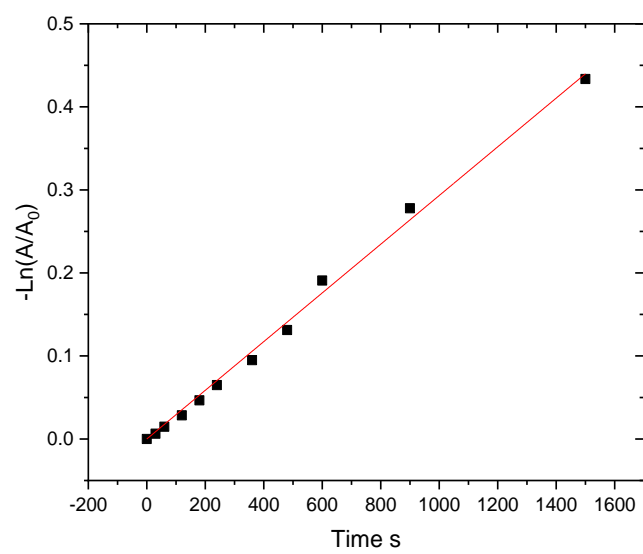
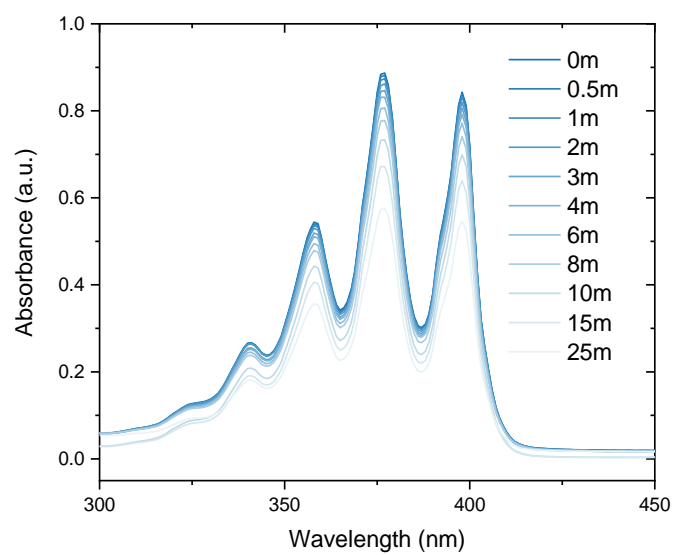
2.2 DMA degradation assays

2.2.1 $[\text{Ru}(\text{bpy})_3]\text{Cl}_2$

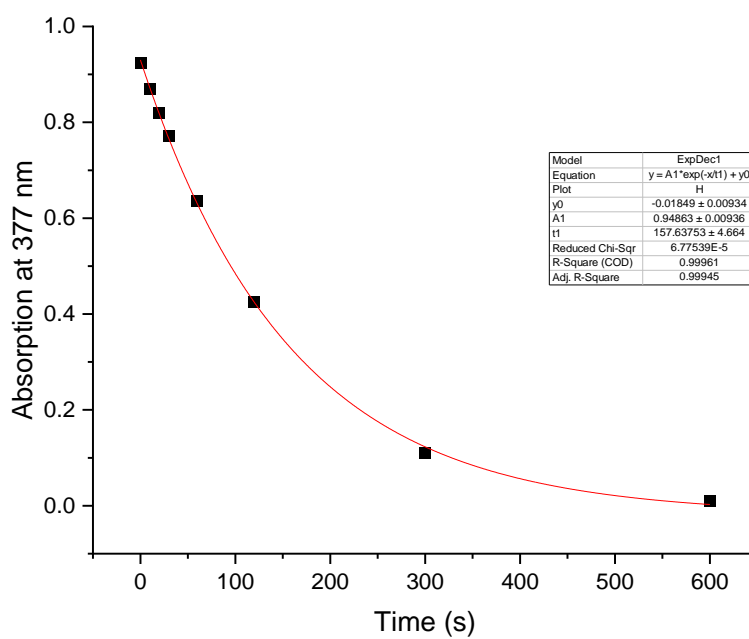
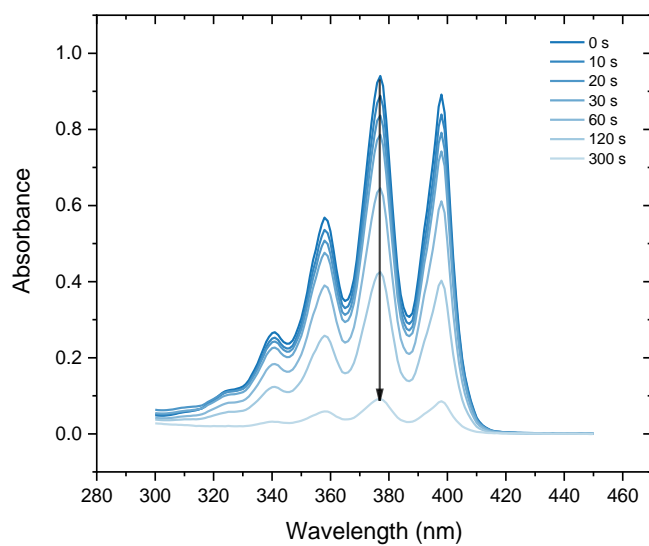


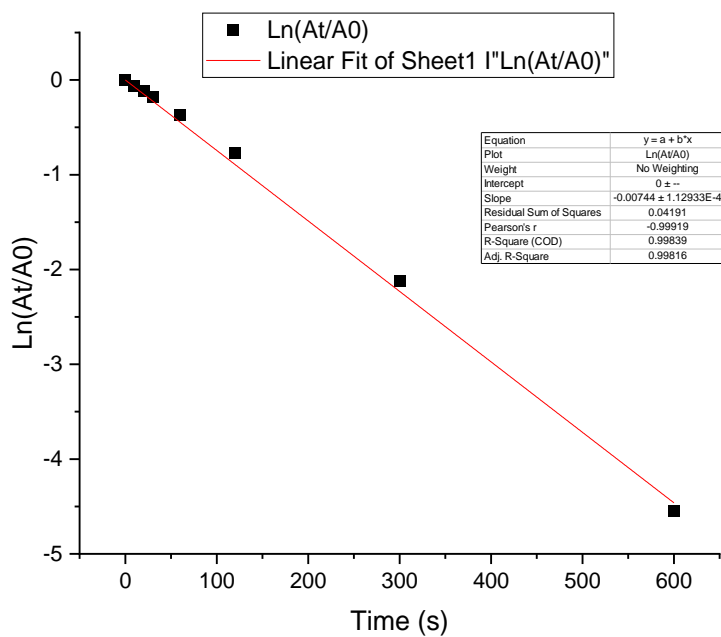


2.3 RuBPS-IRA900 DMA degradation assay



2.4 RuBS-SBA15 DMA degradation assays ($37 \text{ } \mu\text{mol g}^{-1}$)

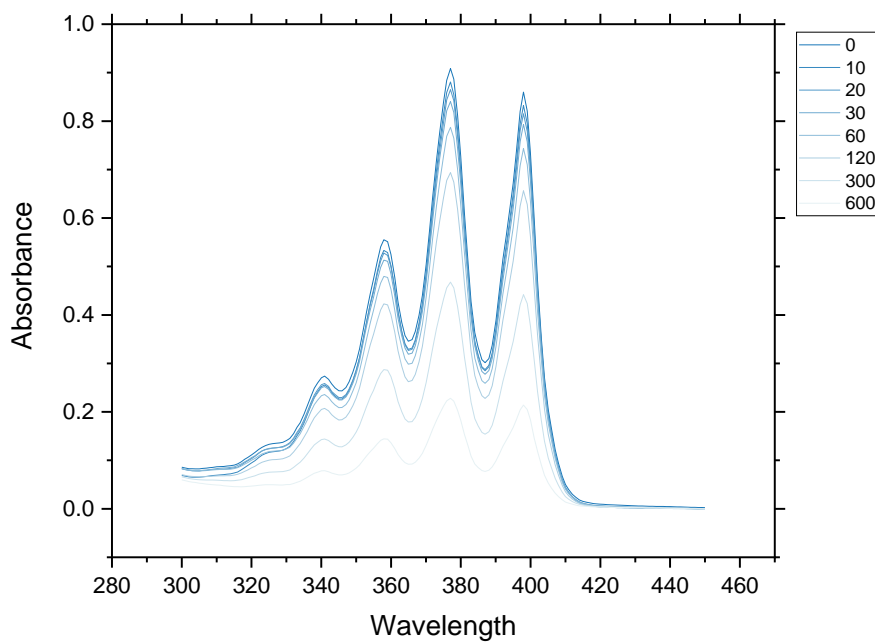


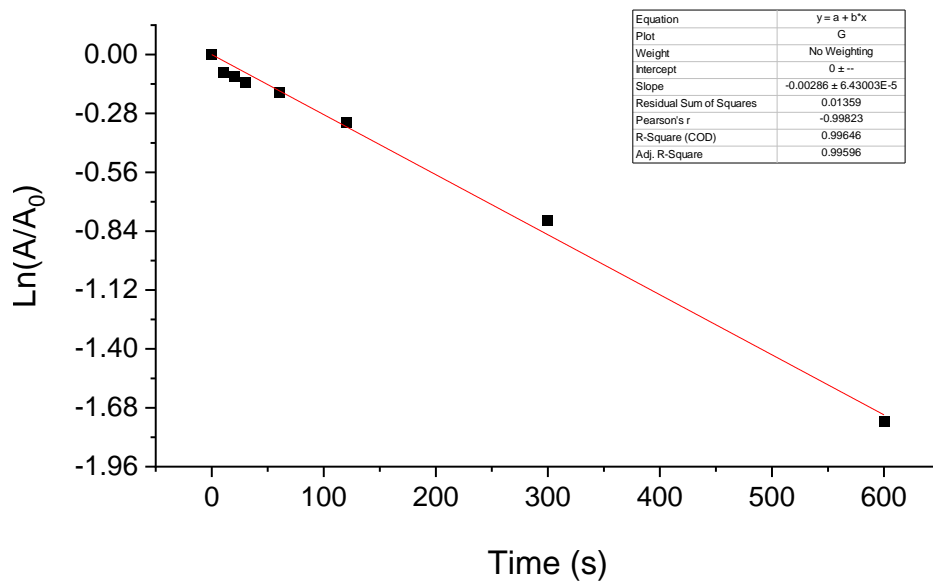
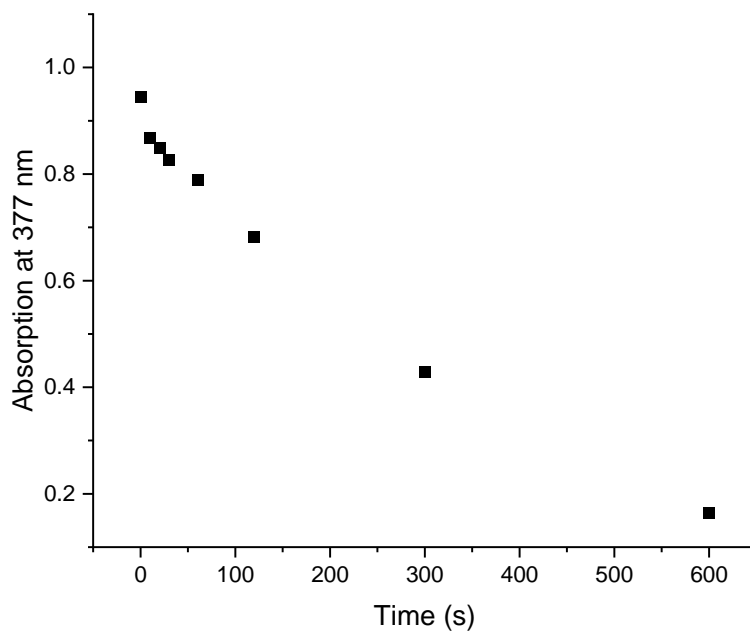


2.5

MCM41 DMA degradation assays (25 $\mu\text{mol g}^{-1}$)

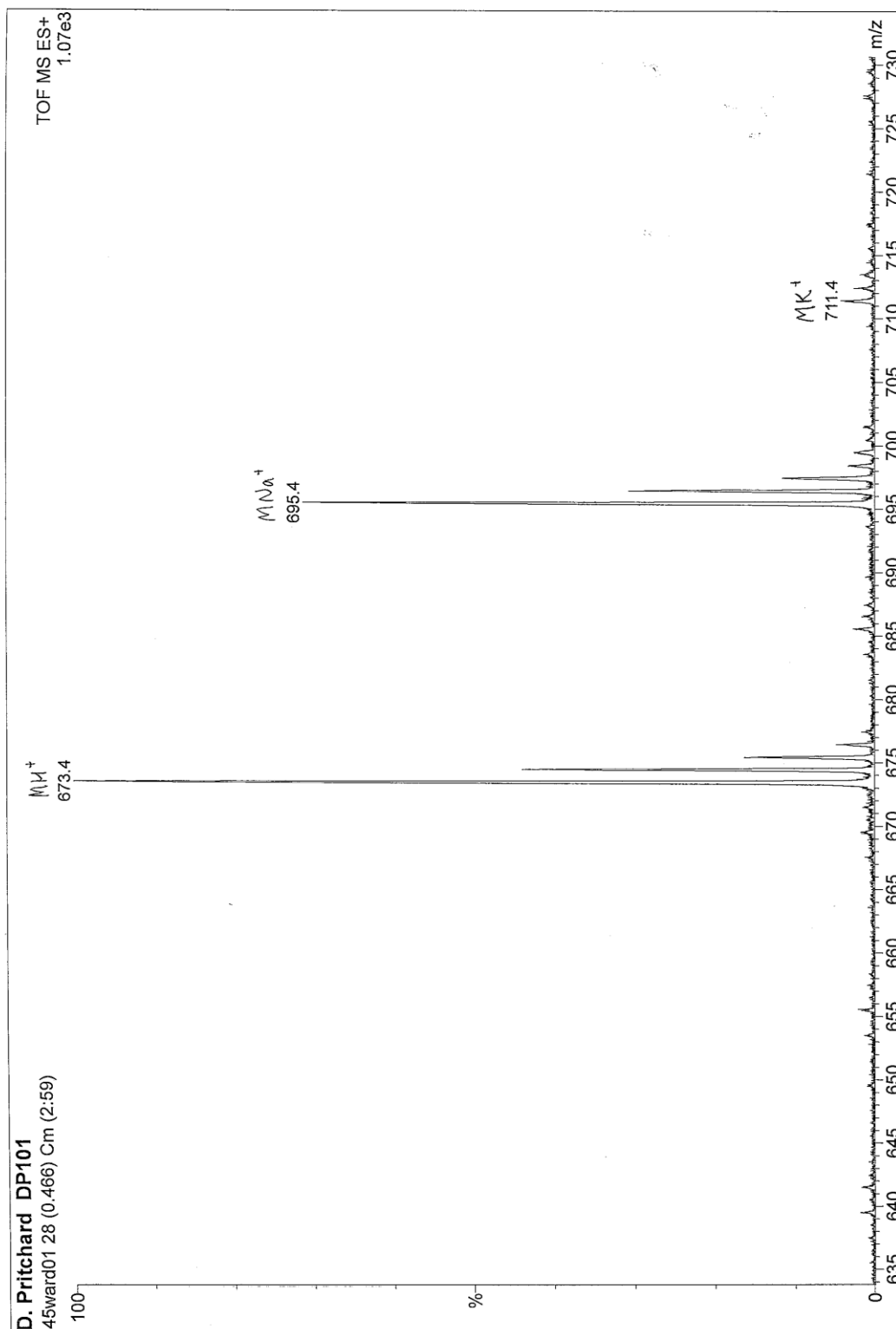
RuBS-



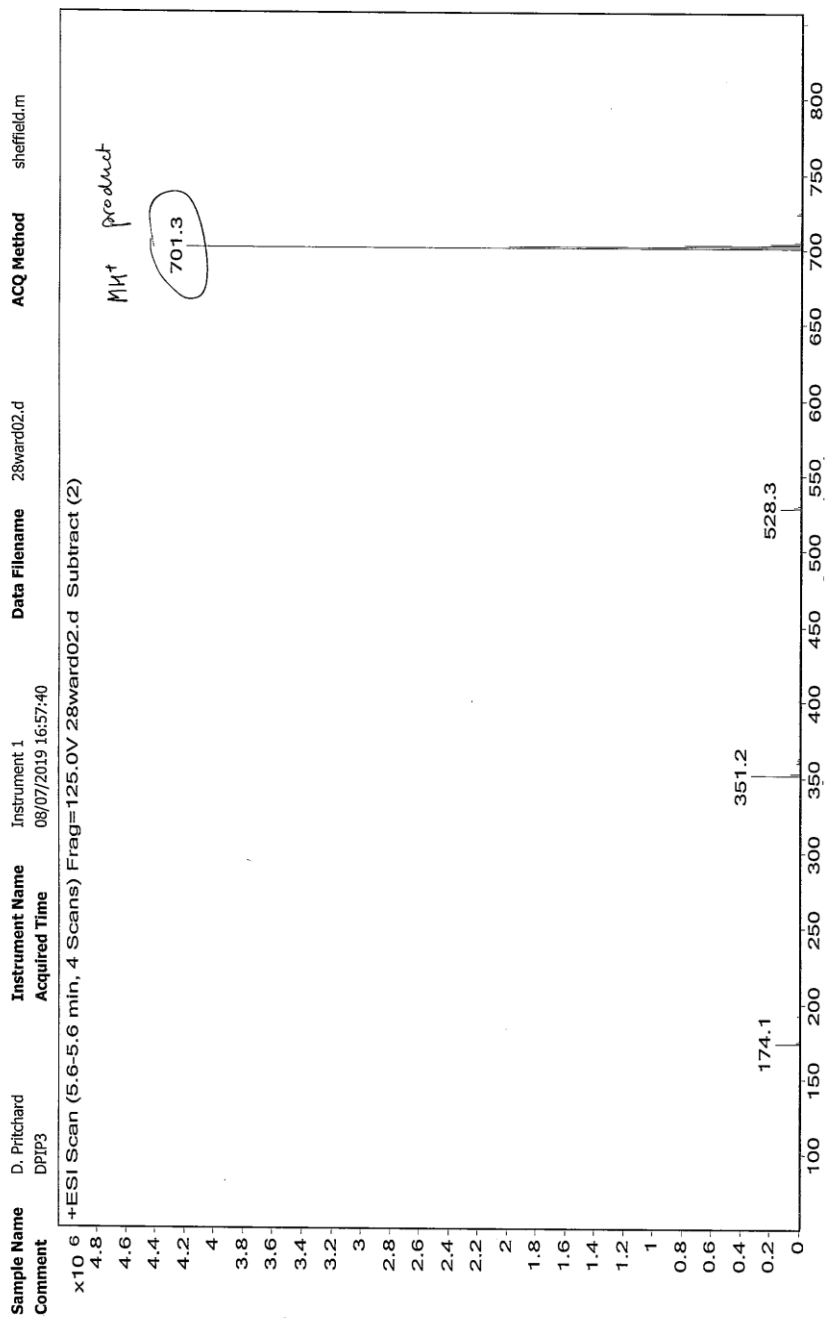


Chapter 5: Experimental

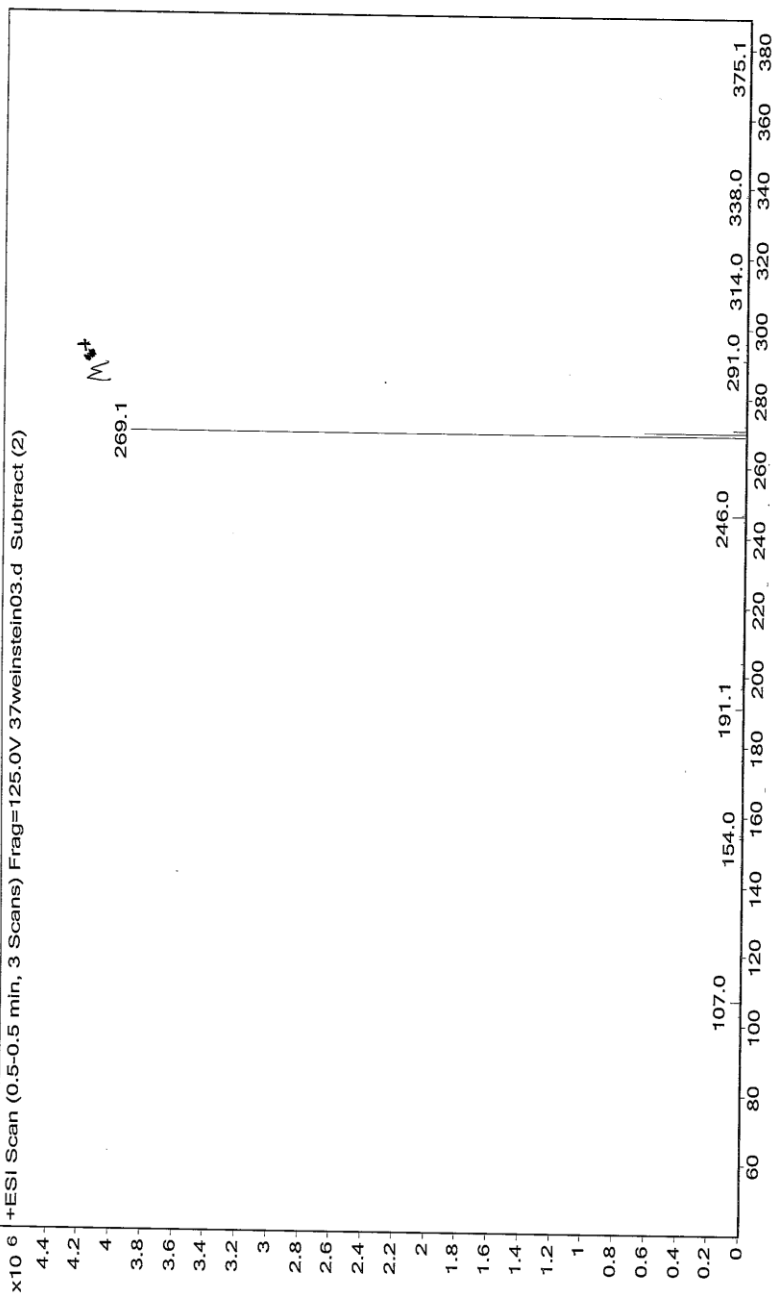
2.6 Bpy-Silatrane



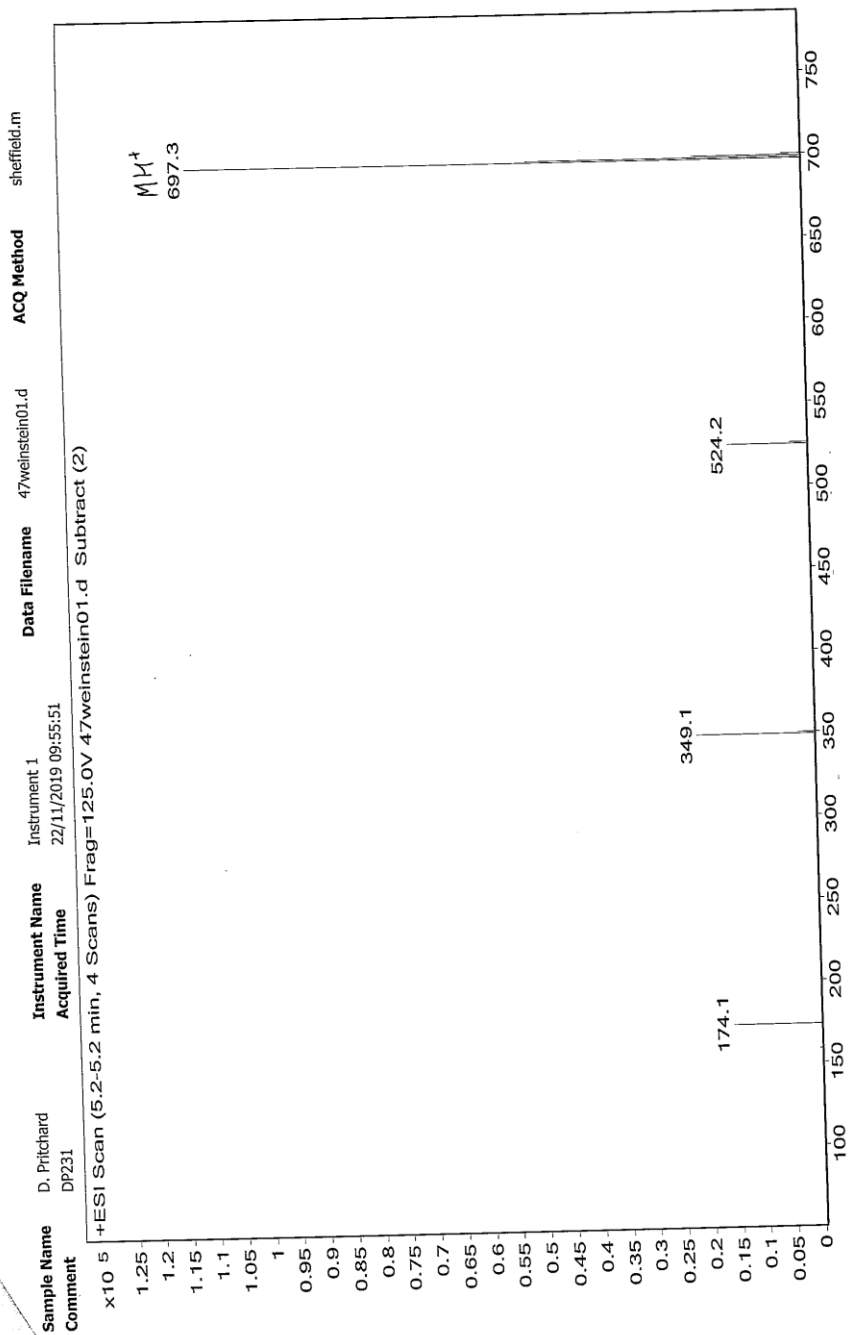
2.7 Bpy-Me-Siltrane



Sample Name D. Pritchard
 Comment DP202 (2nd sample)
 Instrument Name Instrument 1
 Acquired Time 11/09/2019 15:48:03
 Data Filename 37weinstein03.d
 ACQ Method sheffield.m



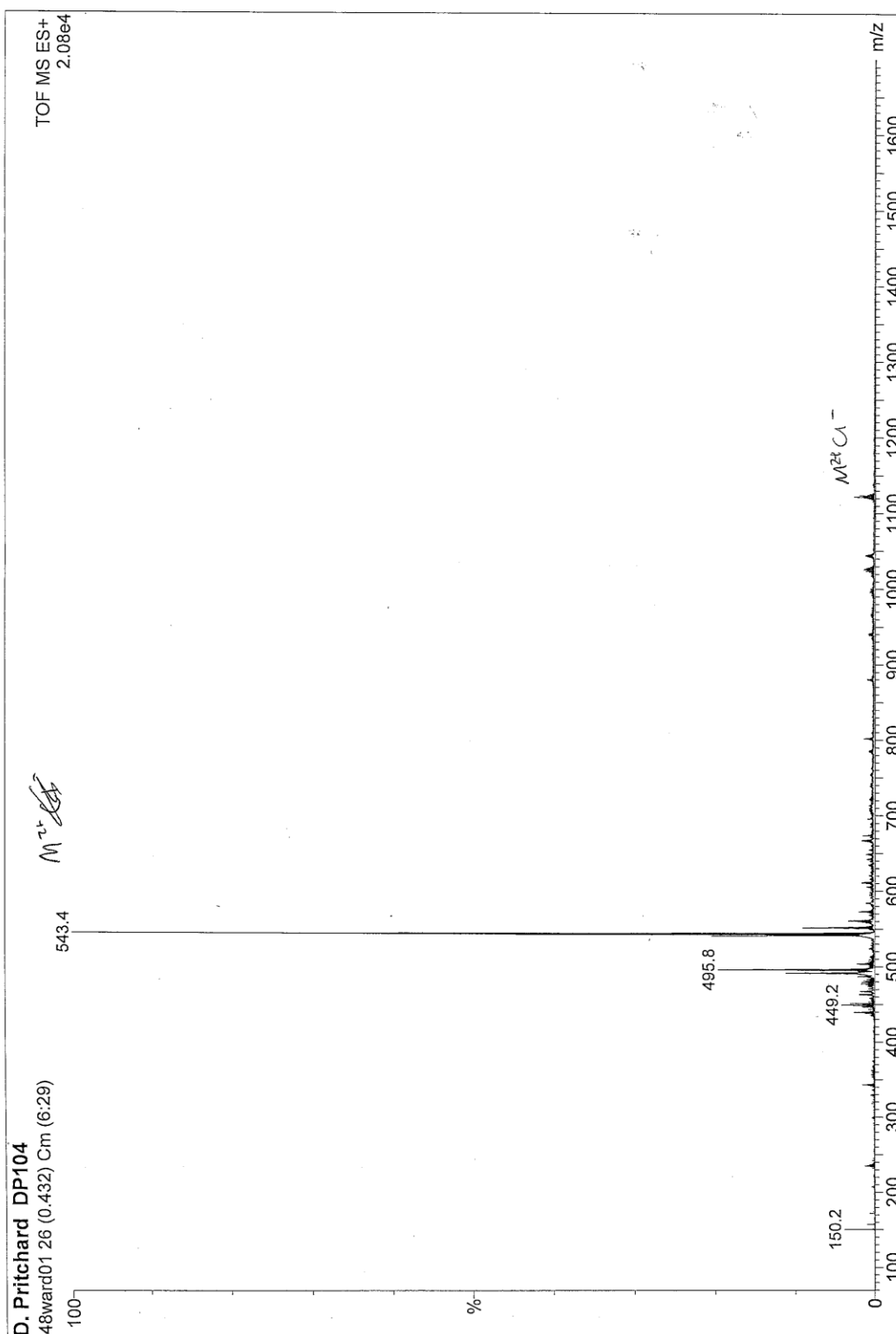
2.9 Phen-Silatrane

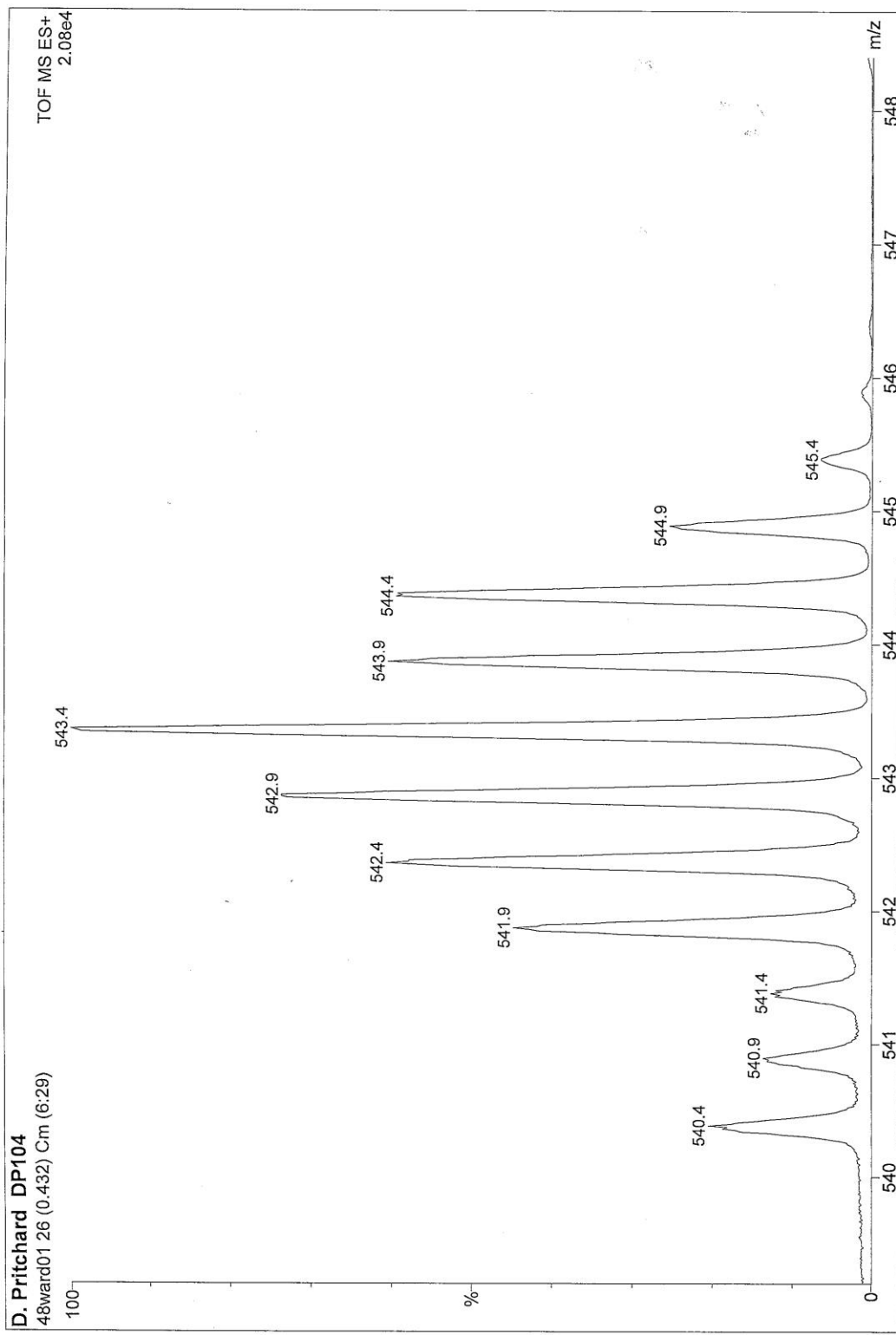


2.10 RuBST

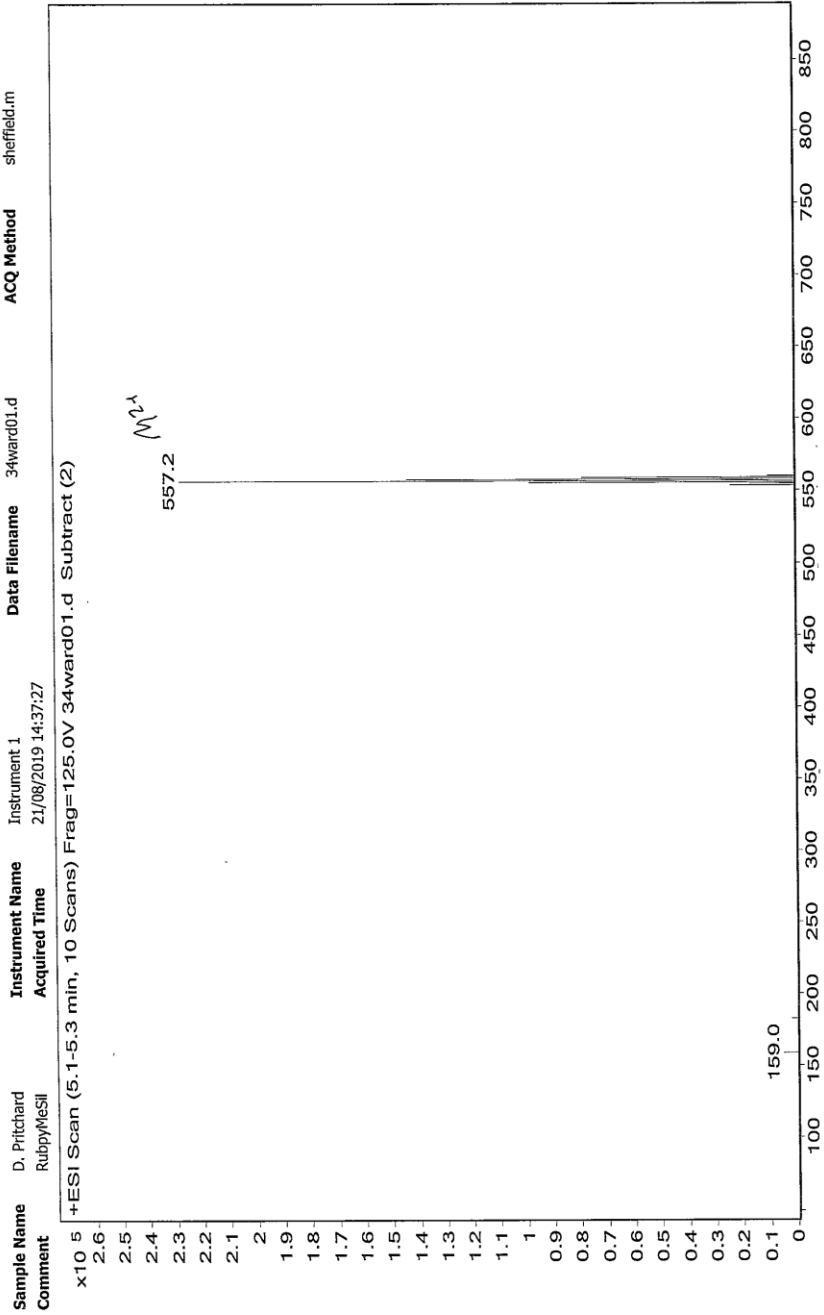
Direct Infusion

Run (bp): 1.173 - 5.174

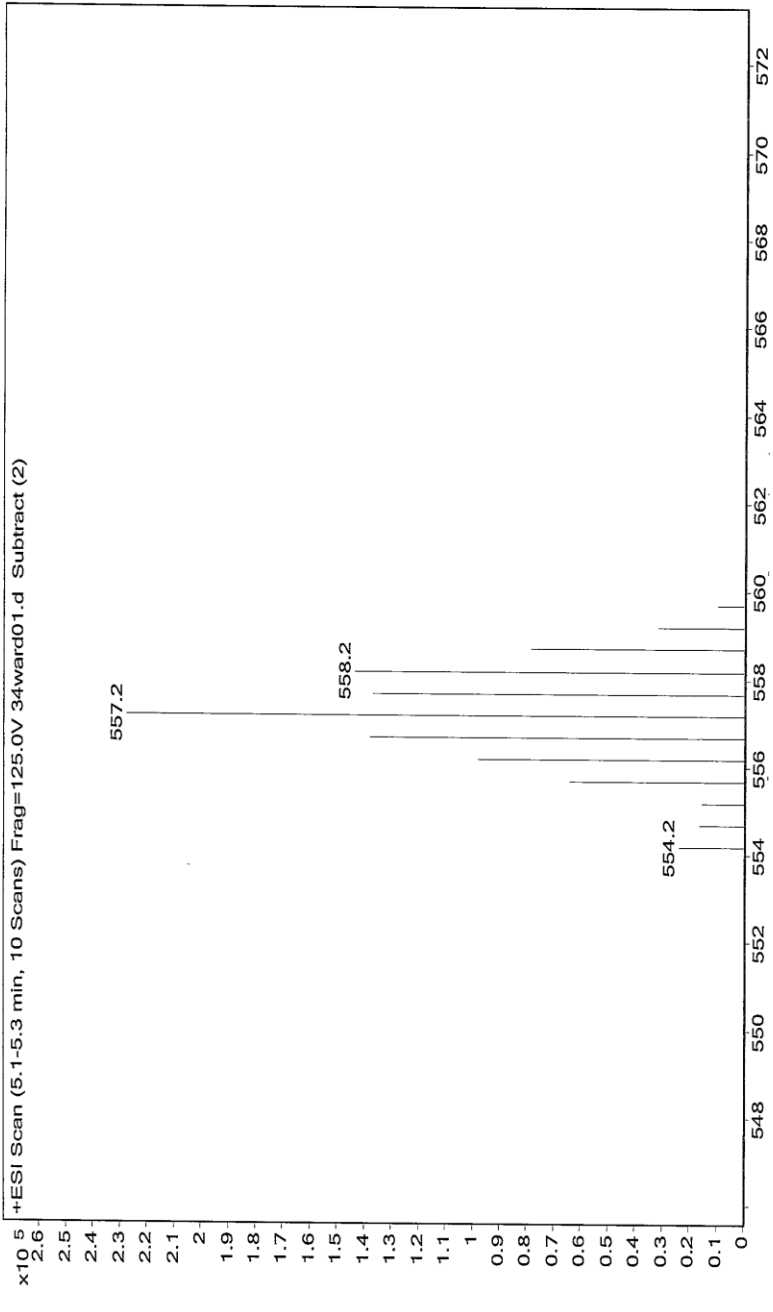


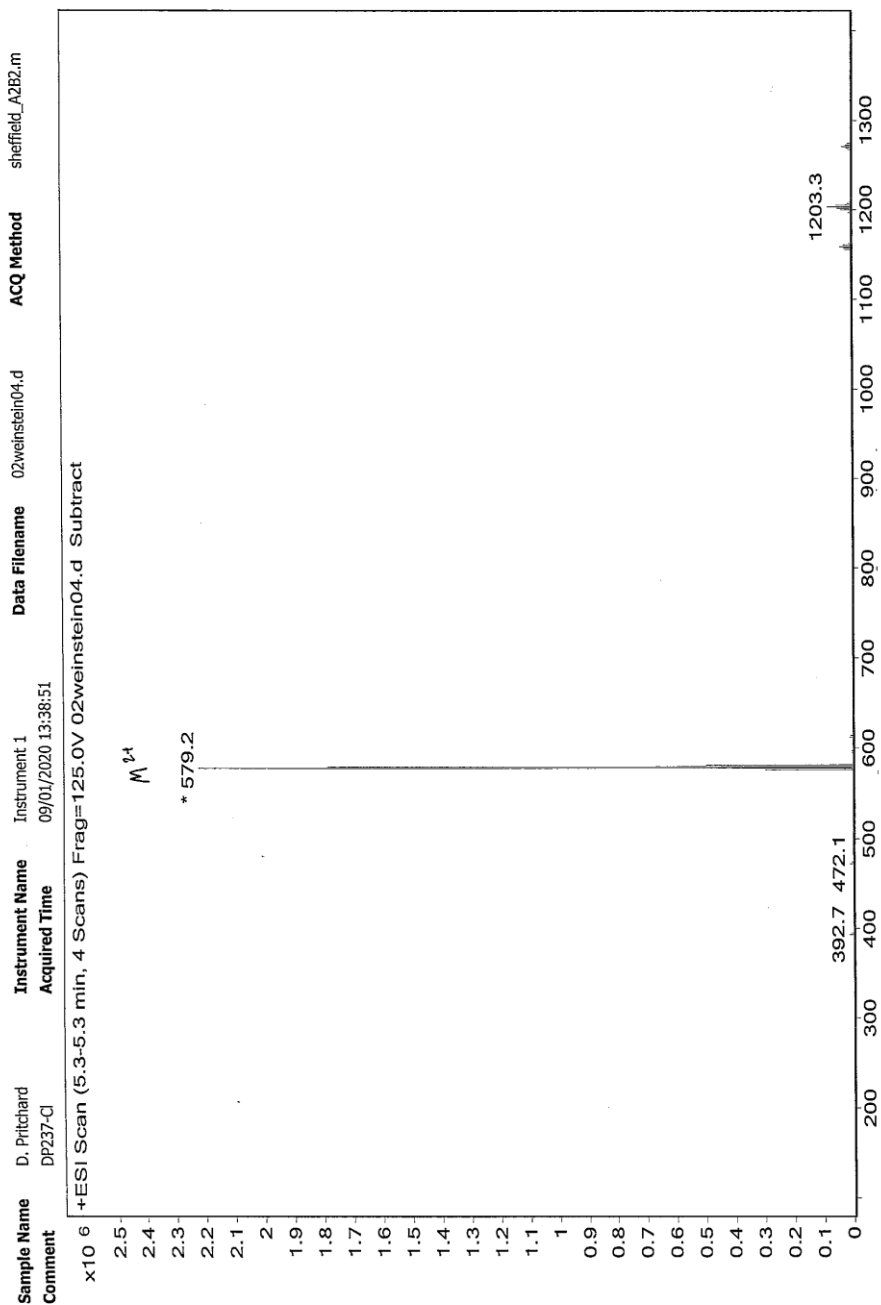


2.11 RuBMS

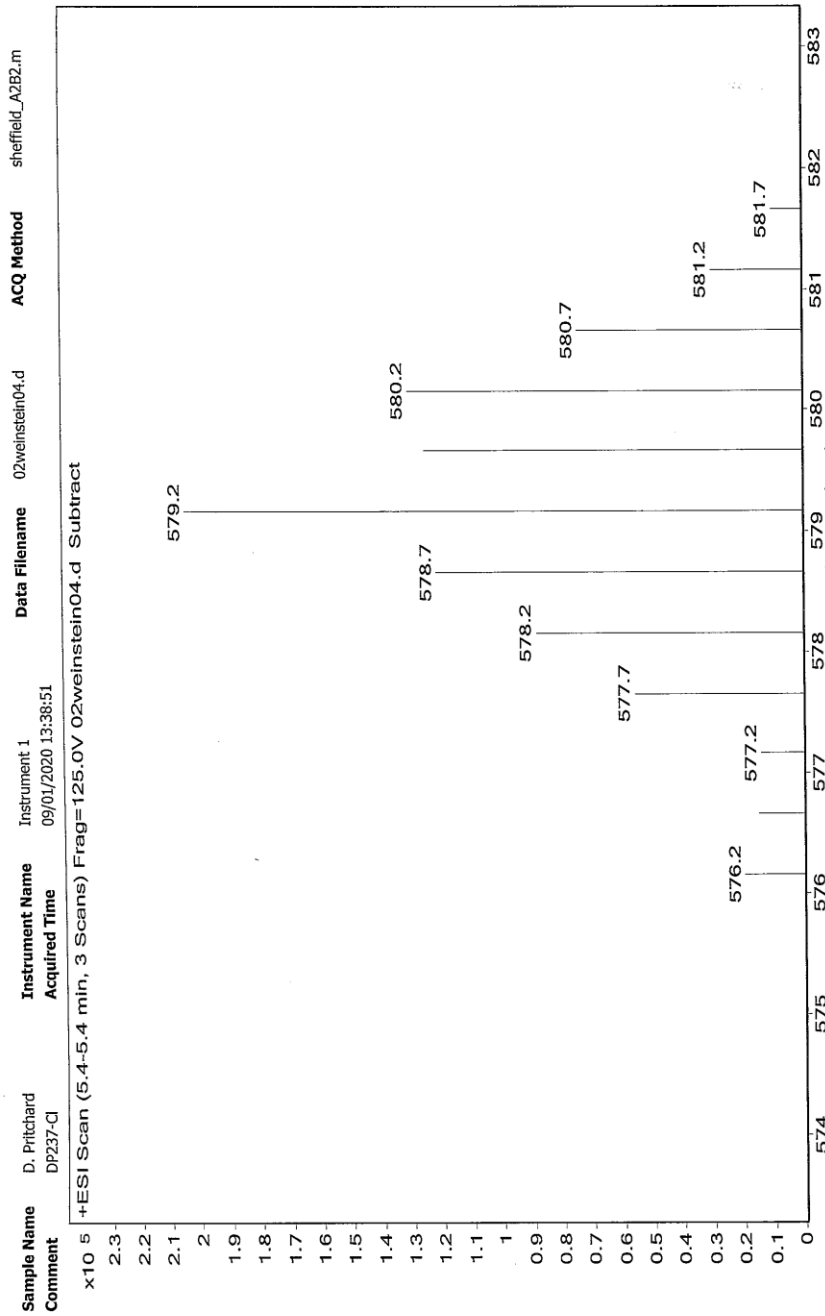


Sample Name D. Pritchard Instrument Name Instrument 1 ACQ Method sheffield.m
Comment RubpyMeSil Acquired Time 21/08/2019 14:37:27 Data Filename 34ward01.d

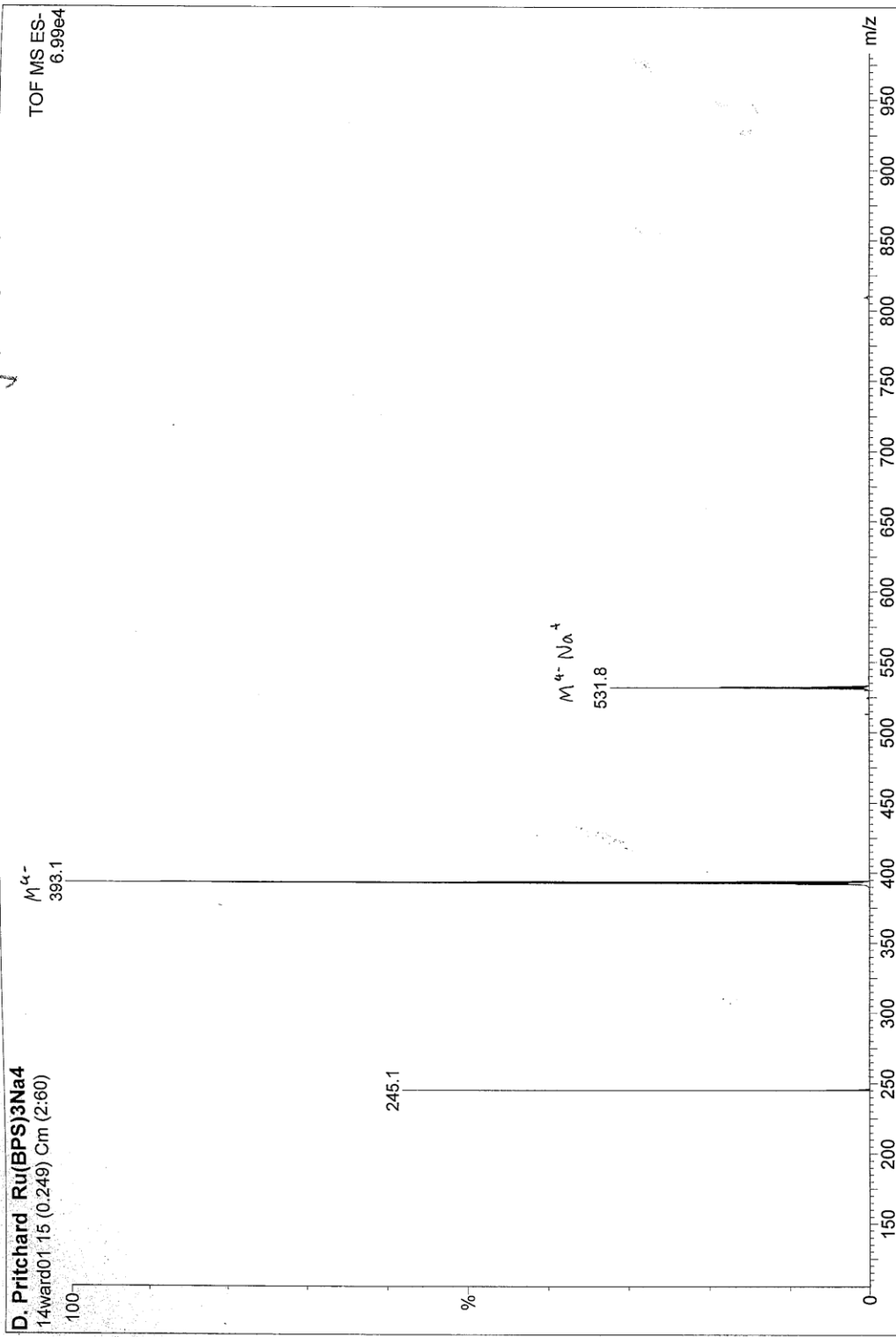


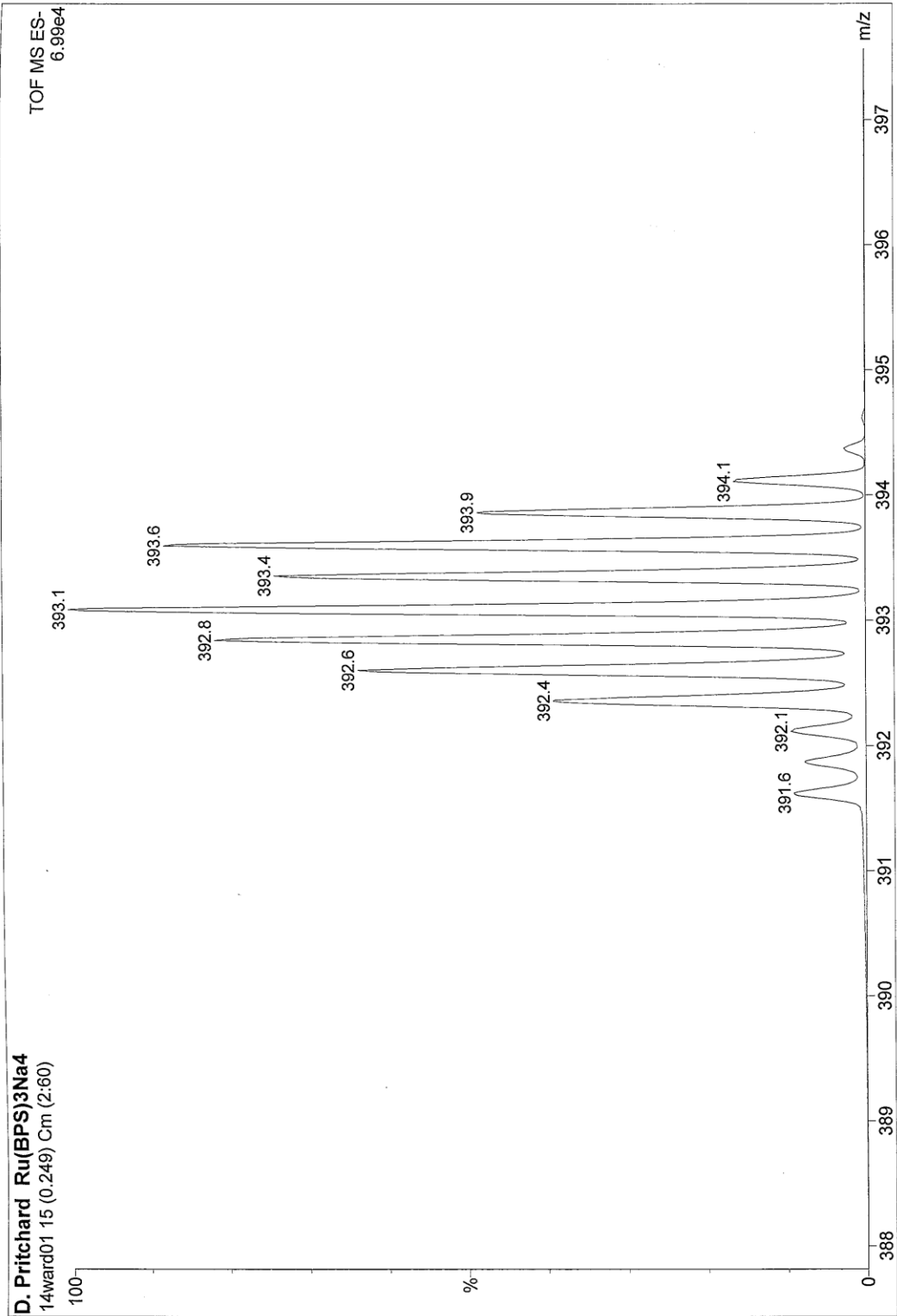


2.13 [RuBPS]Na₄

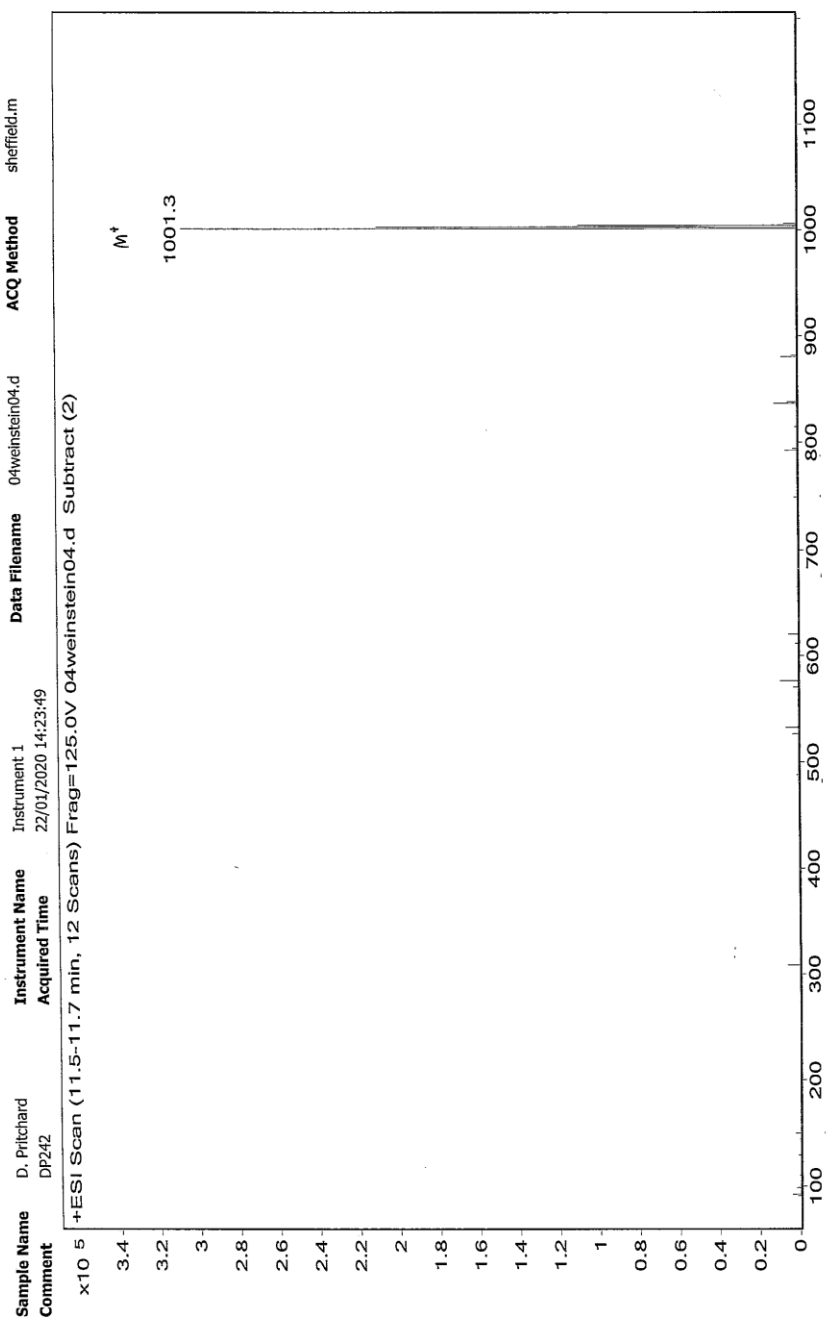


DIRECT INFUSION - didn't work through column

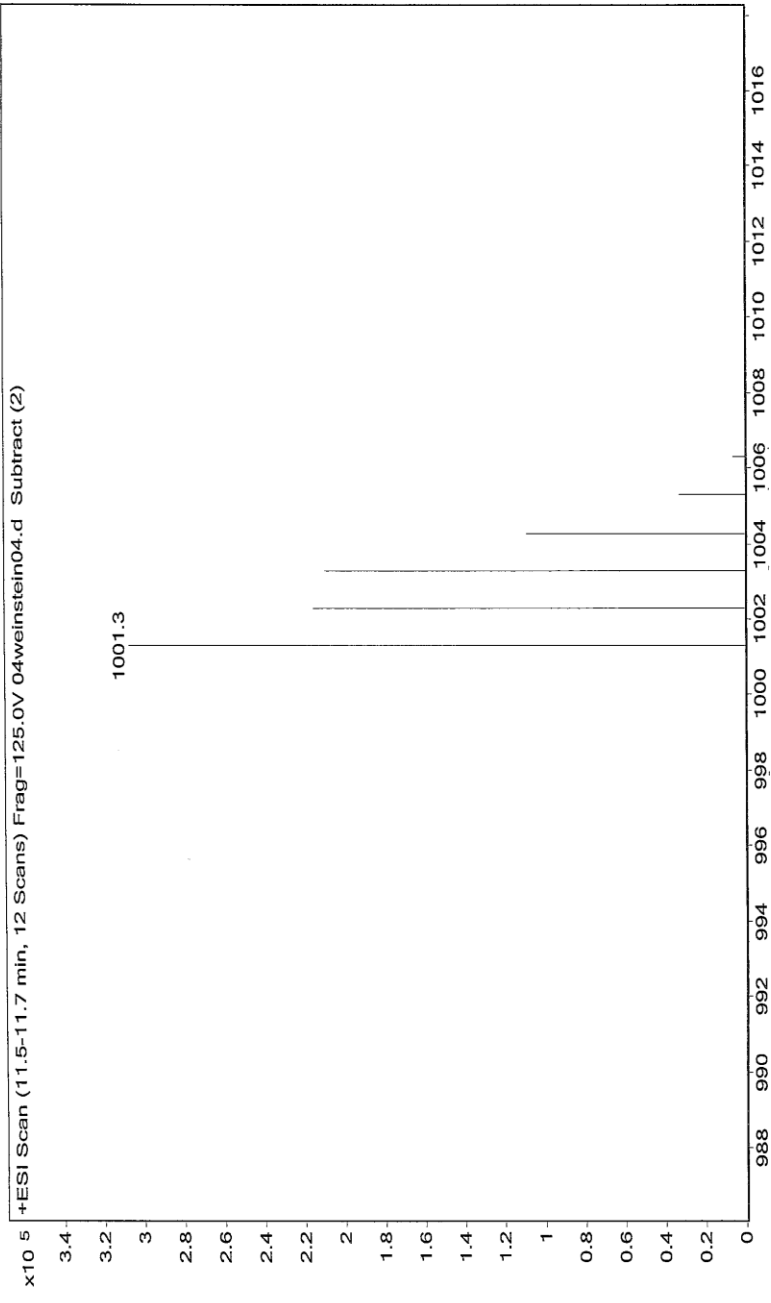




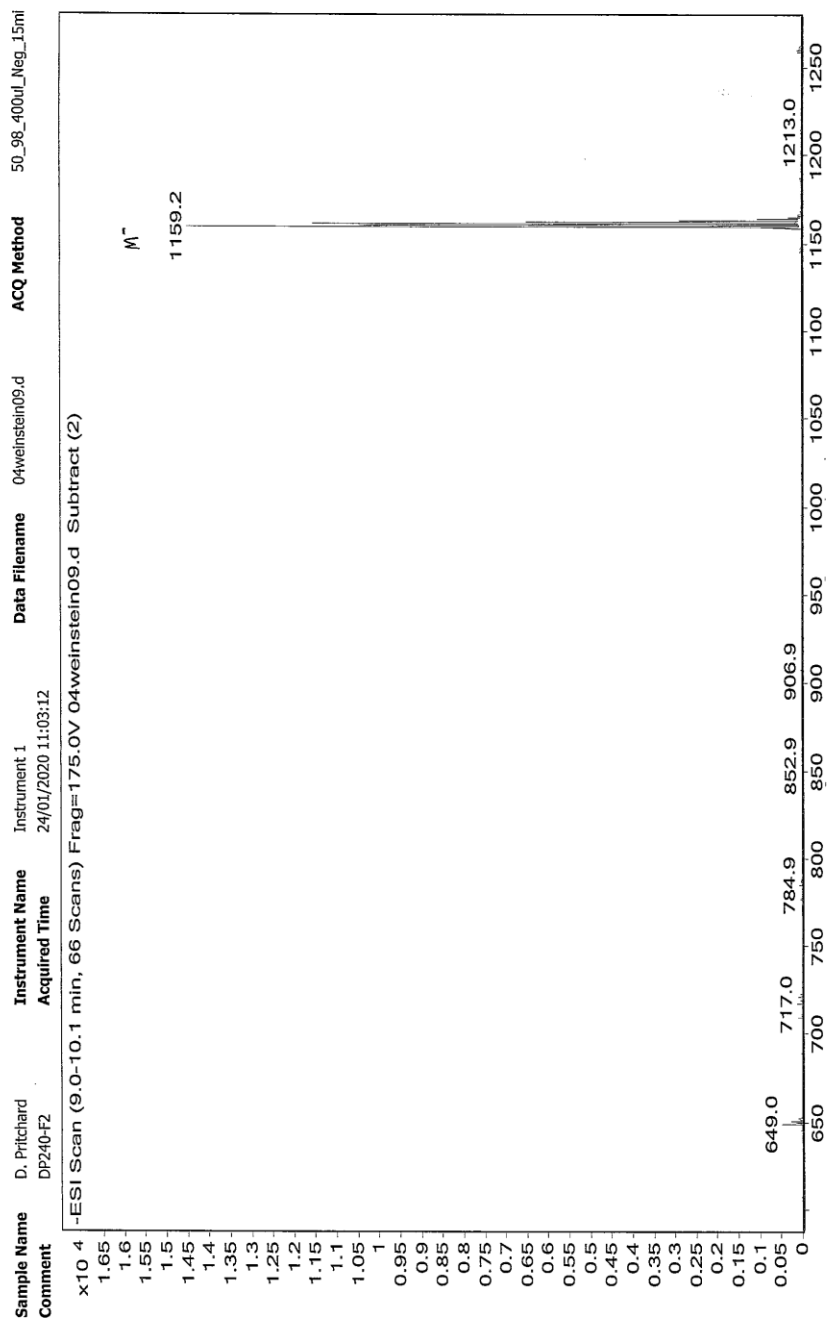
2.14 Cu(BC)(xantphos)



Sample Name D. Pritchard Instrument Name Instrument 1 ACQ Method sheffield.m
Comment DP242 22/01/2020 14:23:49 Data Filename 04weinstein04.d



2.15 [Cu(BCS)(xantphos)]Na



2.16 Cu(dmp)(N-xantphos)

DIRECT INFUSION

